UNIVERSITY OF CALIFORNIA, SAN DIEGO

Development of Microbubble Contrast Agents with Biochemical Recognition and Tunable Acoustic Response

A Dissertation submitted in partial satisfaction of the requirements for the degree Doctor of Philosophy

in

Materials Science and Engineering

by

Matthew Allan Masao Nakatsuka

Committee in charge:

Professor Jennifer N. Cha, Chair
Professor Sadik C. Esener, Co-Chair
Professor Robert F. Mattrey
Professor Donald J. Sirbuly
Professor Liangfang Zhang

2013

The Dissertation of Matthew Allan Masao Nakatsuka is approved, and it is acceptable in quality and form for publication on microfilm and electronically:

_____

_____

_____

_____
Co-Chair

_____
Chair

University of California, San Diego
2013

DEDICATION

For my mom and dad. Thank you for everything.

EPIGRAPH

“Do you see it yet?”
“No,” I replied, “I am certain I do not, but I see how little I saw before.”

Samuel H. Scudder

TABLE OF CONTENTS

LIST OF FIGURES

LIST OF TABLES

ACKNOWLEDGEMENTS

I would like to thank Professor Andrew Goodwin for his continuing mentorship and guidance. It is because of his unyielding effort and patience with me that I am where I am today. I would literally travel halfway across the country to work for him.

Thank you to Professor Jennifer Cha for chairing my committee and serving as an invaluable adviser. I can't imagine how different my career would have been had you not given me that unscheduled interview during my recruiting visit four years ago.

Professor Sadik Esener deserves recognition for acting as a co-chair of my committee, for his constant and invaluable advice and encouragement, especially in the field of ultrasound.

I need to thank Professor Robert Mattrey and his research group for their advice and aid during our collaborative work. Much credit goes to Christopher Barback, Jacqueline Corbeil and Rosemarie Ramirez for their help with animal surgeries and ultrasound imaging. This project would not have been possible without you, and I appreciate the long days you put in with me during the many trips I made to the Hillcrest Medical Center.

My colleagues in Professor Cha and Professor Goodwin's groups have been great scientific resources and even better friends. Thank you to Hyunwoo Noh, Ju Hun Lee, Lauren Forbes, Phyllis Xu, Michael Brasino, Kirsten Fitch, Setareh Azarnoush, Yue Shi, Sarah Chowdhury, and

Taeseok Oh. Without being able to interact with all of you on a daily basis, to share in the same challenges of being a graduate student, this dissertation would not be in the same state it is today. Thank you to Professor Albert Hung, Dr. Dylan Domaille, and Dr. Praveena Mohan for being incredible fonts of knowledge about everything and anything I might have a question about. I only hope I can do the same as a future post-doctoral researcher. Finally thank you to all the undergraduate students with whom I have had the opportunity and pleasure to work; Emi Nakayama, Jade Lee, Alan Toledo, Claudia Shuldberg and Alexander Farwell, I wish the best for all of you.

I owe a great deal of thanks to those in the Esener group for all the support they have provided me over the years. Thanks to Dr. Mark Hsu for the crash-course in optics and acoustics, and Dr. Michael Benchimol for the long troubleshooting sessions and chats regarding bubble theory. Thanks to Dr. Stuart Ibsen, Dr. Inanc Ortac and Carolyn Schutt for their flexibility in letting me share their lab space over the years.

While it has not been as long, I would be remiss to forget Dr. Mark Borden and the rest of his research group, who have made the transition to CU Boulder as seamless as possible, and being very open about collaborations and shared use of his equipment. Thank you to Dr. Shashank Sirsi, Dr. Jameel Feshitan, and Kang-Ho Song for all of their help.

And a final thank you goes to my institutions: UCSD and the Materials Science Department, and CU Boulder and the Chemical and Biological

Engineering Department for providing the resources and support necessary to complete my education.

Chapter 2, in full, is a reprint of the material as it appears in Soft Matter, 2011. Matthew A. Nakatsuka, Joo Hye Lee, Emi Nakayama, Albert M. Hung, Mark J. Hsu, Robert F. Mattrey, Sadik C. Esener, Jennifer N. Cha and Andrew P. Goodwin contributed to this work. The dissertation author was the primary investigator and author of this paper.

Chapter 3, in full, is a reprint of the material as it appears in Advanced Materials, 2011. Matthew A. Nakatsuka, Mark J. Hsu, Sadik C. Esener, Jennifer N. Cha and Andrew P. Goodwin contributed to this work. The dissertation author was the primary investigator and author of this paper.

Chapter 4, in full, is a reprint of the material as it appears in Advanced Materials, 2012. Matthew A. Nakatsuka, Robert F. Mattrey, Sadik C. Esener, Jennifer N. Cha and Andrew P. Goodwin contributed to this work. The dissertation author was the primary investigator and author of this paper.

Chapter 5, in full, is currently being prepared for submission for publication of the material. Matthew A. Nakatsuka, Christopher V. Barback, Kirsten R. Fitch, Alexander R. Farwell, Sadik C. Esener, Robert F. Mattrey, Jennifer N. Cha and Andrew P. Goodwin contributed to this work. The dissertation author was the primary investigator and author of this work.

VITA

2009: Bachelor of Science in Engineering in Materials Science and Engineering, **University of Pennsylvania**, School of Engineering and Applied Science.

2009-2013: Research Assistant, **University of California, San Diego**,

2010: Master of Science in Materials Science and Engineering, **University of California, San Diego**.

2013: Doctor of Philosophy in Materials Science and Engineering, **University of California, San Diego**

PUBLICATIONS

M.A. Nakatsuka, C.V. Barback, K.R. Fitch, A.R. Farwell, S.C. Esener, R.F. Mattrey, J.N. Cha, A.P. Goodwin, "In Vivo Ultrasound Visualization of Non-Occlusive Blood Clots with Thrombin-Sensitive Contrast Agents", Submitted.

P.F. Xu, H. Noh, J.H. Lee, D.W. Domaille, **M.A. Nakatsuka**, A.P. Goodwin, J.N. Cha, "Imparting the Unique Properties of DNA into Complex Material Architecture and Function", *Mater. Today*., In Press

M.A. Nakatsuka, R.F. Mattrey, S.C. Esener, J.N. Cha, A.P. Goodwin, "Aptamer-Crosslinked Microbubbles: Smart Contrast Agents for Thrombin-Activated Ultrasound Imaging", *Adv. Mater.*, **2012**, 24, 6010-6016.

M.A. Nakatsuka, M.J. Hsu, S.C. Esener, J.N. Cha, A.P. Goodwin, "DNA-Coated Microbubbles with Biochemically Tunable Ultrasound Contrast Activity", *Adv. Mater.*, **2011**, 23, 4908-4912.

M.A. Nakatsuka, J.H. Lee, M.J. Hsu, E. Nakayama, A. Hung, R.F. Mattrey, S.C. Esener, J.N. Cha, A.P. Goodwin, "Facile One-Pot Synthesis of Polymer-Phospholipid Composite Microbubbles with Enhanced Drug Loading Capacity for Ultrasound-Triggered Therapy", *Soft Matter*, **2011**, 7, 1656-1659.

ABSTRACT OF THE DISSERTATION

Development of Microbubble Contrast Agents with Biochemical Recognition and Tunable Acoustic Response

by

Matthew Allan Masao Nakatsuka

Doctor of Philosophy in Materials Science and Engineering

University of California, San Diego, 2013

Professor Jennifer N. Cha, Chair
Professor Sadik C. Esener, Co-Chair

Microbubbles, consisting of gas-filled cores encapsulated within phospholipid or polymer shells, are the most widely used ultrasound contrast agents in the world. Because of their acoustic impedance mismatch with surrounding tissues and compressible gaseous interiors, they have high echogenicities that allow for efficient backscatter of ultrasound. They can also generate unique harmonic frequencies when insonated near their resonance frequency, depending on physical microbubble properties such as the stiffness and thickness of the encapsulating shell. Microbubbles are used to detect a number of cardiovascular diseases, but current methodologies lack the ability

to detect and distinguish small, rapidly growing abnormalities that do not produce visible blockage or slowing of blood flow.

This work describes the development, formulation, and validation of microbubbles with various polymer shell architectures designed to modulate their acoustic ability. We demonstrate that the addition of a thick disulfide crosslinked, poly(acrylic acid) encapsulating shell increases a bubble's resistance to cavitation and changes its resonance frequency. Modification of this shell architecture to use hybridized DNA strands to form crosslinks between the polymer chains allows for tuning of the bubble acoustic response. When the DNA crosslinks are in place, shell stiffness is increased so the bubbles do not oscillate and acoustic signal is muted. Subsequently, when these DNA strands are displaced, partial acoustic activity is restored.

By using aptamer sequences with a specific affinity towards the biomolecule thrombin as the DNA crosslinking strand, this acoustic "ON/OFF" behavior can be specifically tailored towards the presence of a specific biomarker, and produces a change in acoustic signal at concentrations of thrombin consistent with acute deep venous thrombosis. Incorporation of the emulsifying agent poly(ethylene glycol) into the encapsulating shell improves microbubble yield and circulation half-life substantially, allowing for the in vivo detection of a blood clot in a rabbit model. The results presented here show a unique marriage of highly specific molecular imaging and sonography that could be tailored towards a wide variety of cardiovascular abnormalities.

Chapter 1: Introduction

1.1: Clinical ultrasound imaging and contrast agents

It is difficult to consider modern medical diagnostics without regarding the impact of ultrasound. As the second most widely-used imaging modality, ultrasound is employed for many different therapeutic and diagnostic applications. Ultrasound works on the basis of sending a wave consisting of alternating high and low pressure phases through a transducer. As the sound wave impacts tissues and various surfaces within the body, the wave is reflected to generate echoes that can be detected by the ultrasound probe, generating a 2D image. The proportion of reflected sound depends on differences in compressibility, material density, and acoustic impedance of the two materials [1].

Current technologies based on simple reflection and reading of sound echoes, called brightness-mode, or “B-Mode”, can produce an image at resolutions down to the millimeter scale. B-Mode imaging is frequently used to detect abnormalities within major organs, arteries, and veins in the cardiovascular system, or to image a growing fetus. In all of these cases, there is a significant acoustic mismatch between the surrounding media, blood or amniotic fluid, respectively, and the targeted tissues, allowing them to show up as bright outlines. However, features such as capillary blood vessels are smaller than the resolution limit, making them difficult to distinguish from

background noise [2]. Additionally, B-mode can be insufficient to diagnose tissue diseases such as thrombosis or cancers because of similarities in tissue compressibility.

To address this limitation, contrast agents, or small particles that can be injected intravenously and have a high echogenicity in comparison to the surrounding tissue, have been developed. The addition of a contrast agent allows for much easier viewing of tissue contours, enabling the clinician to find any physical abnormalities quickly. Many different contrast agents have been developed for ultrasound imaging, including solid silica nanoparticles [3], liposomes [4, 5] and emulsions [6, 7] However, of all the contrast agents, microbubbles are the most common and widely studied [8, 9].

1.2: Microbubble properties:

Microbubbles consist of a gas core stabilized by an encapsulating shell, forming a spherical particle ranging from 1-10 μm in diameter [10, 11]. The first formulations of microbubbles consisted of little more than air temporarily encapsulated by a single monolayer of phospholipids with charged heads and non-polar tails, and the bubble was stabilized by simple hydrophobic/hydrophilic interactions. However, as the phospholipid monolayer provided little resistance to the diffusion of air out of the shell, these microbubbles had lifetimes no longer than a few seconds and would place patients in danger of contracting an embolism. To combat this problem,

microbubbles were formed with thick encapsulating shells made from denatured proteins such as albumin (Albunex®, MolecularBiosystems), which would prevent gas diffusion out of the bubble. Nevertheless, changes in the microbubble encapsulating shell proved to only increase the half-life of the microbubble to ~1 min, and the addition of a thick encapsulating shell considerably dampened acoustic activity, necessitating a far higher dosage of contrast agents. Proteins also are more prone to macrophage absorption and triggering of an immunogenic response than the phospholipids they were replacing [12].

"Second generation" microbubbles were thus improved by replacing the air in the gas core with inert gases that possess lower aqueous solubility and can be safely expelled through the lungs. Examples of this are the commercially available Optison® (GE Healthcare, octafluoropropane), Definity® (Bristol-Meyers Squibb, octafluoropropane), Sonovue® (Bracco, Sulphurhexafluoride), and Sonazoid (Nycomed, perfluorocarbon) [13]. Replacement of the gas increased the half life of the bubbles to several minutes, and has allowed for clinical validation in echocardiography [14] and the imaging of venous thrombosis [15]. Additionally, their persistence within the body has allowed decreased dosages of modern microbubbles as compared to first-generation technologies.

Further enhancements for improving microbubble backscattering in vivo have focused on surface engineering to prevent interaction with macrophages

in vivo. Surface charge has been shown to play a large role in protein adsorption to the bubble shell [16], and the addition of “brush-like” polymer chains such as the polymer-phospholipid conjugate DSPE-PEG or flexible polymer chains such as PLGA [17] were shown to both reduce gas diffusion out of the microbubbles [18] and reduce interaction with macrophages contained within the circulatory system [19] via steric repulsion.

Microbubbles have also been modified to provide simultaneous diagnosis and targeted therapy. The interior of a microbubble shell, particularly one formulated with phospholipids with non-polar tails, can be used as a cargo area to carry aqueous insoluble drugs to a given target [20]. The shell also provides ample sites for attachment of therapeutic drugs [21] and fluorescent labels [22]. Microbubbles are ideal for theranostic purposes, as they can be used as contrast agents at low ultrasound power but are easily ruptured and destroyed by high-powered insonating ultrasound pulses, allowing for a simple and elegant method of imaging and delivery.

1.3: Microbubble Signal Generation

While one would expect gas to reflect sound much more readily than bodily tissue, microbubbles in fact generate a signal distinct from a reflected pulse when insonated due to non-linear oscillation. Bubble dynamics in a pressure wave have been extensively studied for the better part of a century, starting with Lord Rayleigh’s first theoretical descriptions of bubbles exposed

to external cavitating pressure forces, to more recent works on modeling the acoustic behavior of a freely oscillating gas bubble in the linear range.

Rayleigh [23] first proposed a straightforward equation for the oscillation of a spherical, empty bubble first trapped within a liquid media. This model neglects the effects of viscosity, heat transfer and compressibility of the bubble and the media. The Rayleigh-Plesset equation describes an ideal gas trapped within an incompressible liquid media that exerts a constant external pressure on the bubble, while an ultrasound pulse traveling through this liquid media is treated as a repeating series of high and low pressure forces. As such, when an ultrasound pulse encounters a microbubble, the gas trapped within is subjected to repeating changes in external pressure in accordance with the insonating pulse. When the ultrasound pulse exerts a lower external pressure on the gas, the bubble will naturally expand, and when the ultrasound pulse exerts a higher external pressure, the gas bubble will contract. This can be seen in Equation 1 as follows,

$$\frac{P_B(t) - P_\infty(t)}{\rho_L} = R\frac{d^2R}{dt^2} + \frac{3}{2}\left(\frac{dR}{dt}\right)^2 + \frac{4\nu_L}{R}\frac{dR}{dt} + \frac{2S}{\rho_L R}$$

Equation 1: PB = Pressure within the bubble, P_∞ = External Pressure, ρ_L = is the density of the surrounding liquid, R = Bubble radius, v_L = kinematic viscosity, and S = surface tension of the bubble.

As seen from the Rayleigh-Plesset equation, microbubble motion is far from linear. The time it takes for the gas sphere to expand against a lower external pressure and compress against a higher external pressure are

different, leading to non-linear oscillations. Minnaert [24] further refined the Rayleigh-Plesset model to account for this non-linear motion by considering the system as a simple spring, whereby the liquid acts as an inert mass and the interior gas as a spring [25]. By making this approximation, a characteristic resonance frequency could be determined for an air bubble oscillating in water, called the Minnaert resonance, as seen in Equation 2:

$$f = \frac{1}{2\pi R}\left(\frac{3\gamma p_A}{\rho}\right)^{\frac{1}{2}}$$

Equation 2: f = resonance frequency of the microbubble, γ = polytropic gas constant, p_a = ambient pressure, ρ = density of water.

If a microbubble is driven at a frequency far away from this characteristic resonance frequency, sound energy from the insonating wave may be either scattered or absorbed by the microbubble rather than contribute to driving bubble oscillation. Medwin [26] provides an approach to calculate the total backscattered power as a function of the resonance frequency, as well as the power of the insonating wave.

$$\sigma_s = 4\pi R^2\left(\left|\frac{{P_S}^2}{{P_P}^2}\right|\right) = \frac{4\pi R^2}{\left[\left(\frac{f_R}{f}\right)^2 - 1\right]^2 + \delta^2}$$

Equation 3: σ_s = Total scattering cross section of a single bubble, P_s = scattered pressure at the bubble surface, P_p = pressure of the ultrasound incident on the bubble surface, f_R = resonance frequency of the bubble, f = frequency of the incident ultrasound wave, δ = damping constant, dependent on the physical properties of the gas and liquid.

De Jong found that microbubble behavior varied considerably once an encapsulating shell was introduced. Treating an encapsulating shell as multiple layers of elastic material, it was theorized and confirmed by experimentation that the addition of encapsulation results in an increase in resonance frequency and a decrease in scattering. This could be represented within the Rayleigh-Plesset model through the introduction of parameters for shell friction and elasticity, adding a new component to the damping coefficient [27, 28].

$$\omega_r{}^2 = \omega_{rg}{}^2 + \frac{S_{Shell}}{m} \quad S_{Shell} = \frac{8\pi Et}{1-\nu}$$

Equation 4: ω_r =angular resonance frequency, ω_{rg} = angular resonance frequency for an ideal gas bubble, m = effective mass of the system, S_{Shell} = Stiffness of the encapsulating shell, E = elasticity of the shell, t = thickness of the shell, v = Poisson Ratio of the shell.

Church would provide a further derivation of encapsulated bubble motion, showing the dependence of scattering cross-section on the shell viscosity and elastic moduli, among other factors [29]. This was further refined by Hoff [30], showing that the magnitude and frequency of the microbubble-generated signal could be changed dramatically with the addition of a stiff polymer coat.

$$\sigma_s = 4\pi {R_e}^2 \frac{\Omega^4}{(\Omega^2-1)^2+\Omega^2\delta^2} \quad \Omega = \frac{\omega}{\omega_0}$$

$${\omega_0}^2 = \frac{1}{\rho_L {R_e}^2}\left(3\kappa p_0 + 12 G_S \frac{d_{S_e}}{R_e}\right) \quad \delta = \frac{4\mu_L}{\omega_0 \rho_L {R_e}^2} + \frac{12\mu_s \frac{d_{S_e}}{R_e}}{\omega_0 \rho_L {R_e}^2}$$

Equations 5-8: σ_s = scattering coefficient of a shelled microbubble, R_e = equilibrium radius of the microbubble, ω = angular frequency, ω_0 = angular resonance frequency, ρ_L = density of the surrounding liquid, κ = polytropic gas constant, p_0 = external pressure from the liquid, G_s = Shear modulus of the shell, d_{Se} = shell thickness, μ_L = viscosity of the surrounding liquid, μ_s = viscosity of the shell material.

De Jong would go on to compare bubbles with different shell properties to further confirm the behavior of encapsulated bubbles [31]. In the comparison of a thick shelled bubble (Optison), a flexible shell (Sonazoid), and a thin, flexible shell (Albunex), as the shell thickness decreased, the scattered signal increased substantially, and non-linearities within the scattered signal began to form. Other studies on the effect of shell elasticity, viscosity and thickness have demonstrated similar findings [32].

The resulting equations of motion demonstrate that a bubble within a sound field can be described as a second order, non-linear differential equation as a function of the radius over time [33]. The response of microbubbles to acoustic pressure has been generally divided up into three regions of interest. For response at lower pressures (<100kPa), the bubbles oscillate linearly, at moderate pressures (100kPa – 1MPa) they oscillate non-

linearly, and at higher pressures (>1MPa) they are destroyed by cavitation.[34]

Because microbubbles generate resonance frequencies during oscillation that are distinct from the incident ultrasound wave, they can provide especially high signal-to-noise ratios through the application of phase inversion imaging [35, 36]. What this technique entails is to transmit two ultrasound pulses identical in frequency but opposite in phase during the imaging process. By summing the two inverted phase pulses together, all linear echoes resulting from direct backscatter are cancelled out, while any non-linear echoes generated from microbubble oscillation will be magnified [37, 38]. Siemens has developed a specific imaging technique called contrast pulse sequences (CPS), or Cadence™ mode. This involves first transmitting a half-amplitude pulse, followed by a second, full-amplitude, inverted phase pulse, and finally a third half-amplitude pulse identical to the first. This resulting CPS imaging greatly reduces the ultrasound power necessary for imaging [39, 40].

1.4: Deep venous thrombosis diagnosis and risk factors:

Deep venous thrombosis (DVT) occurs in a patient when a blood clot or thrombus forms within a deep vein, most often within the lower body. First described in 1856 by the physician Richard Virchow, the risk factors for thrombosis can be quantified by “Virchow’s Triad”: alterations in blood flow,

endothelial injuries, and hypercoagulability [41]. The early and accurate diagnosis of acute DVT is important, as if left untreated DVT can lead to potentially fatal pulmonary embolisms if the clot reaches the lungs; these account for 60,000 deaths in the United States each year [42].

Thrombosis is the body's natural response to endothelial damage and is designed to slow and prevent the loss of blood, preserving hemostasis. The clot is the end result of the reaction between fibrin and platelets contained within the blood. Fibrin is formed from fibrinogen through the action of thrombin, a protein enzyme that is converted from its inert form prothrombin through a series of tissue factor/cofactor interactions [43, 44]. Thrombin has long been seen as an excellent target for the early determination and prevention of thrombosis, as it is one of the most powerful platelet activators and the production of thrombin during an acute clotting event has been extensively studied [45, 46]. Under normal conditions, the level of activated thrombin contained within the blood vessels is minimal, as it is primarily contained within the zymogen (non-active) form prothrombin and its production is inhibited through the presence of antithrombin iii. However, patients at risk for hypercoagulability stemming from pregnancy, certain cancers, obesity, or invasive surgery may lack this control factor and be at substantially higher risk of contracting DVT.

The current gold standard for diagnosis of DVT is contrast venography [47], in which the veins of the patient are injected with a special dye and

subsequently imaged by x-ray. In this way, physical deformations and damage caused by hypertension can be determined. However, its invasiveness makes angiography unfeasible for general diagnostic use, so acute DVT is currently diagnosed by compression real time ultrasound imaging [48]. The restriction of blood flow upon vein compression is imaged by Doppler imaging, and the overall rigidity of the vessel indirectly confirms that the vein is filled with a clot. However, these techniques alone are insufficient to consistently distinguish acute from chronic DVT. Even angiography cannot easily determine the presence of acute DVT in a chronic DVT patient, further complicating treatment decisions.

Targeted accumulation of contrast agents within a specific organ or disease site has become a popular way to further increase signal to noise ratio, allowing for increased contrast enhancement of important features without the necessity of increasing the overall dose. Many different targeting ligands have been proposed, though some are of limited utility outside of proof-of-concept studies, such as the attachment of biotin [49], or are expensive and inefficient, such as the conjugation of antibodies to the microbubble shell [50]. As a cheaper alternative, DNA strands that specifically bind to certain proteins, blood cells or features within the body have shown great promise [51-54].

1.5: Aptamer design and targeting for therapeutic processes:

Aptamers are ssDNA or RNA sequences that preferentially bind to certain proteins[55] and have shown great potential as targeting ligands. While often compared in functionality to antibodies, aptamers retain several advantages over their protein-based counterparts that make them ideal for molecular imaging. Aptamers are active at a wide range of pHs and temperatures, and they are far easier and less expensive to produce than antibodies. They also exhibit greater specificity, less immunogenicity, and can be loaded at higher densities onto particle surfaces owing to their lower molecular weights [56]. Because they are artificially generated based on affinity to their selected target, aptamers with specific dissociation constants (K_d) can be designed, allowing determination of a “threshold” concentration of activation [57].

Aptamer sequences are carefully chosen by systematic evolution of ligands by exponential enrichment (SELEX) [58, 59]. In this method, an extremely large nucleotide library (~10^{14} sequences) of fixed length sequences is generated flanked by polymerase chain reaction (PCR) primers at the 5’ and 3’ ends. The sequence library is then exposed to the target protein or biomolecule and unbound sequences are washed away. Bound sequences then undergo elution and PCR amplification, and the process is repeated under increasingly rigorous elution conditions to isolate the most strongly binding sequences.

In addition to simple ligand-receptor binding, aptamers have found great use as molecular switches, with systems designed to detect the presence of target proteins through aptamer-target interaction. Sandwich assays require a single target molecule to be bound by two separate aptameric sequences, and this aggregation causes an electrochemical, fluorescence or colorimetric change [60, 61]. Another strategy popularized by Nutiu and Li relies on partial hybridization of an aptamer strand, leaving a “dangling end” containing a partial aptamer sequence. In the presence of the target molecule, this dangling end acts much like a zipper, first interacting with the target biomolecule and then de-hybridizing from the remainder of the strand [62].

Finally, there has been substantial work focused on designing various nanoparticle sensors that utilize the conformational change of aptamer sequences from linear and hybridized to bound and coiled around the active site of a target protein. A surface enhanced resonance Raman scattering (SERRS) sensor [63] was developed whereby in the presence of the target biomolecule, electrostatically immobilized aptamer DNA sequences would be released from the surface of gold particles upon binding to a target molecule. The subsequent aggregation of the two gold particles would be reflected in a decrease in Raman signal. Gold nanoparticle colorimetric detectors [64, 65] have been similarly developed whereby aggregation occurs after the displacement of aptamer DNA sequences from the surface, causing a color

change. Gadolinium MRI contrast agents [66] bound to excess streptavidin by a hybridized aptamer sequence increase their T1 and decrease their relaxivity after the streptavidin/aptamer conjugate preferentially bound to a target biomolecule. Ultimately, all of these “smart” sensors have been developed to convert the specific binding action of an aptamer sequence into a quantifiable secondary signal that can be easily measured.

1.6: Research Motivations and Aims:

Current contrast enhanced imaging utilizing microbubble contrast agents provides a cheap, simple, and non-invasive way to image the cardiovascular system. However, it falls short in diagnosing tissue abnormalities and small but growing thrombi, as the clot must be large enough to produce a filling defect. Because microbubbles oscillate non-linearly, they generate unique pulse echoes with a frequency distinguishable from the insonating ultrasound pulse. Previous studies have shown this unique resonance frequency to be dependent on the shear viscosity and effective elastic modulus of the shell; a mechanically stiffer shell led to less signal being generated at a given insonating frequency and power. Microbubbles are also particularly adept at delivering non-soluble drugs to a given location; the non-polar tails of phospholipid layer provide ample cargo space, and the effect of sonoporation near a living cell has been shown to enhance drug uptake.

With these facts in mind, we set these aims for this work:

1. Measure the change in drug loading and acoustic behavior based on the presence of a crosslinked, polymer coat on the microbubble shell.
2. Design and characterize a microbubble which could change the mechanical properties of its encapsulating shell based on a local chemical environment.
3. Evaluate the ability of an acoustically-tunable contrast agent to specifically find and detect blood clots in vitro and in vivo.

The following hypotheses were made regarding these specific aims:

1. The addition of a polymer coat to a microbubble's encapsulating shell will result in increased hydrophobic drug loading and additional resistance to bubble cavitation caused by insonation.
2. The addition of hybridized DNA-crosslinks within the encapsulating shell will result in a decrease in bubble oscillation. Removal of the crosslinks will result in the restoration of acoustic signal.
3. Modification of a DNA-crosslinked microbubble through the addition of DSPE-PEG will allow for sufficient stability to survive the shear forces present under blood flow within the cardiovascular system, while utilizing aptamer sequences with an affinity towards thrombin as crosslinking strands will allow for specific signal increases only at the site of an acute blood clot.

1.7: References

[1] Sboros V. Response of contrast agents to ultrasound. Adv. Drug Deliv. Rev. 2008;60:1117-36.

[2] Coley BD, Trambert MA, Mattrey RF. Perfluorocarbon-enhanced sonography: value in detecting acute venous thrombosis in rabbits. Am. J. Roentgenol. 1994;163:961-4.

[3] Liu J, Levine AL, Mattoon JS, Yamaguchi M, Lee RJ, Pan XL, et al. Nanoparticles as image enhancing agents for ultrasonography. Phys. Med. Biol. 2006;51:2179-89.

[4] Kimura A, Sakai A, Tsukishiro S, Beppu S, Fujiwara H. Preparation and characterization of echogenic liposome as an ultrasound contrast agent: Size-dependency and stabilizing effect of cholesterol on the echogenicity of gas-entrapping liposome. Chem. Pharm. Bull. 1998;46:1493-6.

[5] Radhakrishnan K, Haworth KJ, Huang SL, Klegerman ME, McPherson DD, Holland CK. Stability of Echogenic Liposomes as a Blood Pool Ultrasound Contrast Agent in a Physiologic Flow Phantom. Ultrasound Med. Biol. 2012;38:1970-81.

[6] Fink IJ, Miller DL, Shawker TH, Girton M, Morrish K. Lipid Emulsions as Contrast Agents for Hepatic Sonography - an Experimental-Study in Rabbits. Ultrasonic Imaging. 1985;7:191-7.

[7] Lanza GM, Wallace KD, Scott MJ, Cacheris WP, Abendschein DR, Christy DH, et al. A novel site-targeted ultrasonic contrast agent with broad biomedical application. Circulation. 1996;94:3334-40.

[8] Calliada F, Campani R, Bottinelli O, Bozzini A, Sommaruga MG. Ultrasound contrast agents: basic principles. Eur. J. Radiol. 1998;27 Suppl. 2:S157-60.

[9] Wilson SR, Greenbaum LD, Goldberg BB. Contrast-enhanced ultrasound: what is the evidence and what are the obstacles? Am. J. Roentgenol. 2009;193:55-60.

[10] Gramiak R, Shah PM. Echocardiography of the aortic root. Invest. Radiol. 1968;3:356-66.

[11] Blomley MJ, Cooke JC, Unger EC, Monaghan MJ, Cosgrove DO. Microbubble contrast agents: a new era in ultrasound. BMJ. 2001;322:1222-5.

[12] Miller DL, Averkiou MA, Brayman AA, Everbach EC, Holland CK, Wible JH, Jr., et al. Bioeffects considerations for diagnostic ultrasound contrast agents. J. Ultras. Med. 2008;27:611-32; quiz 33-6.

[13] Lindner JR. Microbubbles in medical imaging: current applications and future directions. Nat. Rev. Drug Discov. 2004;3:527-32.

[14] Senior R, Becher H, Monaghan M, Agati L, Zamorano J, Vanoverschelde JL, et al. Contrast echocardiography: evidence-based recommendations by European Association of Echocardiography. Eur. J. Echocardiogr. 2009;10:194-212.

[15] Schutt EG, Klein DH, Mattrey RM, Riess JG. Injectable microbubbles as contrast agents for diagnostic ultrasound imaging: the key role of perfluorochemicals. Angew. Chem. Int. Edit. 2003;42:3218-35.

[16] Fisher NG, Christiansen JP, Klibanov A, Taylor RP, Kaul S, Lindner JR. Influence of microbubble surface charge on capillary transit and myocardial contrast enhancement. J. Am. Coll. Cardiol. 2002;40:811-9.

[17] Cui W, Bei J, Wang S, Zhi G, Zhao Y, Zhou X, et al. Preparation and evaluation of poly(L-lactide-co-glycolide) (PLGA) microbubbles as a contrast agent for myocardial contrast echocardiography. J Biomed. Mater. Res. Part B Appl. Biomater. 2005;73:171-8.

[18] Borden MA, Longo ML. Dissolution behavior of lipid monolayer-coated, air-filled microbubbles: Effect of lipid hydrophobic chain length. Langmuir. 2002;18:9225-33.

[19] Chen CC, Borden MA. Ligand conjugation to bimodal poly(ethylene glycol) brush layers on microbubbles. Langmuir. 2010;26:13183-94.

[20] Klibanov AL, Shevchenko TI, Raju BI, Seip R, Chin CT. Ultrasound-triggered release of materials entrapped in microbubble-liposome constructs: A tool for targeted drug delivery. J. Control. Release. 2010;148:13-7.

[21] Tinkov S, Coester C, Serba S, Geis NA, Katus HA, Winter G, et al. New doxorubicin-loaded phospholipid microbubbles for targeted tumor therapy: in-vivo characterization. J. Control. Release. 2010;148:368-72.

[22] Benchimol MJ, Hsu MJ, Schutt CE, Hall DJ, Mattrey RF, Esener SC. Phospholipid/Carbocyanine Dye-Shelled Microbubbles as Ultrasound-Modulated Fluorescent Contrast Agents. Soft Matter. 2013;9:2384-8.

[23] Rayleigh. On the pressure developed in a liquid during the collapse of a spherical cavity. Philos. Mag. 1917;34:94-8.

[24] Minnaert M. On musical air bubbles and the sounds of running water. Philos. Mag. 1933;16:235-48.

[25] Vokurka K. On Rayleigh Model of a Freely Oscillating Bubble .2. Results. Czech J. Phys. 1985;35:110-20.

[26] Medwin H. Counting Bubbles Acoustically - Review. Ultrasonics. 1977;15:7-13.

[27] Dejong N, Hoff L, Skotland T, Bom N. Absorption and Scatter of Encapsulated Gas Filled Microspheres - Theoretical Considerations and Some Measurements. Ultrasonics. 1992;30:95-103.

[28] Dejong N, Hoff L. Ultrasound Scattering Properties of Albunex Microspheres. Ultrasonics. 1993;31:175-81.

[29] Church CC. The Effects of an Elastic Solid-Surface Layer on the Radial Pulsations of Gas-Bubbles. J. Acoust. Soc. Am. 1995;97:1510-21.

[30] Hoff L, Sontum PC, Hovem JM. Oscillations of polymeric microbubbles: Effect of the encapsulating shell. J. Acoust. Soc. Am. 2000;107:2272-80.

[31] Rayleigh J. Heyday (Book Review). Library Journal. 1979;104:2586.

[32] Khismatullin DB, Nadim A. Radial oscillations of encapsulated microbubbles in viscoelastic liquids. Phys. Fluids. 2002;14:3534-57.

[33] Al Dieri R, Peyvandi F, Santagostino E, Giansily M, Mannucci PM, Schved JF, et al. The thrombogram in rare inherited coagulation disorders: its relation to clinical bleeding. Thromb. Haemostasis. 2002;88:576-82.

[34] Hilgenfeldt S, Lohse D, Zomack M. Response of bubbles to diagnostic ultrasound: a unifying theoretical approach. Eur Phys J B. 1998;4:247-55.

[35] Rosenthal SJ, Jones PH, Wetzel LH. Phase inversion tissue harmonic sonographic imaging: a clinical utility study. Am. J. Roentgenol. 2001;176:1393-8.

[36] Ferrara K, Pollard R, Borden M. Ultrasound microbubble contrast agents: fundamentals and application to gene and drug delivery. Annu. Rev. Biomed. Eng.. 2007;9:415-47.

[37] Leen E, Averkiou M, Arditi M, Burns P, Bokor D, Gauthier T, et al. Dynamic contrast enhanced ultrasound assessment of the vascular effects of novel therapeutics in early stage trials. Eur. Radiol. 2012;22:1442-50.

[38] Quaia E. Microbubble ultrasound contrast agents: an update. Eur. Radiol. 2007;17:1995-2008.

[39] Streeter JE, Gessner R, Miles I, Dayton PA. Improving sensitivity in ultrasound molecular imaging by tailoring contrast agent size distribution: in vivo studies. Mol. Imaging. 2010;9:87-95.

[40] Stieger SM, Dayton PA, Borden MA, Caskey CF, Griffey SM, Wisner ER, et al. Imaging of angiogenesis using Cadence contrast pulse sequencing and targeted contrast agents. Contrast Media Mol. Imaging. 2008;3:9-18.

[41] Bagot CN, Arya R. Virchow and his triad: a question of attribution. Brit. J. Haematol. 2008;143:180-90.

[42] Hirsh J, Hoak J. Management of deep vein thrombosis and pulmonary embolism. A statement for healthcare professionals. Council on Thrombosis (in consultation with the Council on Cardiovascular Radiology), American Heart Association. Circulation. 1996;93:2212-45.

[43] Furie B, Furie BC. In vivo thrombus formation. J. Thromb. Haemost. 2007;5 Suppl 1:12-7.

[44] Furie B, Furie BC. Thrombus formation in vivo. J. Clin. Invest. 2005; 115:3355-62.

[45] Hemker HC, Giesen PL, Ramjee M, Wagenvoord R, Beguin S. The thrombogram: monitoring thrombin generation in platelet-rich plasma. Thromb. Haemostasis. 2000;83:589-91.

[46] Ninivaggi M, Apitz-Castro R, Dargaud Y, de Laat B, Hemker HC, Lindhout T. Whole-blood thrombin generation monitored with a calibrated automated thrombogram-based assay. Clin Chem. 2012;58:1252-9.

[47] Bates SM, Jaeschke R, Stevens SM, Goodacre S, Wells PS, Stevenson MD, et al. Diagnosis of DVT: Antithrombotic Therapy and Prevention of Thrombosis, 9th ed: American College of Chest Physicians Evidence-Based Clinical Practice Guidelines. Chest. 2012;141:e351S-418S.

[48] Zierler BK. Ultrasonography and diagnosis of venous thromboembolism. Circulation. 2004;109:I9-I14.

[49] Klibanov AL, Rychak JJ, Yang WC, Alikhani S, Li B, Acton S, et al. Targeted ultrasound contrast agent for molecular imaging of inflammation in high-shear flow. Contrast Media Mol I. 2006;1:259-66.

[50] Villanueva FS, Jankowski RJ, Klibanov S, Pina ML, Alber SM, Watkins SC, et al. Microbubbles targeted to intercellular adhesion molecule-1 bind to activated coronary artery endothelial cells. Circulation. 1998;98:1-5.

[51] Wang CH, Kang ST, Lee YH, Luo YL, Huang YF, Yeh CK. Aptamer-conjugated and drug-loaded acoustic droplets for ultrasound theranosis. Biomaterials. 2012;33:1939-47.

[52] Maul TM, Dudgeon DD, Beste MT, Hammer DA, Lazo JS, Villanueva FS, et al. Optimization of ultrasound contrast agents with computational models to improve selection of ligands and binding strength. Biotechnol. Bioeng. 2010;107:854-64.

[53] Simberg D, Mattrey R. Targeting of perfluorocarbon microbubbles to selective populations of circulating blood cells. J. Drug Target. 2009;17:392-8.

[54] Shi G, Cui W, Benchimol M, Liu YT, Mattrey RF, Mukthavaram R, et al. Isolation of rare tumor cells from blood cells with buoyant immuno-microbubbles. PloS one. 2013;8:e58017.

[55] Ellington AD, Szostak JW. Invitro Selection of Rna Molecules That Bind Specific Ligands. Nature. 1990;346:818-22.

[56] Jayasena SD. Aptamers: an emerging class of molecules that rival antibodies in diagnostics. Clin. Chem. 1999;45:1628-50.

[57] Drabovich AP, Berezovski MV, Musheev MU, Krylov SN. Selection of smart small-molecule ligands: the proof of principle. Anal. Chem. 2009;81:490-4.

[58] Tuerk C, Gold L. Systematic evolution of ligands by exponential enrichment: RNA ligands to bacteriophage T4 DNA polymerase. Science. 1990;249:505-10.

[59] Ellington AD, Szostak JW. In vitro selection of RNA molecules that bind specific ligands. Nature. 1990;346:818-22.

[60] Han K, Liang Z, Zhou N. Design strategies for aptamer-based biosensors. Sensors. 2010;10:4541-57.

[61] Liang G, Cai S, Zhang P, Peng Y, Chen H, Zhang S, et al. Magnetic relaxation switch and colorimetric detection of thrombin using aptamer-functionalized gold-coated iron oxide nanoparticles. Anal Chim. Acta. 2011; 689:243-9.

[62] Nutiu R, Li Y. Aptamers with fluorescence-signaling properties. Methods. 2005;37:16-25.

[63] Cho H, Baker BR, Wachsmann-Hogiu S, Pagba CV, Laurence TA, Lane SM, et al. Aptamer-based SERRS sensor for thrombin detection. Nano Lett. 2008;8:4386-90.

[64] Zhang J, Wang L, Pan D, Song S, Boey FY, Zhang H, et al. Visual cocaine detection with gold nanoparticles and rationally engineered aptamer structures. Small. 2008;4:1196-200.

[65] Zhao W, Chiuman W, Brook MA, Li Y. Simple and rapid colorimetric biosensors based on DNA aptamer and noncrosslinking gold nanoparticle aggregation. Chembiochem]. 2007;8:727-31.

[66] Xu W, Lu Y. A smart magnetic resonance imaging contrast agent responsive to adenosine based on a DNA aptamer-conjugated gadolinium complex. Chem. Commun. 2011;47:4998-5000.

Chapter 2: Facile one-pot synthesis of polymer–phospholipid composite microbubbles with enhanced drug loading capacity for ultrasound-triggered therapy

2.1: Abstract

This chapter reports the one-pot synthesis of perfluorocarbon microbubbles with disulfide-crosslinked encapsulating shells of poly(acrylic acid) and phospholipid. We show that in comparison to a non-polymer stabilized microbubble, this formulation shows less acoustic activity at low incident pressures, due to the increased thickness of the shell and the higher elastic modulus, but also demonstrates greater resistance to cavitation at higher incident pressures.

Additionally, the polymer-shelled microbubbles show a 3-fold increase in the amount of model drug Rhodamine-B encapsulation over the non-shelled formulation. As such, these PAA-SH microbubbles are ideal for theranostic applications, whereby a large amount of hydrophobic, electrostatically charged drug can be loaded into the bubble shell, and imaged via ultrasound at low insonating pressures. Once they arrive at the desired site determined by imaging, the PAA-SH microbubbles can be rapidly destroyed through high-pressure ultrasound to deliver their payload.

2.2: Introduction

Theranostics, or agents that can both be tracked through non-invasive imaging and induce therapy selectively at a diseased site, are highly desired for simultaneous diagnosis and treatment of many diseases. These tools would allow a clinician to obtain detailed information about a potentially diseased site, locate the material within the patient, and induce therapy at that specific location if desired. The ideal theranostic can be imaged non-invasively at low concentrations deep within most tissues, remain benign under imaging conditions, and be loaded with enough drug molecules to impact a diseased site upon activation. In this chapter, we describe a new type of ultrasound theranostic microbubbles stabilized by composite shells of polymer and phospholipid. These microbubbles show similar ultrasound enhancement properties to standard microbubble formulations, but possess greatly improved drug loading capabilities over lipid-shelled bubbles. Furthermore, these microbubbles are synthesized very easily in a one-pot reaction.

While many energy sources have been considered for externally triggered drug release, ultrasound possesses a combination of benefits unmatched by other modalities both for imaging and as a means to trigger drug release from outside the patient. First, ultrasound can pass through most tissues with relatively little attenuation or scattering and can be focused down to ca. 1 mm^3 within a patient with substantial penetration depths at a range of intensities. Furthermore, ultrasound is generally safe and imaging can be

performed with inexpensive, portable equipment found at most hospitals and clinics. As a pressure wave, ultrasound is best able to react with a drug carrier by inducing mechanical stress on the structure [1, 2]. Since ultrasound energy is both deposited and reflected at interfaces of media with large differences in compressibility, microbubbles are very efficient at reflecting incident ultrasound, and when insonated at their resonance frequency with sufficient power they can generate selectively detectable harmonic signals through oscillation at harmonic and subharmonic modes [3-5]. In addition, at larger ultrasound intensities the microbubbles may cavitate violently, generating shock waves that perforate cell membranes and allow macromolecules such as DNA, proteins, or polymers to pass directly into the cytoplasm [6].

Despite the advantages of microbubbles as imaging contrast agents, the large, fluorinated gas core limits the amount of drug that can be loaded into each bubble and thus limits the microbubbles' effectiveness as drug delivery vehicles. Most microbubbles are stabilized by a monolayer of phospholipids that can hold only a thin layer of drugs [7, 8]. While functional groups may be added to the structure of poly(ethylene glycol)-based or albumin-based bubbles, the necessary covalent conjugation of drugs requires an additional mechanism to release the drug molecules in their active form [9] The best option therefore appears to be to create a shell that contains excess drug molecules that can potentially be ejected into the surroundings. In initial attempts, drugs were formulated in an oil layer surrounding the bubbles [10],

but the presence of the oil reduced the ability of the microbubble to cause drug release [11]. Other ultrasound contrast agents like acoustically active liposomes possess poorer echogenicity and are less efficient contrast agents [12-14]. In response to these challenges, some research groups have worked on attaching liposomes to the outside of the microbubbles for additional drug storage via biotin–streptavidin interactions [15], while others have used a layer-by-layer technique to adsorb polymers and DNA for gene delivery [16] using postformulation modification. Finally, microfluidics has also been used to create both shelled microbubbles with layers of drug encapsulation [17-19].

Here, we report a novel method to create microbubbles with high drug loading capacity through the co-mixing of lipids and a polymer that has a reversible affinity for the lipid headgroup. The key component for the successful synthesis of the polymer–lipid microbubble shells is poly(acrylic acid) (PAA), which binds to phosphocholine headgroups below its pKa of 4.5 but has little affinity at physiological pH [20-24]. When simply mixed with preformed liposomes at acidic pH, PAA is thought to either intercalate into the alkyl tail groups or cause ripples in the bilayer, destabilizing the assembly and causing liposome rupture. However, if the PAA and lipid are first mixed together at acidic pH to promote polymer–lipid association and crosslinked into place, the resultant assemblies are stable to biological conditions. Thus our strategy is to mix partially thiolated PAA with a phospholipid suspension, sonicate the mixture under perfluorocarbon gas to form the microbubbles, and

then induce disulfide crosslinking to generate microbubbles that each possess a thick stable polymer–lipid shell which would enable high drug loading.

2.3: Materials and methods

2.3.1: Synthesis of partially thiolated poly(acrylic acid)

This synthesis was adapted from a literature procedure [9]. 200 mg poly(acrylic acid) (PAA, 2.77 mmol per monomer unit, Mw ~ 5000, 5 50% wt% in water, Aldrich) was mixed with 14 mL deionized water and 46 mg sodium hydroxide (Fisher). 192 mg N-hydroxysuccinimide (NHS, 1.662 mmol, Pierce) and 159 mg 1-ethyl-3-(3-dimethylaminopropyl)carbodiimide hydrochloride (EDC, 0.831 mmol, Pierce) were dissolved and agitated 20 min. 95 mg cysteamine hydrochloride (0831 mmol, Aldrich) was added in one portion, and the mixture was agitated at RT overnight. The mixture was transferred to a regenerated cellulose 10 dialysis tube (MWCO ~ 3500) and dialyzed 2 d against several changes of distilled water, followed by removal of water through lyophilisation (116 mg, 42.2%). 1H NMR (500 MHz, D2O): δ 1.34-1.89 (m,138H), 2.05-2.60 (m, 69H), 2.63-2.81 (m, 18H), 2.91-3.10 (m, 18H).

2.3.2: Synthesis of 5(6)-fluoresceinyl-2-maleimidoethyl-thiourea (FITC-Mal)

Dissolved 31 mg 2-15 maleimidoethylammonium triflate (0.124 mmol) in 0.4 mL dimethyl sulfoxide (EMD). Added 29 µL triethylamine (0.206 mmol, Alfa

Aesar) and mixed. Added fluorescein isothiocyanate (FITC, 0.103 mmol, Pierce) and stirred in dark 2 d. Added aqueous 1 M HCl until pH ~ 3. Centrifuged at 5000G for 5 min to obtain pellet and removed supernatant. Added 2 mL methanol to dissolve solid, then re-precipitated into 15 mL water. Centrifuged again, removed supernatant, and removed remaining 20 water via lyophilisation to obtain orange fluffy solid (43 mg, 80.7%). 1H NMR (500 MHz, DMSO-d6):δ 3.59-3.80 (m, 4H), 6.42-6.78 (m, 6H), 7.01-7.25 (m, 2H), 7.60-7.78 (m, 2H), 7.82-7.94 (m, 1H),8.00-8.21 (m, 2H), 10.05-10.21 (m, 2H).

2.3.3: Synthesis of fluorescein-labeled partially thiolated poly(acrylic acid) (PAA-SH-FITC)

Dissolved 25 53 mg PAA-SH (0.00883 mmol; See Supporting Information) 2 mL deionized water in vial with stirbar. In separate tube, dissolved 4.3 mg FITC-Mal (0.00883 mmol; See Supporting Information) in 3 mL methanol (Fisher). Combined mixtures, stirred overnight in dark. Added to regenerated cellulose dialysis tubing (MWCO ~ 1000), dialyzed against several changes of distilled water 2 d. Lyophilized to obtain an orange fluffy solid (25 mg, 43.6%). 1H NMR (500 MHz, D2O): δ 1.32-1.89, 5 (m, 138H), 2.05-2.40 (m, 69H), 2.63-2.81 (m, 18H), 2.91-3.10 (m, 20H), 6.42-6.78 (m, 4H), 7.01-7.25 (m, 2H), 7.60-7.78 (m, 2H), 7.82-7.94 (m, 1H), 8.00-8.21 (m, 2H), 10.05-10.21 (m, 2H).

2.3.4: Preparation of DSPC suspension

1,2-distearoyl-sn-glycero-3-phosphocholine (DSPC, Avanti Polar Lipids) was dissolved in chloroform (EMD) at a concentration of 20 mg/mL. Under air flow at room temperature, chloroform was evaporated to form a thin film; this film was then placed under vacuum for at least 12 h to ensure total removal of solvent. The film was then suspended in distilled water at a concentration of 4 mg/mL and heated to 80°C for 30 min while stirring. The suspension was allowed to cool back to RT prior to use in microbubble suspension. For Rhodamine-B loaded microbubbles, 2 μL/mg DSPC of 0.05 mg/mL Rhodamine-B (Aldrich) in methanol (Fisher) was added prior to evaporation of the chloroform.

2.3.5: Preparation of uncrosslinked PAA-SH-FITC solution

Prior to microbubble formation, PAA-SH-FITC was dissolved in 10 mM phosphate buffer at a concentration of 0.25 mg/mL. Dithiothreitol (DTT, Pierce) was added at a concentration of 2.5 mg/mL, and solution 20 was mixed and allowed to sit overnight.

2.3.6: Preparation of microbubbles

In a 1.6 mL centrifuge tube, the following stock solutions were combined, in order: 259.4 μL deionized water, 50 μL 100 mM aqueous acetic acid solution, 50 μL 1.5M NaCl solution, 15.6 μL PAA-SH-FITC solution, and

125 µL of DSPC suspension to make 500 µL total volume in a buffer containing 10 mM acetic acid and 150 mM NaCl (acetate buffered saline at pH 3.4, ABS). Perfluorobutane (PFB, Synquest Labs) was flowed twice through the solution and into the headspace above the solution twice, and the mixture was sonicated at the gas-liquid interface continuously for 10 s at 70% amplitude (Fisher Scientific Sonic Dismembrator 150T). The opaque suspension was washed once by centrifuging at 300 g for 3 min at RT to cause the bubbles to float, followed by removal of the subnatant via syringe and needle and replacement with ABS. Hydrogen peroxide (Fisher) was added to a final concentration of 10 mM, and the solution was mixed and allowed to sit without agitation. After 20 minutes, bubbles were centrifuge washed three times as above, replacing each time with PBS (Gibco) instead of ABS. The bubble solution was then diluted 10 2X with PBS, drawn slowly into a syringe, and allowed to sit for 15 min, plunger upwards, to let large bubbles float to the surface. The middle 80% of the solution was retained for analysis.

2.3.7: Fluorescence microscopy

Bright field and fluorescence images were obtained on a Nikon Eclipse TE200 inverted microscope with a Spot Idea 5Mp Color Mosaic camera. High magnification images 15 were obtained with a Nikon 100X objective with oil immersion. Green and red fluorescence were obtained using appropriate filter cubes.

2.3.8: Ultrasound backscatter measurements

An agar phantom measuring 7x7x4.5 cm with a central rectangular cavity measuring 2.5x2.5x3.5 cm was weighed down in a fish tank filled with water to the 20 top of the phantom. A 2.25 MHz ultrasound transducer (Panametrics V306) was placed on a flat side of the phantom and aligned with the center of the sample cavity. Ultrasound signal was provided as an impulse via a Panametrics Computer Controlled Pulser/Receiver Model 5800 connected to and synchronized with an oscilloscope (Tektronix TDS 3032), which was connected to a PC (Dell) running Labview (National Instruments). First, PBS was placed into the cavity of the phantom and the backscatter was recorded. Next, microbubbles were added to the PBS to a final dilution of 100 fM, mixed, and allowed to settle at least 5 min to prevent scattering due to sample currents. At least 100 consecutive impulses were sent into the sample at 2.25 MHz center frequency at 100 kHz repetition rate, receiving at 40 dB gain with a 300 kHz and 10 MHz high pass and low pass filter, respectively. Backscatter power was calculated as the square of the voltage difference between the signal and the baseline of the AC coupled signal, integrated over the entire time corresponding to the length of the sample, not including the walls of the chamber. This was converted to dB, setting 1 V2 equal to 0 dB. Net backscatter was calculated by subtracting the backscatter from the sample of PBS prior to microbubble addition. The phantom was washed at least three

times between runs to remove any microbubbles adhered to the sidewall. Pulse peak pressure was measured with a calibrated needle hydrophone (Onda HND-0200, amplified by Onda AH-2020-DCBSW) placed on the opposite side of the phantom.

2.3.9: Ultrasound attenuation experiments

A different ultrasound setup was used to reach insonation peak pressures beyond 110 kPa. Experiments were set up as with backscatter experiments, except signal was generated as a single sine wave at 2.25 MHz (HP 8116A Pulse/Function Generator), amplified (T&C Power Conversion AG Series Amplifier), and transmitted through the agar block and received by a needle hydrophone (Onda HND-0200, amplified by Onda AH-2020-DCBSW). The pulse was found to have a peak pressure of 357 kPa through calibrated hydrophone measurements. Attenuation was taken as the difference between the signal at 2.25 MHz measured with blank PBS and with added sample.

2.3.10: Microbubble counting and sizing

At least ten images per sample were taken at 20X in bright field at random locations in the sample. The microbubbles were counted and sized using ImageJ (NIH), using a polystyrene bead standard (Duke Scientific) to calibrate pixels/μm. The concentration was calculated by determining the area of spot size against known volumes of buffer and was checked against silica

microparticle standards (Bangs Labs). Microbubbles were also counted in an Invitrogen Countess Automated Cell Counter to confirm the accuracy of microbubble counting.

2.4: Results and discussion

2.4.1: Microbubble formulation and sizing

First, PAA (MW 5,000 Da) was partially functionalized with cysteamine to add thiol groups and then labeled with a maleimidyl fluorescein isothiocyanate derivative (FITC; **Figure 2.1**). The polymer was combined with a premade suspension of 1,2-distearoyl-sn-glyerco-3-phosphocholine (DSPC) in pH 3.4 acetate buffered saline (ABS). Perfluorobutane (PFB) was flowed into the headspace above the suspension and the mixture was probe sonicated at the gas–liquid interface for 10 s, forming the microbubbles. The microbubbles were then centrifuged at 300g for 3 min to float the bubbles, followed by removal of the subnatant and replacement with ABS. The microbubbles were exposed to 10 mM hydrogen peroxide for 20 min to form disulfide bridges, followed by centrifuge washing three times with PBS. The gas-filled microbubbles are easily visualized by transmission optical microscopy due to the large difference refractive index compared to the surrounding buffer, and the polymer is identified by fluorescence microscopy; the overlay of these images confirms the co-localization of the polymer to the

microbubble surface (**Figure 2.1**). During the synthesis at pH 3.4, while the protonated PAA alone can also stabilize larger bubbles, these are not stable at neutral pH (data not shown). Microbubbles formed with DSPC alone are stable but are formed at a yield of 6 ±1 x 10^7 microbubbles per mL as compared to 7 ± 1 x 10^7 microbubbles per mL with PAA and DSPC (**Figure 2.2**). This increase in yield is most likely due to the steric and electronic repulsion between anionic PAA chains that resist coalescence and promote bubble stability. Irrespective of PAA addition, the bubble size means and distributions are about the same, with average bubble diameters of 2.4 ± 0.8 mm and 2.5 ± 0.8 mm, respectively (**Figure 2.2**). This microbubble size range similar to commercial formulations and thus is appropriate for in vivo imaging [5].

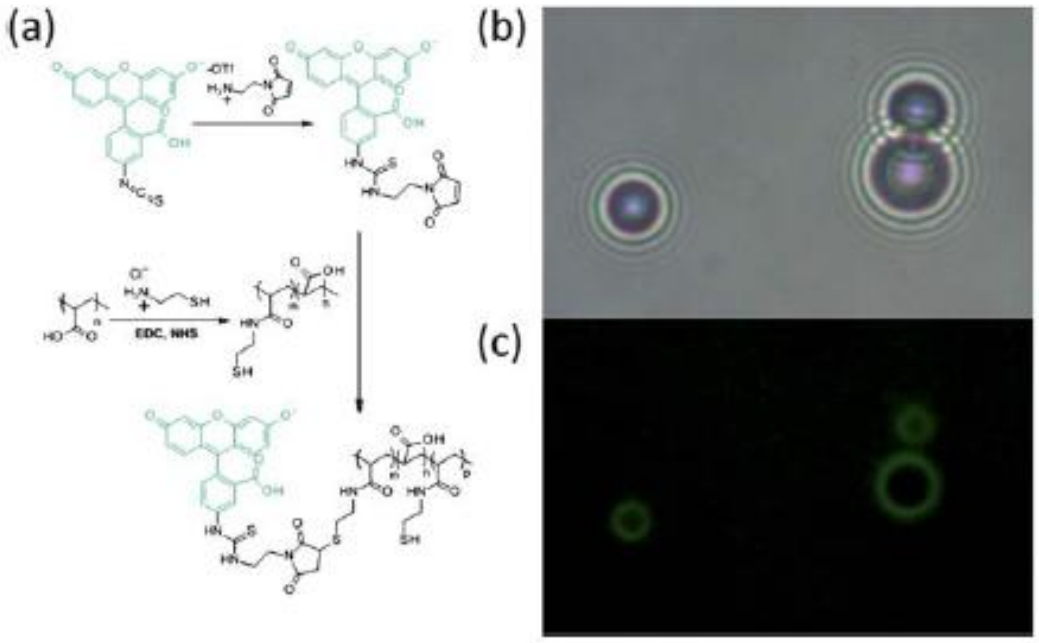

Figure 2.1: (a) Synthesis of FITC-labeled thiolated poly(acrylic acid). Thiol groups were functionalized on 11% of monomer units. (b) Bright field transmission image of microbubbles comprised of DSPC and PAA–SH–FITC, showing location of perfluorobutane gas. (c) Green fluorescence image of the same, showing PAA–SH–FITC.

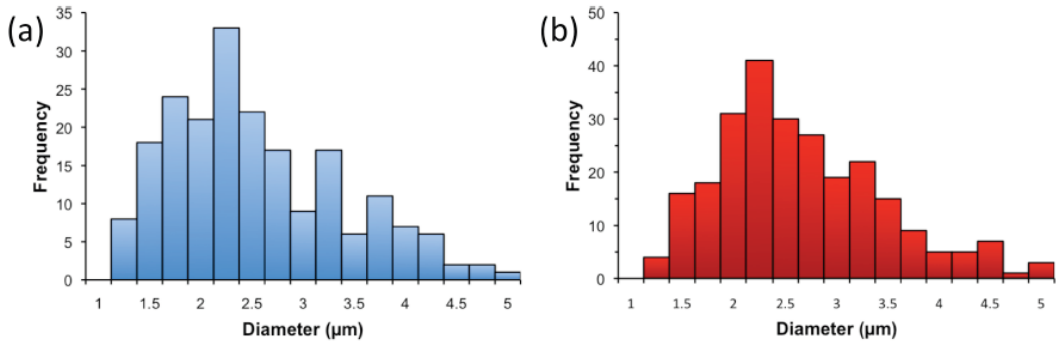

Figure 2.2: Size histograms for DSPC microbubbles made without (a) and with (b) added PAA from bright field microscopy. There were no bubbles larger than 5 μm found for either sample.

2.4.2: Chemical characterization of microbubble shell

The characterization of the composition of the bubbles indicated the shell was comprised of both PAA–SH and DSPC. First, the microbubbles were washed of excess polymer and lipid and examined by NMR spectroscopy, which showed the clear presence of the PAA–SH–FITC in the washed microbubble sample. Next, attempts were made to characterize the shell by transmission electron microscopy (TEM), but the microbubbles proved unstable to the conditions of the TEM. To approximate the shell on a more stable substrate, the same DSPC/PAA–SH–FITC shell was formed on the surface of a silica microparticle. The microparticle was first rendered hydrophobic through reaction with N,N,N,N’,N’,N’-hexamethyldisilazane (HMDS), and then the film was formed on the microparticle through sonication in the presence of DSPC and PAA–SH–FTIC and hydrogen peroxide oxidation. The particles containing the DSPC/PAA–SH–FITC shell were stained with uranyl acetate to stain primarily the PAA in the presence of the lipids. As shown in **Figure 2.3**, the film appears to be 6–9 nm, although it is difficult to draw direct conclusions about substructure from these images alone. However, since lipids are known to form monolayers on the microbubble surface [25, 26], the shell appears to contain a composite of phospholipid and polymer that may be used to encapsulate drug.

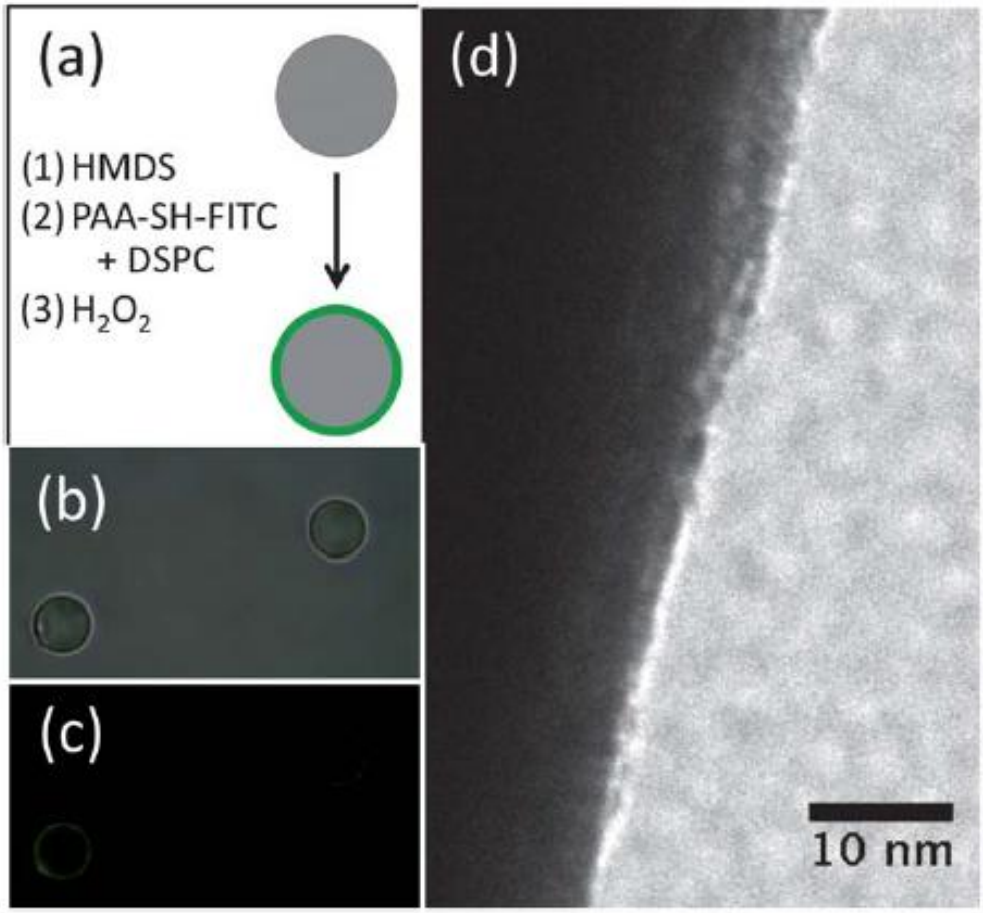

Figure 2.3: Examination of model shell on silica microparticles by TEM. (a) Schematic of hydrophobic functionalization of silica and formation of shell. (b) Bright field image of silica particles containing silica with shells. (c) Green fluorescence image of silica particles containing silica with shells. (d) TEM image of PAA–DSPC formed on hydrophobic silica microparticles. The shell is approximately 6–9 nm thick.

2.4.3: Ultrasound characterization of PAA-crosslinked microbubbles

The microbubbles must reflect the ultrasound efficiently so that their pharmacokinetics can be tracked within the patient. Thus it was important for the microbubbles to retain their ultrasound properties despite the addition of the crosslinked shell. The standard of comparison for these studies was

microbubbles formulated to be similar to Definity®, a common lipid-shelled microbubble that contains a stabilizing layer of poly(ethylene glycol) conjugated to a lipid. For these studies, microbubbles were formulated with the same mass ratios of DPPC, DPPA, and DSPC–mPEG corresponding to Definity®. The ultrasound reflectivity of these microbubbles was measured in vitro in an agar phantom. As shown in **Figure 2.4e**, the resonance frequency of the microbubbles shifts only slightly from 1.5 MHz, consistent with Definity® at this frequency range [27] to 1.7MHz. This slight increase in shell thickness and rigidity due to crosslinking is consistent with theoretical descriptions.

Next, suspensions of microbubbles at 1 fM were added to an agar phantom and pulsed at 2.25 MHz at diagnostic pressures ranging from 24 kPa to 89 kPa (**Figure 2.4a–d**). The backscattered signal of the microbubbles is slightly poorer at 24 kPa, about the same for 43 kPa and 69 kPa, and slightly greater at 89 kPa. We attribute the signal dampening at 24 kPa to the slight reduction in bubble compressibility caused by the presence of the shell, a change which would be observed best at incident pressures insufficient to cause size fluctuations in the stiffer bubbles. However, this same polymer shell provides added stability, and so the sharp decrease at the beginning of the insonation at 89 kPa is most likely due to the destruction of bubbles with resonance frequencies near that of the incident pulse (Fig. 2d). Thus lower diagnostic pressures may be used to image the bubbles without destroying them. When the ultrasound pressure is increased to 89 kPa, also within

diagnostic range, the microbubbles degrade steadily. When the microbubbles were pulsed at 357 kPa, still within diagnostic range, they degrade quite readily, losing over half of their attenuation within one minute (**Figure 2.5**).

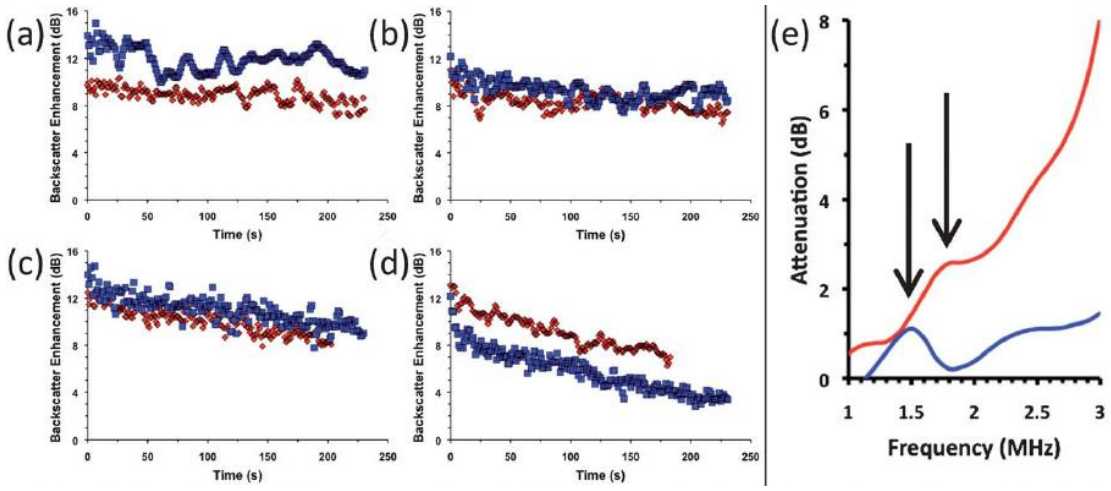

Figure 2.4: Ultrasound characterization of microbubbles with different polymer shells (blue ¼ PEG–DSPE, red ¼ PAA–SH–FITC). (a–d): Backscatter of impulse at 2.25 MHz (100 kHz repetition rate) was measured in an agar phantom at RT. Signal is expressed as enhancement over PBS blank. Backscatter measurements at (a) 24 kPa, (b) 43 kPa, (c) 69 kPa, and (d) 89 kPa peak pressure vs. time. (e): Acoustic attenuation spectra of microbubbles with one sine wave at 2.25 MHz. Attenuation is expressed as loss of through signal compared to PBS blank.

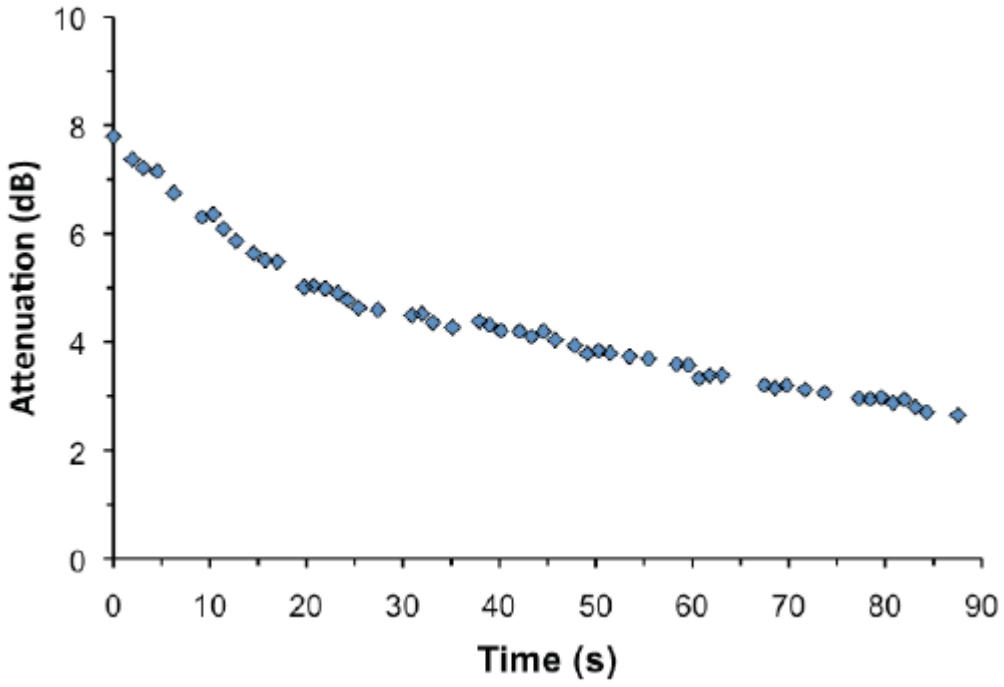

Figure 2.5: Attenuation of PAA-microbubbles at 2.25 MHz while insonated continuously at 357 kPa at 100 Hz with a center frequency of 2.25 MHz. The attenuation was measured by needle hydrophone and compared to PBS blank as with backscatter studies.

2.4.4: Model drug loading of microbubbles

To determine the microbubbles' ability to act as drug carriers, Rhodamine B was used as a model lipophilic drug. The dye was mixed into the lipid mixture prior to formulation and prepared as before, producing bubbles that show much stronger red fluorescence than their lipid-only labeled counterparts (**Figure 2.6**).

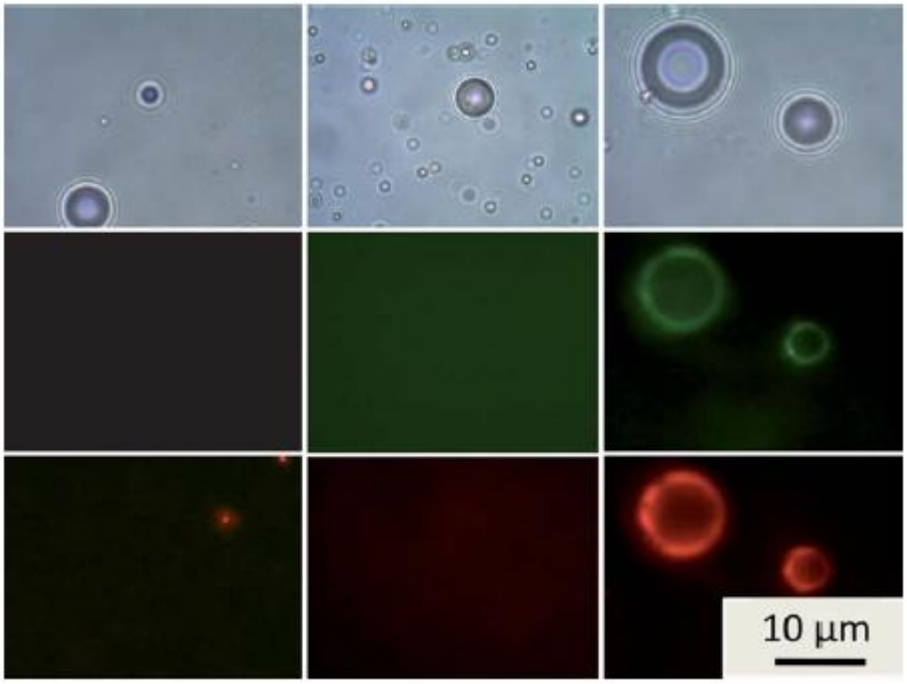

Figure 2.6: Comparison of Rhodamine B loading for microbubbles with DSPC only (left), DPPC/DPPA/DSPE–mPEG (center), and with DSPC/PAA–SH–FITC (right). Top images: bright field transmission mode. Middle images: green fluorescence shows the presence of PAA–SH–FITC. Bottom images: red fluorescence shows the presence of Rhodamine B. The exposure time for lipid-only and mPEG bubbles is 16 times greater than for PAA bubbles, confirming the great difference in Rhodamine B loading.

According to flow cytometry studies (**Figure 2.7**), the bubbles with PAA–SH showed an average of 3-fold greater fluorescence than those without PAA. In addition, when Rhodamine B was formulated into PPC/DPPA/DSPE–mPEG, little fluorescence from the Rhodamine B could be observed on the bubbles. Fluorescence microscopy also shows that the red fluorescence of the dye is co-localized with the green fluorescence of the PAA–SH–FITC, even in areas of uneven polymer coating. The increase in dye loading may be due to formation of lipid networks that can be filled with organic molecules or also to

electrostatic binding between Rhodamine B and the PAA. If the latter case is true, the presence of the negatively charged PAA should be sufficient to bind drugs containing cationic groups, such as doxorubicin [28]. If neither hydrophobicity nor positive charge is present for a potential drug, the PAA may be appended further to include additional functional groups that show affinity for such drugs. Regardless, it is clear that the increase in dye loading in the study shows that a multicomponent shell is able to load larger amounts of cargo than a simple lipid shell.

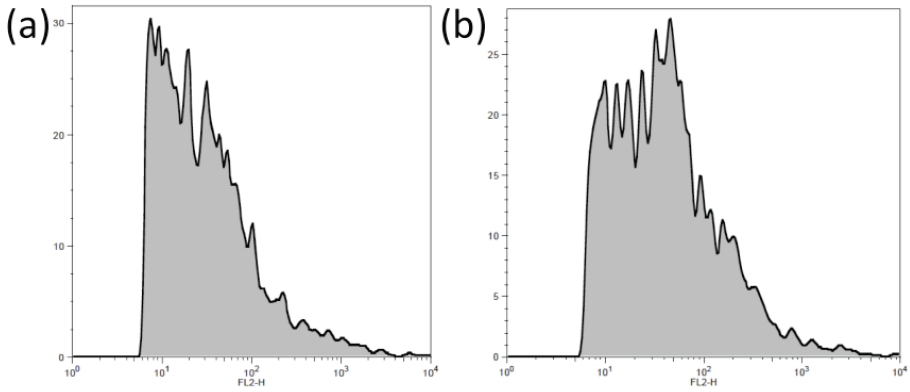

Figure 2.7: Histogram of Rhodamine B fluorescence encapsulated in DSPC microbubbles synthesized without (a) and with (b) added PAA. The average relative fluorescence is approximately 3-fold greater for bubbles with PAA than without.

2.5: Conclusions

In conclusion, we have shown that stable phospholipid–polymer microbubbles with enhanced drug loading can be made in a simple one-pot synthesis. These microbubbles are effective ultrasound contrast agents that

also showed improved echogenicity as well as overall stability compared to lipid-only bubbles. Furthermore, because these DSPC/PAA–SH microbubbles appear to possess crosslinked composites of lipid and polymer, they are able to load much more dye than other lipid-stabilized microbubbles, which should translate well to future drug loading studies. Finally, while the polymer–lipid microbubbles are stable to normal imaging conditions, the bubbles degrade at increased ultrasound pressures that are still within the diagnostic range, enabling the future use of these structures as theranostic agents that can be tracked within a patient and externally triggered to release high amounts of drug at a specified site of inflammation.

2.6: Acknowledgements

The authors thank Dr. Davorka Messmer and Dr. Ana Sanchez for help with FACS.

This chapter was reproduced in full from: M. A. Nakatsuka, J. H. Lee, E. Nakayama, A. M. Hung, M. J. Hsu, R. F. Mattrey, S. C. Esener, J. N. Cha, A. P. Goodwin, Soft Matter, 2011, 7, 1656-1659. **DOI:** 10.1039/C0SM01131B – Reproduced by permission of the Royal Society of Chemistry

2.7: References

[1] Berkowski KL, Potisek SL, Hickenboth CR, Moore JS. Ultrasound-induced site-specific cleavage of azo-functionalized poly(ethylene glycol). Macromolecules. 2005;38:8975-8.

[2] Hickenboth CR, Moore JS, White SR, Sottos NR, Baudry J, Wilson SR. Biasing reaction pathways with mechanical force. Nature. 2007;446:423-7.

[3] Church CC. The Effects of an Elastic Solid-Surface Layer on the Radial Pulsations of Gas-Bubbles. J. Acoust. Soc. Am. 1995;97:1510-21.

[4] Hoff L, Sontum PC, Hovem JM. Oscillations of polymeric microbubbles: Effect of the encapsulating shell. J. Acoust. Soc. Am. 2000;107:2272-80.

[5] Schutt EG, Klein DH, Mattrey RM, Riess JG. Injectable microbubbles as contrast agents for diagnostic ultrasound imaging: the key role of perfluorochemicals. Angew. Chem. Int. Ed. 2003;42:3218-35.

[6] Ferrara K, Pollard R, Borden M. Ultrasound microbubble contrast agents: fundamentals and application to gene and drug delivery. Annu. Rev. Biomat. Eng. 2007;9:415-47.

[7] Lentacker I, Geers B, Demeester J, De Smedt SC, Sanders NN. Design and evaluation of doxorubicin-containing microbubbles for ultrasound-triggered doxorubicin delivery: cytotoxicity and mechanisms involved. Mol. Ther. 2010;18:101-8.

[8] Treat LH, McDannold N, Vykhodtseva N, Zhang Y, Tam K, Hynynen K. Targeted delivery of doxorubicin to the rat brain at therapeutic levels using MRI-guided focused ultrasound. Int. J. Cancer. 2007;121:901-7.

[9] Klibanov AL. Ligand-carrying gas-filled microbubbles: Ultrasound contrast agents for targeted molecular imaging. Bioconjugate Chem. 2005;16:9-17.

[10] Unger EC, McCreery TP, Sweitzer RH, Caldwell VE, Wu Y. Acoustically active lipospheres containing paclitaxel: a new therapeutic ultrasound contrast agent. Invest. Radiol. 1998;33:886-92.

[11] Lentacker I, De Smedt SC, Sanders NN. Drug loaded microbubble design for ultrasound triggered delivery. Soft Matter. 2009;5:2161-70.

[12] Hernot S, Klibanov AL. Microbubbles in ultrasound-triggered drug and gene delivery. Adv. Drug. Deliver. Rev. 2008;60:1153-66.

[13] Ophir J, Parker KJ. Contrast agents in diagnostic ultrasound. Ultrasound Med. Biol. 1989;15:319-33.

[14] Wheatley MA, Lathia JD, Oum KL. Polymeric ultrasound contrast agents targeted to integrins: importance of process methods and surface density of ligands. Biomacromolecules. 2007;8:516-22.

[15] Kheirolomoom A, Dayton PA, Lum AFH, Little E, Paoli EE, Zheng HR, et al. Acoustically-active microbubbles conjugated to liposomes: Characterization of a proposed drug delivery vehicle. J. Control. Release. 2007;118:275-84.

[16] Becker AL, Zelikin AN, Johnston AP, Caruso F. Tuning the formation and degradation of layer-by-layer assembled polymer hydrogel microcapsules. Langmuir. 2009;25:14079-85.

[17] Hettiarachchi K, Lee AP. Polymer-lipid microbubbles for biosensing and the formation of porous structures. J. Colloid Interf. Sci. 2010;344:521-7.

[18] Hettiarachchi K, Zhang S, Feingold S, Lee AP, Dayton PA. Controllable microfluidic synthesis of multiphase drug-carrying lipospheres for site-targeted therapy. Biotechnol. Progr. 2009;25:938-45.

[19] Talu E, Hettiarachchi K, Zhao S, Powell RL, Lee AP, Longo ML, et al. Tailoring the size distribution of ultrasound contrast agents: possible method for improving sensitivity in molecular imaging. Mol. Imaging. 2007;6:384-92.

[20] Seki K, Tirrell DA. Interactions of Synthetic-Polymers with Cell-Membranes and Model Membrane Systems .5. Ph-Dependent Complexation of Poly(Acrylic Acid) Derivatives with Phospholipid Vesicle Membranes. Macromolecules. 1984;17:1692-8.

[21] Thomas JL, Tirrell DA. Polyelectrolyte-Sensitized Phospholipid-Vesicles. Accounts Chem. Res. 1992;25:336-42.

[22] Fujiwara M, Grubbs RH, Baldeschwieler JD. Characterization of pH-dependent poly(acrylic acid) complexation with phospholipid vesicles. J. Colloid Interf. Sci. 1997;185:210-6.

[23] Zelikin AN, Li Q, Caruso F. Disulfide-stabilized poly(methacrylic acid) capsules: Formation, cross-linking, and degradation behavior. Chem. Mater. 2008;20:2655-61.

[24] Zelikin AN, Quinn JF, Caruso F. Disulfide cross-linked polymer capsules: En route to biodeconstructible systems. Biomacromolecules. 2006;7:27-30.

[25] Borden MA, Martinez GV, Ricker J, Tsvetkova N, Longo M, Gillies RJ, et al. Lateral phase separation in lipid-coated microbubbles. Langmuir. 2006;22:4291-7.

[26] Ferrara KW, Borden MA, Zhang H. Lipid-shelled vehicles: engineering for ultrasound molecular imaging and drug delivery. Accounts Chem. Res. 2009;42:881-92.

[27] Chatterjee D, Sarkar K, Jain P, Schreppler NE. On the suitability of broadband attenuation measurement for characterizing contrast microbubbles. Ultrasound Med. Biol. 2005;31:781-6.

[28] Tinkov S, Winter G, Coester C, Bekeredjian R. New doxorubicin-loaded phospholipid microbubbles for targeted tumor therapy: Part I--Formulation development and in-vitro characterization. J. Control. Release. 2010;143:143-50.

Chapter 3: DNA-Coated Microbubbles with Biochemically Tunable Ultrasound Contrast Activity

3.1: Abstract

In this chapter, we describe the formulation of a microbubble contrast agent that incorporates a phospholipid-poly(acrylic acid)-poly(adenine) conjugate into its encapsulating shell. Upon the introduction of a long, bridging poly(thymine) DNA strand, crosslinks between adjacent PAA chains substantially increased the stiffness of the microbubble shell leading to vast changes in ultrasound-induced bubble dynamics and signal generation when imaged with contrast enhanced ultrasound imaging. Through the use of accousto-optic laser light scattering, the oscillatory behavior of single bubbles is determined, showing that crosslinked microbubbles require an additional 291kPa to initiate oscillation as compared to non-crosslinked microbubbles.

The rigidification of these crosslinked microbubbles is also shown to be partially reversible through the addition of a competing poly(adenine) DNA strand to competitively hybridize the poly(thymine) crosslinking strand and remove it from the bubble shell. Microbubbles measured after being “reactivated” increased their oscillatory behavior two-fold, and showed a vast increase in scattered signal when utilizing contrast enhanced ultrasound imaging, demonstrating their potential as a simple and highly versatile platform for the detection of biochemical stimuli.

3.2: Introduction

Imaging is a vital weapon in the clinician's arsenal with uses at almost every stage of patient care, including routine screening, diagnostic testing, disease staging, surgical assistance, and post-treatment monitoring. Of the many imaging modalities available, ultrasound is one of the most widely employed. The incident sound waves are safe, penetrate deeply into most tissues, and provide millimeter resolution imaging, while multiple tests may be performed relatively cheaply and in real-time with equipment already present in most hospitals and clinics. The main drawback of ultrasound is poor sensitivity to abnormalities in tissue; as most tissues have similar densities and compressibilities only a small fraction of the incident sound is reflected back to the transducer [1]. To address this, colloids and particles with large differences in acoustic impedance, such as microbubbles [2-6], emulsions [7, 8], and air-containing liposomes [9, 10], have been employed successfully as ultrasound contrast agents owing to their inherent ability to scatter sound more effectively. Gas-filled microbubbles in particular are especially effective for cardiovascular imaging, with success in applications such as determining the presence of thrombosis [11] or malignant prostate carcinomas [12, 13]. Recent advances have included the addition of targeting ligands to the contrast agent to enhance their accumulation in a specific area [14]. However, a contrast agent that activates only in the presence of specific biomarker would relay a positive (bright) signal instead of a void (dark), reducing

background and allowing a clinician to distinguish a growing area of inflammation from an imaging artifact or acoustic shadowing. For example, microbubbles that become active only in the presence of thrombin, a biomarker for the clotting cascade, would allow imaging of small but growing clots that are difficult to image by standard methods for early detection of malignant thrombosis [15].

To reduce the potential for non-specific background signal, we have designed a strategy to create “smart” contrast agents that only enhance ultrasound signal in a specific chemical environment through modulation of nonlinear echoes. In response to the compression and rarefaction phases of an ultrasonic pressure wave, a microbubble will expand and contract, or oscillate, in a nonlinear fashion; this motion creates additional sound waves at different frequencies that can be distinguished from the initial pulse [16, 17]. Theoretical modeling and empirical studies have both shown that the microbubble’s response to ultrasound is partly related to the mechanical properties of the encapsulating shell, as stiffer shells do not deform as easily as their flexible counterparts [18, 19]. To utilize this effect we created microbubbles with a network of crosslinkable oligonucleotides on their shell. Here, one DNA sequence is appended to the microbubble shell covalently, which allows free movement of the lipid membrane (**Figure 3.1a**, “ON”). Then a strand complementary to the shell DNA is added and the resultant hybridization of these oligonucleotides creates a crosslinked network

surrounding the bubble (“OFF”). If, however, an analyte is added with preferential affinity for the crosslinking strand, the microbubble loses its crosslinks and becomes flexible again (“ON”). While similar strategies have been applied to complex hydrogels [20] and fluorescence-based sensing mechanisms [21, 22], such approaches have never been applied to ultrasound.

3.3: Materials and Methods

3.3.1: Synthesis of DSPE-PAA:

Poly(acrylic acid) (PAA, 100 mg, 0.02 mmol per chain, MW ~ 5000, 50% wt% in water, Aldrich) was mixed with dimethylsulfoxide (4 mL, EMD) in a scintillation vial with stirbar, titrating in 1 M hydrochloric acid to solubilize, if necessary. N-hydroxysuccinimide (NHS, 46 mg, 0.40 mmol, Pierce) and 1-ethyl-3-(3-dimethylaminopropyl)carbodiimide hydrochloride (EDC, 38 mg, 0.20 mmol, Pierce) were dissolved and the solution was stirred 30 min at RT. In a separate vial, 1,2-distearoyl-*sn*-glycero-3-phosphoethanolamine (15 mg, 0.02 mmol, Aldrich) was mixed with chloroform (4 mL, EMD) and triethylamine (1 mL, Alfa Aesar). The mixture was incubated at 60°C until clear. The two solutions were combined and stirred at 60°C for 1 h, then stirred overnight at RT. The volatiles (chloroform and triethylamine) were removed via a stream of air, and the remaining solution was diluted with water (16 mL) and transferred

to a regenerated cellulose dialysis tube (MWCO 1000, SpectraPor) and dialyzed two days against distilled water with at least four changes of water. The dialyte was lyophilized to obtain a white powder. Yield: 106 mg (0.0184 mmol, 92%). ^{1}H NMR (500 MHz, DMSO- d_6, δ *):* 2.93-3.09 (m, 41H), 2.71 (d, *J* = 3 Hz, 15H), 2.09-2.30 (br s, 48H), 1.10-1.82 (br m, 140H), 0.92-0.99 (m, 8H), 0.82-0.85 (m, 6H).

3.3.2: Synthesis of DSPE-PAA-A15.

DSPE-PAA : (0.25 mg, 44 μmol) was mixed with amine-terminated $(adenine)_{15}$ (A15 -NH_2, 1.025 mg, 213 μmol, Integrated DNA Technologies) and EDC (0.417 mg, 2.17 mmol) in 50 mM phosphate buffer (pH 7.0, 800 μL) on a rotisserie mixer at RT overnight. The product was dialyzed (MWCO 12–14k, Fisher Brand) for two days against distilled water with four changes of water. The dialyte was frozen and lyophilized to remove water and obtain a white powder. Yield: 1.1 mg (86%). DNA attachment was quantified by UV-Vis spectroscopy (Beckman Coulter DU 730). 1.1 mg of DSPE-PAA-A15 was dissolved in 1.4 mL of water. The absorbance at 260 nm was measured to be 0.188, which with the A15 –NH_2 absorption coefficient being 183,400 A/mol/cm, corresponded to a coupling yield of 2.1 A15 –NH_2 per DSPE-PAA.

3.3.3: Microbubble formulation, crosslinking, and decrosslinking:

Microbubbles were formulated in a similar manner as described previously [23]. In order to add crosslinks to the encapsulating shell, (thymine) 30 (T 30 , IDT) was added to pre-formed microbubbles in a 1.5:1 molar ratio to the total number of $(adenine)_{15}$. The bubbles were then allowed to sit at RT for 30 min. To remove crosslinks by competitive association, $(adenine)_{30}$ (A30, IDT) was added to crosslinked microbubbles in a 3:1 molar ratio with the number of $(thymine)_{30}$ added during the crosslinking step. The bubbles were then allowed to sit at room temperature for 45 min prior to fractionation and sizing.

3.3.4: Measurement of modulated light scattering

This equipment has been described previously [24]. To measure microbubble dynamics, ultrasound was pulsed in bursts of 15 sine waves of 2.25 MHz at a repetition rate of about 1 Hz. Light scattering data was collected from the oscilloscope using Labview (National Instruments) on a PC. The AC variance was determined for the noise floor, and the threshold was set to a value slightly greater than this. Microbubble samples were counted as described above, diluted to a concentration of 10 5 mL^{-1}, and flowed through the setup continuously. The gated AC variance time domain spectra, their Fourier transformations, and the data time stamps were collected and processed in Matlab (MathWorks) offline.

3.3.5: Determination of microbubble fractions and correlation to size:

The counting procedure has been described previously [18]. The microbubble count was plotted versus collection time and the linear fit was determined for all non-zero samples. $R^2 > 0.98$ for all non-zero samples except for crosslinked bubbles at 345 kPa, for which $R^2 > 0.95$. To determine microbubble fraction, the largest count rate was set to unity and the other count rates were scaled against this value. Correlation of size to bubble fraction was determined by calculating radius from raw ImageJ data from the counting experiment and ranking these against count fraction (count number divided by total sample count). For example, if the radius of the 480th largest bubble out of 850 was 0.99 μ m, then a fraction of 0.565 of the bubbles in the sample was considered to be larger than 0.99 μ m. This radius value was substituted for the fraction obtained from the pressure-oscillation count experiment, and plotted as pressure vs. 1/R, removing the 571 kPa point as an outlier for uncrosslinked microbubbles and the 196 kPa point for crosslinked bubbles (1/R > 0). Linear fits were obtained through Microsoft Excel. Uncrosslinked bubbles: slope = 295 mN m − 1; intercept = −32 kPa; R 2 = 0.975. Crosslinked bubbles: 293 mN m − 1; intercept = 260 kPa; R 2 = 0.954.

3.3.6: Contrast enhanced ultrasound imaging:

Samples were imaged with Siemens Acuson Sequoia 512 set in dual cadence mode (B-mode and contrast-enhanced ultrasound obtained

simultaneously). The samples were diluted to a concentration of 20,000 bubbles mL – 1 and placed in a transfer pipette in a water tank. Images in Figure 3 were obtained at 1.5 MHz and MI = 0.12 (peak pressure = 147 kPa), Figure 5 at 1.5 MHz and MI = 0.16 (257 kPa). Brightness analysis was performed with ImageJ (NIH) by integrating the brightness level inside the phantom minus an average of four background regions of the same size and shape at similar imaging depth. Data from this analysis: crosslinked raw brightness, 4966993; crosslinked average background, 4754288; decrosslinked raw brightness, 27466036, decrosslinked average background, 4316435.4. Calculations: crosslinked net brightness, 212705; decrosslinked net brightness, 23149600.6; ON/OFF ratio, 108.8.

3.4: Results and Discussion

3.4.1: Microbubble formulation and sizing

Here, microbubbles were fabricated with a stabilizing shell containing DNA attached to a polymer-lipid conjugate. Poly(acrylic acid) (PAA) was coupled to the amine of 1.2-distearoyl-*sn*-glycero-3-phosphoethanolamine (DSPE) via carbodiimide-mediated amidation, followed by a similar reaction to attach an average of 2.1 amine-terminated A15 (polyadenine) per PAA-DSPE as determined by UV-Vis absorbance measurements (**Figure 3.1b**). DSPE-PAA-A 15 was then mixed with 1,2-palmitoyl-*sn*-glycero-3-phosphocholine

(DPPC) and 1,2-palmitoyl-*sn*-glycero-3-phosphatic acid (DPPA) in phosphate buffered saline (PBS) to create a suspension with a 153:17:1 DPPC:DPPA:DSPE-PAA-A15 molar ratio (**Figure 3.1**). Finally, the entire mixture was probe sonicated under a headspace of perfluorobutane gas to form the microbubbles (**Figure 3.1d**). After floatation for 15 min to remove the foam, microbubbles of mostly 1–5 μm were isolated in a yield of approximately 10^8 bubbles per milliliter PBS (**Figure 3.2**). The bubble count and size dispersity were very similar to those generated from a suspension of DPPC:DPPA:DSPE-PAA without DNA attached.

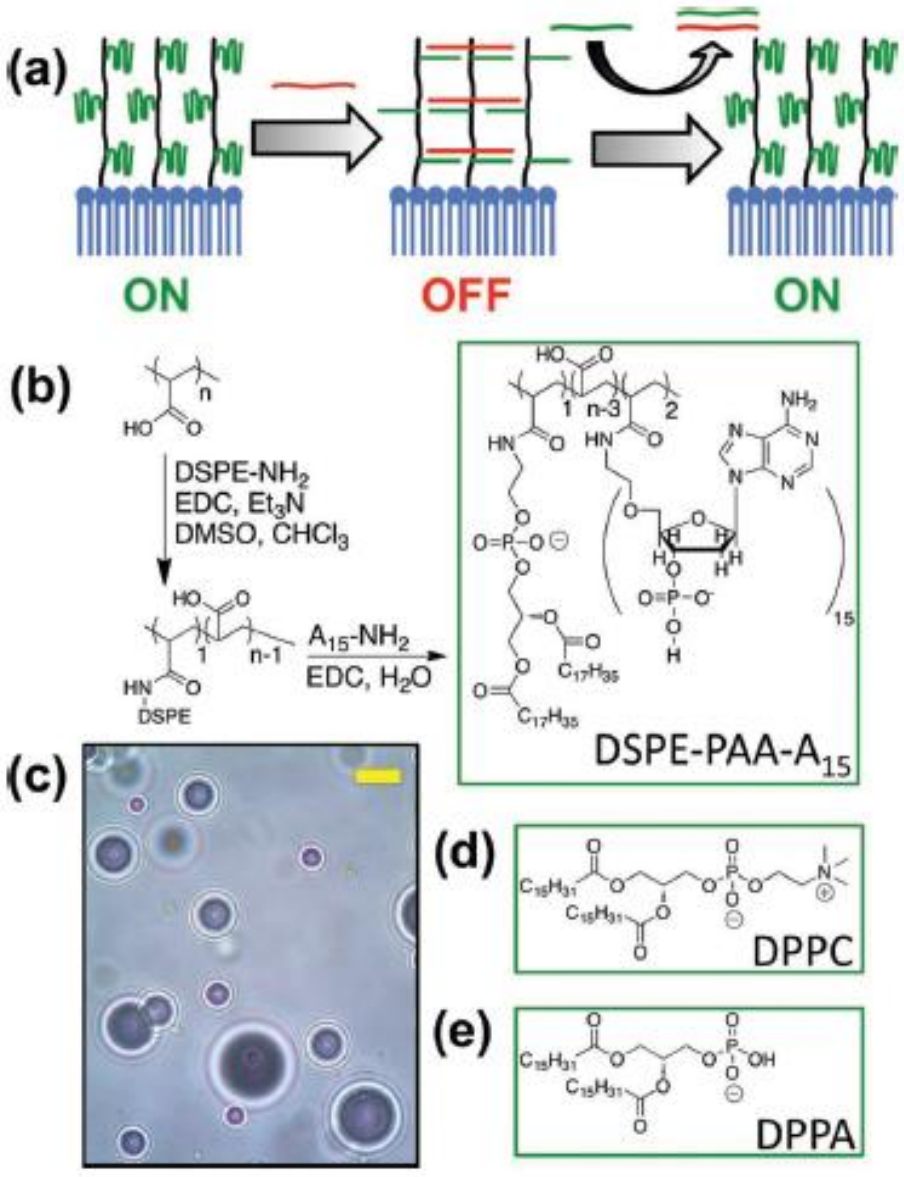

Figure 3.1: Microbubble design and synthesis. (a) Schematic of crosslinking and reactivation in a microbubble shell. (b) Synthesis of DSPE-PAA-A15 . (c) Bright field optical micrograph of synthesized microbubbles. Scale bar (yellow) = 5 μ m. (d, e) 1,2-Dipalmitoyl- *sn* -glycero-3-phosphocholine and 1,2-dipalmitoyl-*sn* -glycero-3-phosphatic acid form the dominant portion of the shell.

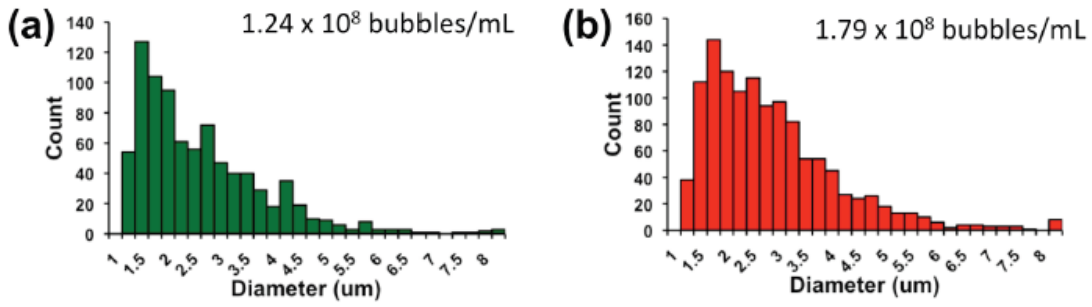

Figure 3.2: Microbubble count and size distribution for (a) Uncrosslinked and (b) crosslinked microbubbles after addition of T30.

3.4.2: Single bubble light scattering to measure oscillation

Since the generation of nonlinear echoes depends on the size oscillations of the microbubble under ultrasound, we employed a home-built modulated light scattering apparatus described previously to distinguish oscillating microbubbles from static ones (**Figure 3.3a**) [24, 25]. Briefly, a dilute flowing stream of microbubbles stabilized by DPPC:DPPA:DSPE-PAA-A 15 was interrogated with a series of pulses containing 15 sine waves at 2.25 MHz while irradiated with a continuous wave laser. The ultrasound induced changes in microbubble size were measured through the resultant changes in light scattering while gating for an AC variance above the noise floor (**Figure 3.3b,c**). At low peak pressure (194 kPa), the oscillation of the microbubble shows strong peaks corresponding not only to the fundamental frequency at 2.25 MHz, but also at harmonics 4.5, 6.75, and 9 MHz, as well as subharmonics at 1.12 MHz (**Figure 3.3d**). These peaks confirm the expected nonlinearity of oscillation of the microbubbles, which is necessary to obtain effective contrast enhanced imaging. At larger interrogation intensities, the

peaks begin to lose their sharpness and a strong broadband contribution is observed. This broadband signal is most likely due to the cavitation of microbubbles, which occurs when the microbubble expands too rapidly and subsequently becomes unstable and collapses, producing a large broadband signal.

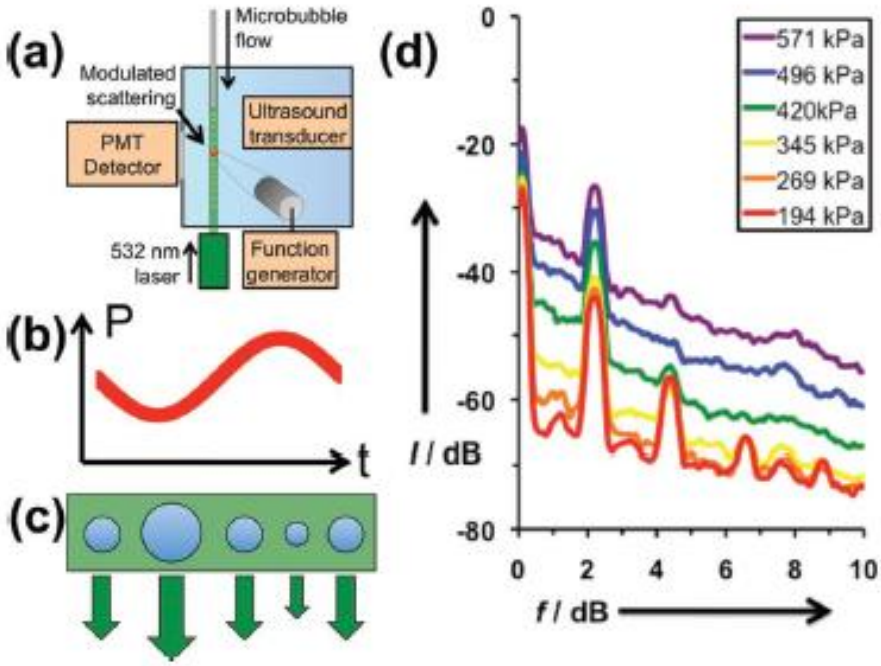

Figure 3.3: Analysis of uncrosslinked, DPPC:DPPA:DSPE-PAA-A15 microbubbles. (a) Schematic of modulating light scattering apparatus. Microbubbles are fl owed through a tube into a water tank, where they are simultaneously interrogated by an ultrasound pulse and a continuous wave laser. If the microbubble oscillates in response to the sine wave ultrasound pulse (b), the microbubble will expand and contract accordingly (c), changing the intensity of light scattering. (d) Fourier Transforms of received light scattering signal gated by AC variance, averaged over 100 oscillating bubbles each.

The as-determined flexible DPPC:DPPA:DSPE-PAA-A15 microbubbles were then crosslinked via incubation with a T30 (polythymine) strand to bridge

the A15 strands on adjacent polymers. Successful hybridization was determined by incubating the adenine microbubbles with FAM-labeled T30 and performing fluorescence microscopy (**Figure 3.5b,c**). Despite the potential rigidification of the shell, as well as the possible rearrangement of lipids to accommodate the crosslinking strands, the act of crosslinking had little effect upon either the concentration or size distribution of the microbubble suspension, nor was bubble aggregation observed by bright field microscopy. Standardized concentrations of crosslinked and uncrosslinked bubbles were run through the modulated light scattering instrument, again gating against AC variance to select for oscillating bubbles. Microbubbles with oscillatory behavior were counted over time and normalized to the maximum count rate of the instrument. The fraction of oscillating bubbles was taken as the slope of the linear fit (R 2 > 0.95 for all non-zero samples; **Figure 3.4**).

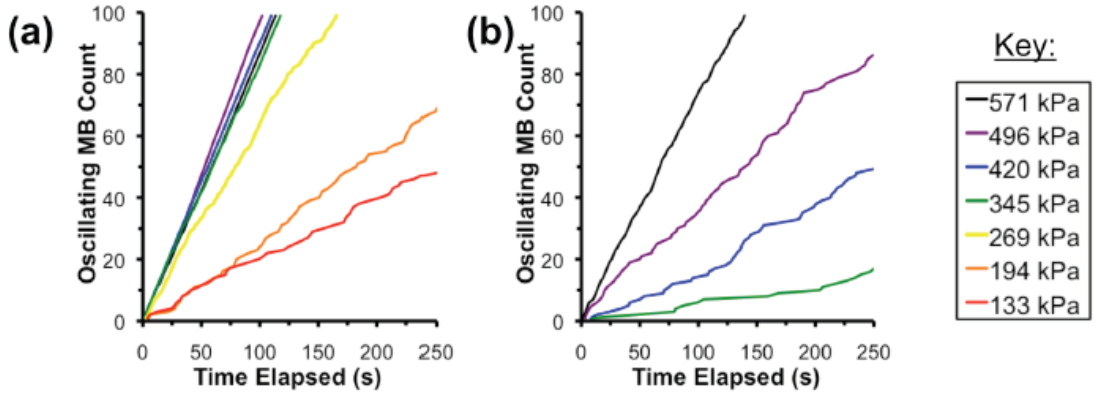

Figure 3.4: Number of bubbles that have oscillated over a given time period for (a) uncrosslinked and (b) crosslinked microbubbles at pressures between 133 and 571kpa.

For uncrosslinked bubbles at 345, 420, 496, and 571 kPa, over 80% of microbubbles were found to show oscillatory behavior. At 269 and 194 kPa, the fractions dropped to 20% and 6%, respectively (**Figure 3.5a**). After addition of the T30 crosslinking strand however, the microbubble count rate decreased significantly when compared at the same insonation pressures as the uncrosslinked DPPC/ DPPA/DSPE-PAA-A 15 microbubbles. In particular, there was a sharp decrease at 345 and 420 kPa, at moderate pressures. At 194 and 269 kPa, no oscillating bubbles were detected at all, implying that oscillation was suppressed almost completely. By controlling the incident ultrasound power during imaging, the difference in bubble dynamics may be exploited to obtain substantial differences in ultrasound image contrast. **Figure 3.5e** shows uncrosslinked (left) and crosslinked (right) microbubbles in phantoms imaged at 147 kPa in contrast-enhanced mode, which suppresses elastic reflection to isolate signal from harmonic oscillation. The signal is substantially brighter for uncrosslinked than crosslinked microbubbles, and both are distinct from the phantom, the walls of which can be seen clearly in B-mode ultrasound (**Figure 3.5d**).

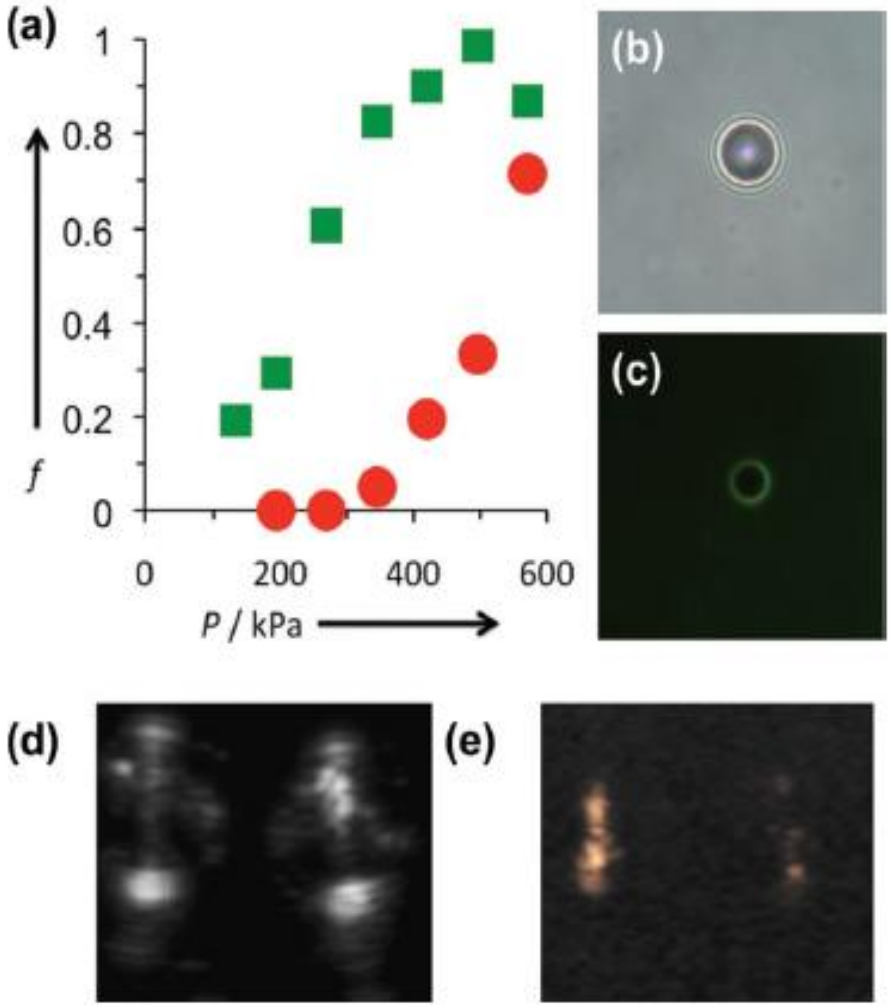

Figure 3.5: Examination of effect of T30 crosslinking on ultrasound-induced microbubble dynamics. (a) Comparison of percentage of oscillating microbubbles vs. incident pressure for uncrosslinked (green) and crosslinked (red) microbubbles. (b, c) Bright field and green fluorescence micrographs of DPPC:DPPA:DSPE-PAA-A15 microbubbles with FAM-T30 added. The green fluorescence of the crosslinking strand only appears on the microbubble shell. (d) B-mode and (e) contrast-enhanced ultrasound images obtained simultaneously for uncrosslinked (left) and crosslinked (right) microbubbles in a phantom. The bright spots at the top and bottom of the B-mode image are caused by elastic reflection of ultrasound from the front and back walls of the phantom, respectively. The outline of the round phantom is observed as well. The contrast-enhanced image (e) shows that the uncrosslinked bubbles (left) are significantly brighter than crosslinked bubbles (right). A comparison of these images reveals that the contrast-signal overlays with the interior of the phantom, demonstrating the selectivity of microbubble imaging.

3.4.3: Dynamics of oscillating crosslinked microbubbles

Analysis of the microbubble oscillation through modulated light scattering provides some intriguing insight into the mechanism of crosslink-induced microbubble oscillation. Recent findings by de Jong and coworkers found that small microbubbles require a minimum ultrasound intensity to initiate oscillation, and this threshold appears to have an inverse relationship with microbubble radius [26, 27]. In our study, the size distribution of microbubbles can be used to find the size threshold corresponding to a given fraction of the bubbles. Plotting the inverse of this diameter against the incident pressure reveals a linear fit (**Figure 3.6a**). The y-intercepts of the two plots reveal that an additional 291 kPa is required to initiate oscillation for crosslinked bubbles. As the slopes of the fitted lines are the same for both crosslinked and uncrosslinked bubbles, this value appears to be valid for all bubble sizes. Since pressure is force per area and the number of DNA strands per shell unit area is known, this corresponds a “ripping” force of ~ 25 pN per DNA strand, which is consistent with literature reports for single oligonucleotide force measurements [28, 29]. Once this threshold is surpassed, the uncrosslinked bubbles show increasing oscillation amplitude with increasing pressure (**Figure 3.6b–f**). However, the amplitude for oscillating crosslinked bubbles stays about the same, and even decreases. One possible explanation for this observation is that for the gas

bubble to begin to expand and contract, only some of the DNA-DNA bonds need to be broken. As the gas bubble approaches a certain size, the remaining DNA-DNA bonds restrain the bubble from expanding further. These studies indicate that the act of crosslinking plays a dual role in suppressing ultrasound contrast activity, and both modes are advantageous for clinical imaging.

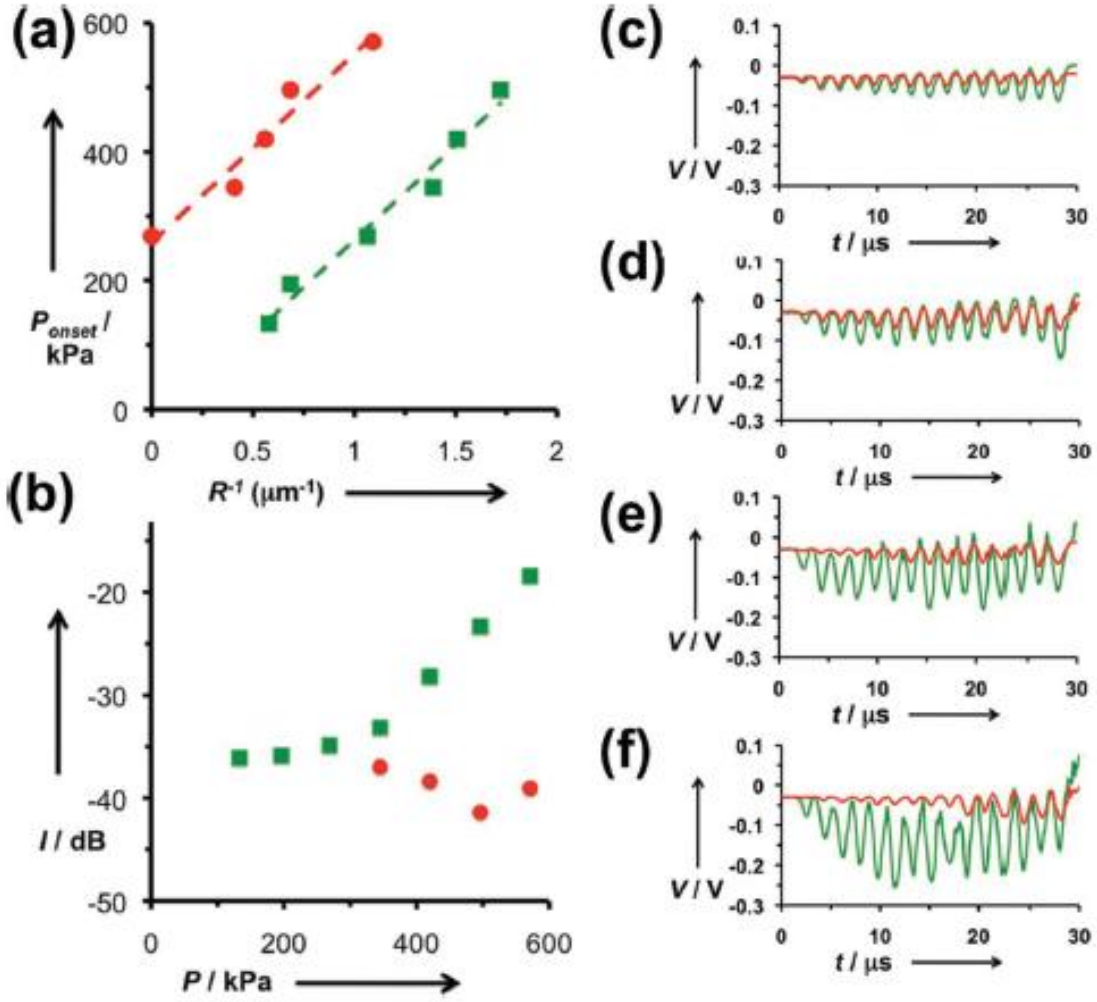

Figure 3.6: Analysis of oscillating microbubble dynamics. (a) Plotting microbubble pressure versus inverse minimum microbubble radius yields a linear fit for uncrosslinked (green) and crosslinked (red) microbubbles. The intercept corresponds to an activation pressure of 291 kPa. (b) Integrated light scattering signal for oscillating uncrosslinked (green) and crosslinked (red) microbubbles. While the size fluctuations of uncrosslinked bubbles appear to increase steadily with increasing incident pressure, the crosslinked bubbles lose signal as pressure increases. (c–f) Time domain plots of the modulated light scattering of *oscillating* uncrosslinked (green) and crosslinked (red) microbubbles at (c) 345 kPa, (d) 420 kPa, (e) 496 kPa, and (f) 571 kPa.

3.4.4: Reactivation of crosslinked microbubbles

Ultimately, the application of this work is to design microbubbles capable of sensing specific biomolecules in vivo and go from a dark “OFF” state to a bright “ON” state. To study this, T30 - crosslinked microbubbles were re-activated by adding excess A 30 to competitively bind to the T30 and remove it from the microbubble shell (**Figure 3.7a**). The competitive displacement of T30 was confirmed by fluorescence microscopy, where the addition of three equivalents of A30 per T30 caused transfer of most of the FAM-labeled T30 from the microbubble surface into the background (**Figure 3.7b–e**). The competitive displacement of the crosslinking T30 strands from the microbubbles appeared to increase the oscillating microbubble fraction by more than two-fold (**Figure 3.7f**), although not to its original level. However, this result indicates that the excess complementary strand can compete for the crosslinking strand to pull many of them from the bubble. This activation also appears to be mostly reversible, with only a slight reduction in microbubble population as a result of the decrosslinking (**Figure 3.8**).

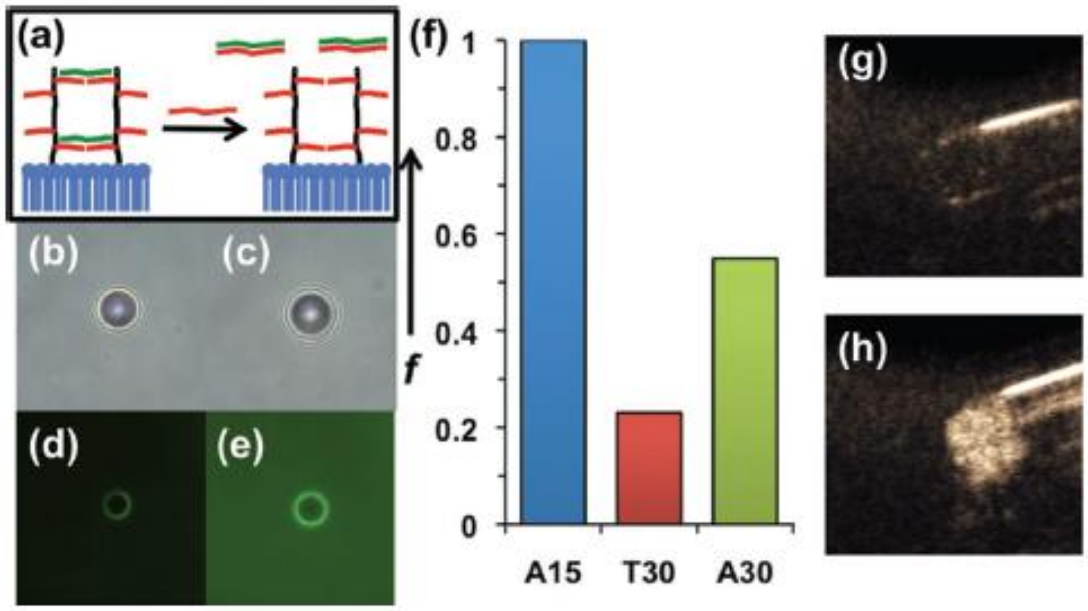

Figure 3.7: Analysis of A30 decrosslinking of DPPC:DPPA:DSPE-PAA-A15 microbubbles precrosslinked with T30 . (a) Schematic of re-activation through addition of longer oligonucleotide (A30) complementary to crosslinking strand (T30). (b, d) Bright field and green fluorescence microscopy images of microbubbles crosslinked with FAM-T30 . (c, e) Microscopy images of same sample after addition of A 30 . (f) Comparison of oscillating microbubble fraction for uncrosslinked (A15), crosslinked (T30), and decrosslinked (A30) microbubbles. (g) Contrast enhanced ultrasound image of crosslinked microbubbles in phantom. (h) Contrast enhanced ultrasound image of same suspension after addition of A30.

Next, crosslinked microbubbles subjected to A30 addition were imaged via contrast-enhanced ultrasound at 257 kPa in a phantom. The crosslinked bubbles showed little signal inside the walls of the phantom (**Figure 3.8g**). After addition of A30, the signal was found to increase quite dramatically, visibly filling the region of interest (**Figure 3.8h**). Brightness analysis (ImageJ) revealed that decrosslinked bubbles were approximately 100 times brighter than crosslinked bubbles. Thus the reactivation of oscillatory behavior has a

profound effect on ultrasound contrast activity using pre-existing clinical ultrasound imaging protocols.

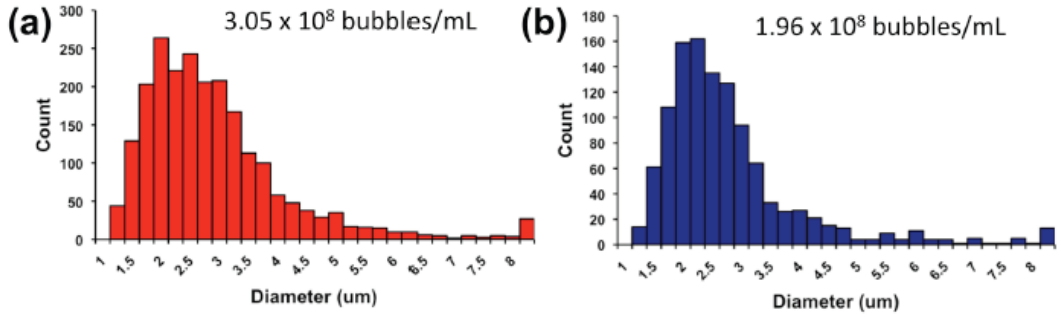

Figure 3.8: Microbubble count and size distribution for (a) crosslinked and (b) de-crosslinked microbubbles after addition of A30.

3.5: Conclusions

In this study, it was found that the ultrasound contrast activity of gas-filled microbubbles could be tuned by using the properties of the encapsulating shell to control the generation of nonlinear echoes. Microbubbles were fabricated with a shell consisting of a mixture of phospholipids and synthetic oligonucleotide-polymer-phospholipid conjugates. The addition of a crosslinking oligonucleotide caused the microbubbles to lose their ability to oscillate in an ultrasound field and create non-linear echoes. Analysis of the microbubbles' modulated light scattering revealed that the crosslinking not only added a resistance to oscillation of 291 kPa for all bubble sizes, but it also decreased the amplitude of microbubble oscillation. Addition of a competitively-binding oligonucleotide resulted in the recovery of ultrasound signal based on removal of the crosslinking oligonucleotide. In future studies, the DNA will be reformulated to include biomarker binding aptamer strands, to

allow the possibility of site-specific detection of deep-lying disease, a highly sought-after goal for clinical imaging.

3.6: Acknowledgements

The authors thank Prof. Robert F. Mattrey of the Department of Radiology at UCSD for helpful discussions and use of his Siemens Acuson Sequoia™ 512 Imaging System, and Prof. Clark Wu of the Department of Radiology at UCSD for help with ultrasound imaging.

This chapter was reproduced in full from M.A. Nakatsuka, M. J. Hsu, S. C. Esener, J. N. Cha, A. P. Goodwin, Advanced Materials, 2011, 23, 4908-4912 DOI: 10.1002/adma.201102677 – Reproduced by permission of John Wiley and Sons, Co.

3.7: References

[1] Schutt EG, Klein DH, Mattrey RM, Riess JG. Injectable microbubbles as contrast agents for diagnostic ultrasound imaging: the key role of perfluorochemicals. Angew. Chem. Int. Edit. 2003;42:3218-35.

[2] Gramiak R, Shah PM. Echocardiography of the aortic root. Invest. Radiol. 1968;3:356-66.

[3] Klibanov AL, Hughes MS, Wojdyla JK, Marsh JN, Hall CS, Miller JG, et al. Targeting of ultrasound contrast material: selective imaging of microbubbles in vitro. Acad. Radiol. 1998;5 Suppl 1:S243-6.

[4] Porter TR, Iversen PL, Li S, Xie F. Interaction of diagnostic ultrasound with synthetic oligonucleotide-labeled perfluorocarbon-exposed sonicated dextrose albumin microbubbles. J. Ultras. Med. 1996;15:577-84.

[5] Unger E, Shen D, Fritz T, Kulik B, Lund P, Wu GL, et al. Gas-filled lipid bilayers as ultrasound contrast agents. Invest. Radiol. 1994;29 Suppl 2:S134-6.

[6] Unger EC, Lund PJ, Shen DK, Fritz TA, Yellowhair D, New TE. Nitrogen-filled liposomes as a vascular US contrast agent: preliminary evaluation. Radiology. 1992;185:453-6.

[7] Lanza GM, Wallace KD, Scott MJ, Cacheris WP, Abendschein DR, Christy DH, et al. A novel site-targeted ultrasonic contrast agent with broad biomedical application. Circulation. 1996;94:3334-40.

[8] Forsberg F, Roy R, Merton DA, Rawool NM, Liu JB, Huang M, et al. Conventional and hypobaric activation of an ultrasound contrast agent. Ultrasound Med. Biol. 1998;24:1143-50.

[9] Huang SL, Hamilton AJ, Pozharski E, Nagaraj A, Klegerman ME, McPherson DD, et al. Physical correlates of the ultrasonic reflectivity of lipid dispersions suitable as diagnostic contrast agents. Ultrasound Med. Biol. 2002;28:339-48.

[10] Alkan-Onyuksel H, Demos SM, Lanza GM, Vonesh MJ, Klegerman ME, Kane BJ, et al. Development of inherently echogenic liposomes as an ultrasonic contrast agent. J. Pharm. Sci. 1996;85:486-90.

[11] Coley BD, Trambert MA, Mattrey RF. Perfluorocarbon-enhanced sonography: value in detecting acute venous thrombosis in rabbits. Am. J. Roentgenol. 1994;163:961-4.

[12] Ragde H, Kenny GM, Murphy GP, Landin K. Transrectal ultrasound microbubble contrast angiography of the prostate. Prostate. 1997;32:279-83.

[13] Frauscher F, Klauser A, Halpern EJ, Horninger W, Bartsch G. Detection of prostate cancer with a microbubble ultrasound contrast agent. Lancet. 2001;357:1849-50.

[14] Borden MA, Sarantos MR, Stieger SM, Simon SI, Ferrara KW, Dayton PA. Ultrasound radiation force modulates ligand availability on targeted contrast agents. Mol. Imaging. 2006;5:139-47.

[15] Kearon C, Ginsberg JS, Hirsh J. The role of venous ultrasonography in the diagnosis of suspected deep venous thrombosis and pulmonary embolism. Ann. Intern. Med. 1998;129:1044-9.

[16] Krishna PD, Newhouse VL. Second harmonic characteristics of the ultrasound contrast agents albunex and FSO69. Ultrasound Med. Biol. 1997;23:453-9.

[17] Ophir J, Parker KJ. Contrast agents in diagnostic ultrasound. Ultrasound Med. Biol. 1989;15:319-33.

[18] Church CC. The Effects of an Elastic Solid-Surface Layer on the Radial Pulsations of Gas-Bubbles. J. Acoust. Soc. Am. 1995;97:1510-21.

[19] Hoff L, Sontum PC, Hovem JM. Oscillations of polymeric microbubbles: Effect of the encapsulating shell. J. Acoust. Soc Am. 2000;107:2272-80.

[20] Um SH, Lee JB, Park N, Kwon SY, Umbach CC, Luo D. Enzyme-catalysed assembly of DNA hydrogel. Nat Mater. 2006;5:797-801.

[21] Yang H, Liu H, Kang H, Tan W. Engineering target-responsive hydrogels based on aptamer-target interactions. J. Am. Chem. Soc. 2008;130:6320-1.

[22] Nutiu R, Li Y. Structure-switching signaling aptamers. J. Am. Chem. Soc. 2003;125:4771-8.

[23] Nakatsuka MA, Lee JH, Nakayama E, Hung AM, Hsu MJ, Mattrey RF, et al. Facile one-pot synthesis of polymer-phospholipid composite microbubbles with enhanced drug loading capacity for ultrasound-triggered therapy. Soft Matter. 2011;7:1656-9.

[24] Hsu MJ, Eghtedari M, Goodwin AP, Hall DJ, Mattrey RF, Esener SC. Characterization of individual ultrasound microbubble dynamics with a light-scattering system. J. Biomed. Opt. 2011;16:067002.

[25] Guan JF, Matula TJ. Using light scattering to measure the response of individual ultrasound contrast microbubbles subjected to pulsed ultrasound in vitro. J. Acoust. Soc. Am. 2004;116:2832-42.

[26] Emmer M, Vos HJ, Goertz DE, van Wamel A, Versluis M, de Jong N. Pressure-dependent attenuation and scattering of phospholipid-coated microbubbles at low acoustic pressures. Ultrasound Med. Biol. 2009;35:102-11.

[27] Tang MX, Eckersley RJ, Noble JA. Pressure-dependent attenuation with microbubbles at low mechanical index. Ultrasound Med. Biol. 2005;31:377-84.

[28] Strunz T, Oroszlan K, Schafer R, Guntherodt HJ. Dynamic force spectroscopy of single DNA molecules. P. Natl. Acad. Sci. USA. 1999;96:11277-82.

[29] MacKerell AD, Lee GU. Structure, force, and energy of a double-stranded DNA oligonucleotide under tensile loads. Eur. Biophys. J. Biophy. 1999;28:415-26.

Chapter 4: Aptamer-Crosslinked Microbubbles: Smart Contrast Agents for Thrombin-Activated Ultrasound Imaging

4.1: Abstract

This chapter describes the adaption of the previously studied DNA-crosslinked microbubbles so they produce ultrasound harmonic signal only in the presence of elevated thrombin levels. Previously, we described a microbubble contrast agent stabilized with phospholipid-poly(acrylic acid)-DNA conjugates with tunable acoustic activity based on the presence or absence of a DNA crosslinking strand. By incorporating the thrombin-binding aptamer sequence GGTTGGTGTGGTTGG as part the crosslinking strand, the presence of thrombin will remove crosslinks and result in an increase in generated signal.

The ability of thrombin to remove hybridized DNA crosslinks is shown here through fluorescence imaging, and the generation of harmonic signal is measured as a function of thrombin concentration via a home built system, with a detection limit of 20 nM thrombin. Thrombin sensitive microbubbles were also imaged via contrast enhanced ultrasound in thrombin-spiked and freshly clotting blood, and showed up to a 10-fold increase in signal after three minutes.

4.2: Introduction

Thrombosis, or malignant blood clot formation, has been associated with numerous cardiovascular diseases, including myocardial infarction, coronary artery disease, and deep venous thrombosis, the latter of which can develop into pulmonary embolism. The most common method of imaging thrombosis is to fill blood vessels with X-ray or ultrasound contrast media and locate clots as filling defects [1, 2]. However, these methods do not provide biochemical information necessary to determine clot activity, which is vital for establishing a method of treatment, particularly to prevent acute active thrombosis from leading to pulmonary embolism. To analyze clot biochemistry, Weissleder et al [3]. and Tsien et al.[4] developed optical probes that sense thrombin through increased fluorescence emission; however, optical imaging is limited in its ability to image deep-lying blood vessels.

Ultrasound is an attractive imaging tool for detecting and monitoring cardiovascular health due to its widespread availability, safety, penetration depth, real-time image acquisition, millimeter resolution, and portability. Most importantly, ultrasound is currently the primary imaging tool for diagnosis of deep venous thrombosis. However, ultrasound is quite limited in its ability to discern abnormalities from surrounding tissue owing to the similar physical properties of soft tissues within the body [5]. A popular strategy to address this limitation is to administer an ultrasound contrast agent with a large acoustic impedance mismatch with the surrounding tissue. Although these agents allow

for the detection of thrombi [2], they cannot distinguish acute from chronic disease. To bias contrast enhancement towards sensing disease, researchers have attached ligands to ultrasound contrast to target fibrin or platelets within thrombi [6-8]. Such methods rely on the accumulation of microbubbles at the site of disease, tethering microbubbles by direct interaction with targeting ligands such as P-Selectin or GPIIb/GPIIIa, and they have proven to be effective at increasing the signal generated in specific areas. However, they are still limited in their ability to sense changes in biomarker concentration, and the total enhancement is theoretically limited by the surface area of the targeted tissue. The alternative method presented here seeks to improve the noninvasive detection of thrombosis by using a stimulus responsive or “smart” contrast agent that becomes active only in the presence of a biochemical environment specifically indicative of thrombus formation [9-12].This strategy also reduces background signal and should even be able to image inflammation near the resolution limit of the instrument. We recently showed that DNA hybridization and dehybridization can be employed to reversibly change the way in which a microbubble responds to ultrasound [13]. Since the ultrasound pressure wave causes a lipid-shelled microbubble to undergo nonlinear size oscillations that result in the generation of nonlinear sound waves [14], crosslinking and decrosslinking of the microbubble shell modulates the generation of these selectively-detectable harmonics [15].

Here, we report the design, fabrication, and validation of microbubbles that only show ultrasound contrast activation at levels of thrombin associated with clot formation. First, the components of the microbubble shell were synthesized and validated for their ability to respond to thrombin. To form the shell that stabilizes the microbubbles, poly(acrylic acid) (PAA) was coupled to the amine of 1,2-distearoyl- *sn* -glycero-3-phosphoethanolamine (DSPE) via carbodiimide-mediated amidation, followed by a similar reaction to attach two amine terminated DNA strands (H 2 N-CCAACCACAAAA and AAAACACCAACCNH2) [13]. Next, a DNA crosslinking strand was added with the sequence TTGGTGTGGTTGGTGTTTTTTTTTGTGGTTGGTGTGGTTGG.
This thrombin aptamer crosslinking strand (TACS) contains a portion complementary to the polymer-DNA to induce crosslinking, as well as two flanking 15-base DNA aptamer sequences (GGTTGGTGTGGTTGG), each of which possesses a half maximal inhibitory concentration (IC 50) on the order of 25 n M for thrombin [16]. Nine of the fifteen aptamer bases are left unbound at the ends of the crosslinking strand so that the binding of thrombin results in the complete displacement of the TACS from the polymer-DNA strands.

4.3: Materials and methods

4.3.1: Synthesis of DSPE-PAA

Synthesis of the DSPE-PAA conjugate was described previously [13], as well as covered extensively in Chapter 3.

4.3.2: Synthesis of DSPE-PAA-DNA

DSPE-PAA (80.8 μ g) was mixed with either 5 ′ amine - CCAACCCACAAA - dabcyl or 5 ′ fluorescein – AAACAACCAACC - amine, (187.5 nmol, Integrated DNA Technologies) with N-hydroxysulfosuccinimide (8.70 mg, 40 μmol, Pierce) and 1-ethyl-3-(3-dimethylpropyl)carbodiimide hydrochloride (EDC, 3.83 mg, 20 μmol, Pierce) in 50 mM 2-(N-morpholino) ethanesulfonic acid (MES, Sigma- Aldrich) buffer (pH 4.95, 1 mL) under agitation at 60 °C overnight. The product was subsequently purified by filtration through a regenerated cellulose filter (MWCO 10,000 kDa, Millipore) at 14,000g for 20 min three times. The retentate was subsequently lyophilized to produce a white powder. DNA attachment was quantified by comparing the UV absorbance at 260 nm (Beckman Coulter DU 730) with the mass of the collected powder. This procedure typically produced a product with an average of 2.7 DNA strands per DSPE-PAA.

4.3.3: Fluorescence analysis

DSPE-PAA-DNA-FAM (20 pmol) and DSPEPAA-DNA-Dabcyl (20 pmol) were mixed in 20 mM Tris actetate buffered saline (200 μL) and measured by fluorometry (Perkin Elmer LS 55; λ ex = 490 nm). To achieve crosslinking and quenching, an equimolar amount of TACS was added, and the system was allowed to remain at RT for 30 min. To dissolve the tripartite DNA hybrid molecule, an equimolar amount of thrombin from human plasma (Sigma-Aldrich) was added.

4.3.4: Microbubble formulation, sizing and crosslinking

Microbubbles were formulated and sized in a similar manner to that described previously [17]. Briefly, ten images per sample were taken at 20 × in bright field at random locations in the sample. The microbubbles were counted and sized using ImageJ (NIH). Concentration was calculated by determining the area of spot size against known volumes of buffer. In order to add crosslinks to the encapsulating shell, a symmetric thrombin binding aptamer (IDT) was added to pre-formed microbubbles in a 3:1 molar ratio to each pair of fluorescence–quencher DNA strands. The bubbles were then allowed to sit at RT for 30 min to allow for the hybridization of the crosslinking strand to the complementary bound strands. Images were taken with a Nikon Eclipse TE200, for fluorescence images gain = 0.2, exposure = 5 set in Spot Basic.

4.3.5: Analysis of microbubble harmonic scattering

Samples were diluted to a concentration of 100 000 bubbles mL − 1 in 2 mL of phosphate buffered saline within the bulb of a transfer pipette held upside down. The pipette bulb was fixed in a submerged position within a large fish tank centered to the focus of a 1” focused 2.25 MHz transducer (Panametrics V305), then insonated with a single pulse from a function generator (Tektronics TDS 2012C) at room temperature open to the atmosphere. Harmonic side scatter signal was collected by an unfocused 5 MHz transducer (Panametrics V308) perpendicular to the sending transducer, and amplified by 30 dB (Olympus 5072PR Pulser/Receiver). Focus was determined by maximizing the signal reflected off of a needle placed upright inside the pipet bulb prior to adding microbubbles.

4.3.6: Contrast enhanced ultrasound imaging in whole blood

Samples were imaged with a Siemens Acuson Sequoia 512 set in dual cadence mode (B-mode and contrast-enhanced ultrasound obtained simultaneously). The samples were diluted to a concentration of 10,000 bubbles/mL^{-1} in 2 mL of EDTA-treated bovine whole blood (Sigma Aldrich), or a concentration of 1.0×10^6 bubbles/mL^{-1} in 2 mL of freshly drawn rabbit blood (1 year old, New Zealand White, 4.5 kg) within a stationary 15 mL centrifuge tube submerged within a large water tank at room temperature open to the atmosphere. Images were obtained at 2.0 MHz and MI = 0.10. Brightness

analysis was performed with ImageJ by integrating the brightness level inside the phantom minus an average of four background regions of the same size and shape at similar imaging depth, as done previously [13].

4.4: Results and discussion

4.4.1: Fluorescence Analysis of Thrombin-Aptamer Activity

The activity of thrombin towards these DSPE-PAA-DNA conjugates was studied by attaching a fluorescent dye, 6-carboxyfluorescein (FAM) to the end of the phospholipid-polymer-DNA, and its corresponding quencher, 4-(4-dimethylaminophenyl) azobenzoic acid (Dabcyl) was appended to the other [18]. When separate, the FAM fluorescence emission is bright and unaffected by the presence of the Dabcyl in solution (**Figure 4.1b**). After addition of TACS, the two strands are pulled together such that the dye and quencher come into close proximity, and the fluorescence emission decreases. Addition of thrombin in a 1:1:1:1 ratio of thrombin:DSPE-PAA-DNA-FAM:DSPEPAA-DNA-Dab:TACS results in the partial recovery of fluorescence emission, indicating that the thrombin is preferentially removing the crosslinking strands from the DNA conjugates. The incomplete recovery of fluorescence is most likely due to the equilibrium established by the PAA-DNA:TACS:thrombin system.

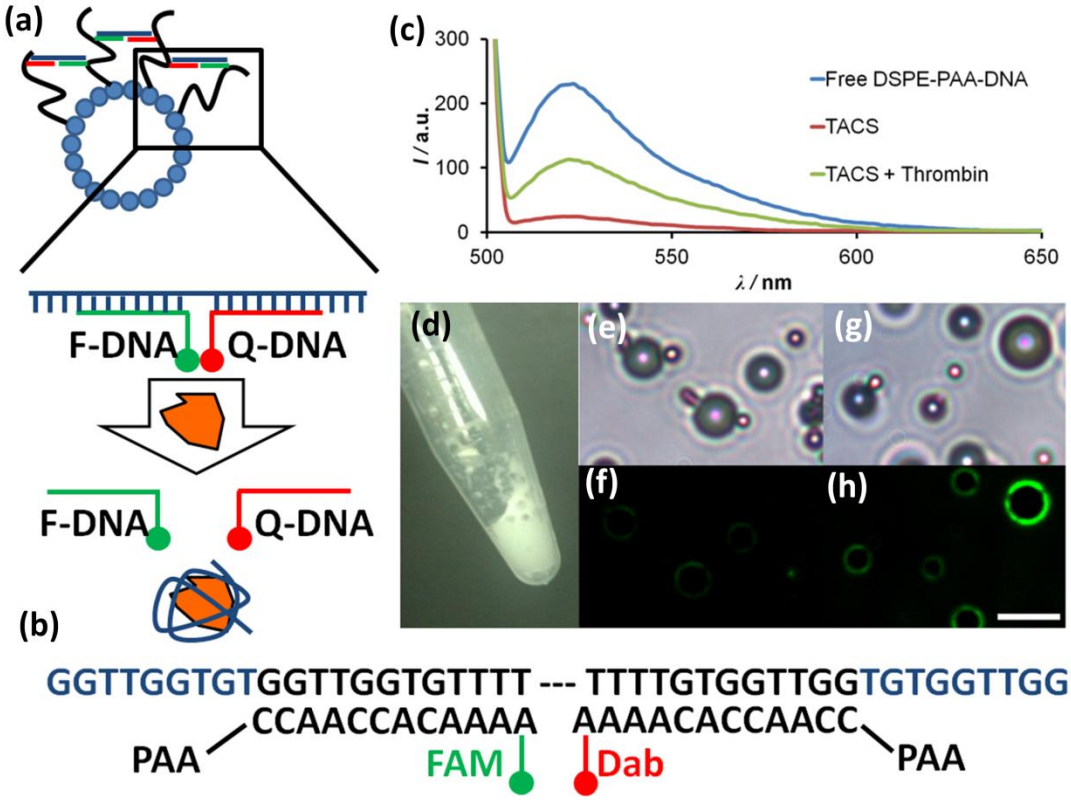

Figure 4.1: Design of aptamer-activated microbubble. (a) Schematic representation of fluorescence activation by thrombin binding. (b) Thrombin aptamer crosslinking strand (TACS). (c) Fluorescence emission spectra of DSPE-PAA-FAM and DSPE-PAA-Quencher (blue), after addition of TACS (red), and addition of thrombin (green) (λ_{ex} = 465nm). (d) Microbubble suspension after sonication. (e) Bright field and (f) fluorescence images of crosslinked bubbles. (g) Bright field and (h) fluorescence images of crosslinked bubbles after addition of thrombin. Fluorescence increases after TACS interacts with thrombin. Scale bar = 5 µm.

4.4.2: Microbubble formulation and sizing

To form microbubbles, the DSPE-PAA-DNA conjugates were melted with 1,2-palmitoyl-*sn*-glycero-3-phosphocholine (DPPC) and 1,2-palmitoyl-*sn*-glycero-3-phosphatic acid (DPPA) in 20 mM Tris Acetate buffered saline. This mixture was probe sonicated under a headspace of perfluorobutane gas to

form microbubbles mostly in the range of 1–5 μ m at a concentration of approximately 10^8 bubbles per milliliter (**Figure 4.2**).

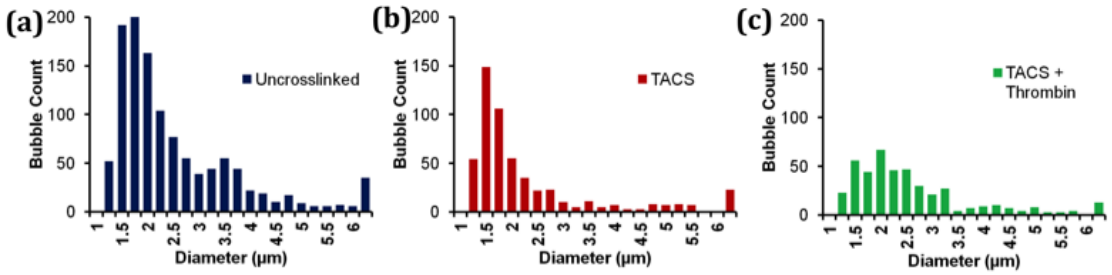

Figure 4.2: Typical microbubble size distributions. (a) Microbubbles prior to addition of TACS. Average diameter = 2.38 μm, concentration = 4.31e8 mL^{-1}. (b) Microbubbles after addition of TACS. Average diameter = 2.23 μm, concentration = 1.90e8 mL^{-1}. (c) Microbubbles with TACS after addition of 100 nM thrombin. Average diameter = 2.53 μm, concentration = 1.53e8 mL^{-1}.

Addition of the TACS did not affect the bubble concentration significantly. Fluorescence microscopy of the microbubble suspension revealed highly-dampened green fluorescent rings that correlated with the bright field images of the microbubble suspension. After introduction of thrombin at 100 nM, a significant increase in green fluorescence was observed on the bubble surface, indicating that the removal of the crosslinker occurred even when the DNA was incorporated into a self-assembled encapsulating shell (**Figure 4.1e-h)**. Thrombin-induced removal of the TACS did not significantly affect the microbubble concentration.

4.4.3: Side scatter analysis of microbubble harmonic signal generation

The effect of thrombin activation on the acoustic contrast properties of the microbubbles was studied through the use of homebuilt instrumentation designed to measure the generation of harmonic signals (**Figure 4.3**). A dilute sample of microbubbles in phosphate buffered saline contained within a submerged transfer pipette bulb in a large water tank was insonated with a 2.25 MHz single sine pulse sent through a focused single element transducer at 290 kPa. Signals generated by the oscillation of the insonated microbubbles were then collected by a 5 MHz unfocused transducer angled perpendicular to the ultrasound wave, followed by subtraction of the signals generated by a blank sample containing only PBS. The average nonlinear power output was determined by integrating the signal from 4.0 to 6.0 MHz, which was outside the pulse width of the original sine pulse. By comparing the power output generated around the 5 MHz peak listening frequency before and after thrombin addition, we could determine that the interaction between the TACS-microbubbles and thrombin had a significant effect on the harmonic signals generated by the microbubble, increasing the side scatter signal 10 dB over non-activated bubbles. To further confirm that this effect was specific to the thrombin-TACS interaction, we also measured the signal generated by microbubbles crosslinked with a DNA strand in which the thrombin binding aptamer sequence was replaced with a mixed sequence (GGTTGGGTGTGTGTG) with no affinity for thrombin (scrambled aptamer

crosslinking sequence, or SACS). The resulting signal from the SACS microbubbles showed little change in side scatter signal power before and after thrombin addition, demonstrating that the signal enhancement observed shows excellent specificity for thrombin. Interestingly, the power generated by the bubbles crosslinked with the SACS DNA strand prior to thrombin addition was slightly higher than the corresponding signal generated by the TACS bubbles. This may be attributed to the greater repetition of sequence motifs within the TACS strand, enabling crosslinks to be more easily formed within the encapsulating shell. In the case of the SACS strand, hybridization between the polymer DNA strands and the crosslinker must be well-aligned, while for the TACS strands, partial hybridization may occur at the hanging aptamer tails.

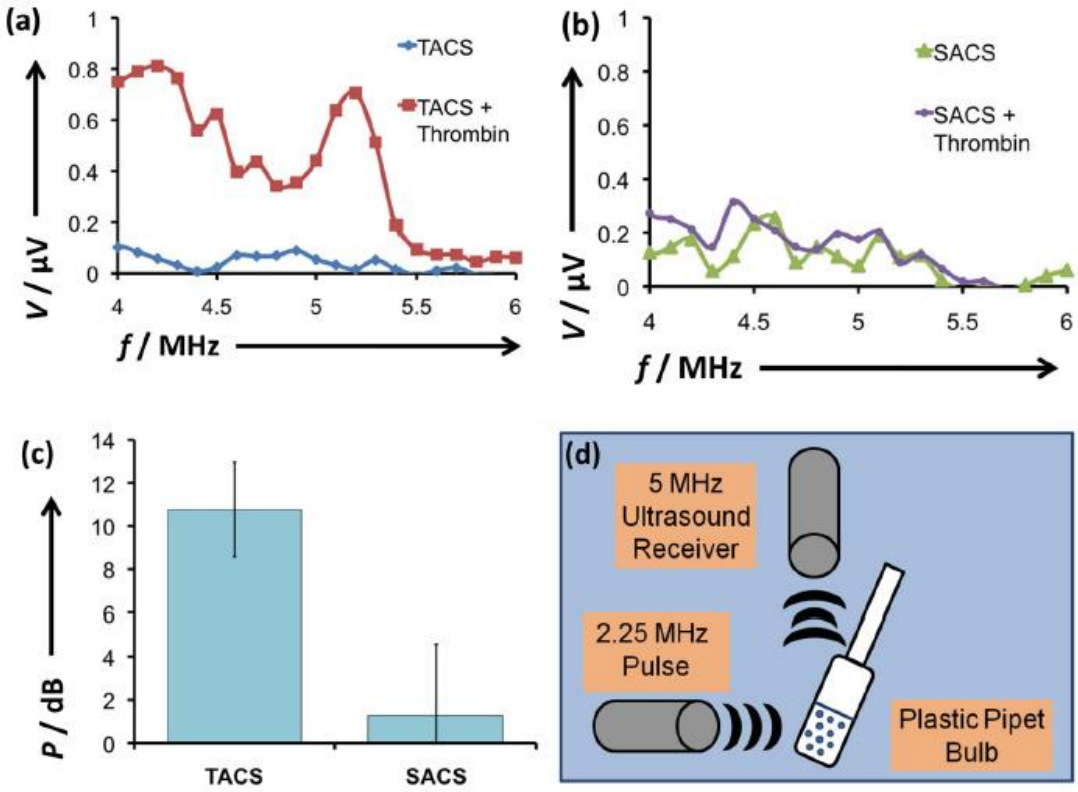

Figure 4.3: Characterization of the effect of thrombin on microbubble acoustic properties. (a) Signal acquired from microbubbles crosslinked with TACS before and after addition of thrombin. Curves shown are the mean of 10 sequential trials, standard error shown. (b) Signal acquired from microbubbles crosslinked with DNA strand containing a scrambled aptamer sequence (SACS), before and after addition of thrombin. (c) Comparison of the change in the reflected power after thrombin addition between TACS bubbles and SACS bubbles. (d) Schematic of home-built side-scatter measurement system.

4.4.4: Dependence of ultrasound signal on thrombin concentration

In order to measure the dynamic detection range of these microbubbles, different concentrations of thrombin were added to microbubble suspensions and the ultrasound signal was measured as before (**Figure 4.4a**). At 10 nM, enhancement was essentially zero and comparable to that of

microbubbles unexposed to thrombin (**Figure 4.4b**), while a very sharp and dramatic increase in power output was observed as concentration was increased from 10 to 25 nM. Interestingly, increasing thrombin levels beyond this inflection point had little effect on the total received signal but resulted in noticeable sharpening of the second harmonic peak. This response suggests that at lower concentrations of thrombin, TACS strands are not fully removed from the encapsulating shell, leaving the shell with regions of increased and decreased stiffness. This shell heterogeneity results in more heterogeneous bubble dynamics and thus a broadband signal. As the thrombin concentration increases, TACS strands are completely removed from the bubble shell, and full, unhindered oscillation can occur, producing very sharp harmonic peaks. It should be emphasized that since in phase inversion mode all frequencies outside the sending pulse contribute to the detected signal, broadband signal generation can produce a very highly detectable signal. Secondly, because the microbubbles can generate nonlinear signal with only partial shell softening, the received signal exhibits a nonlinear dependence on thrombin concentration, so the microbubble “turns on” at concentrations greater than about 20 n M. Thus while it is difficult to differentiate between thrombin concentrations of 100 or 200 nM, it is relatively easy to distinguish thrombin concentrations of 10 and 25 nM. This correlates extremely well with expected levels of thrombin in blood clots, which begin clotting at thrombin concentrations of about 25 nM and increase further as the clot grows [19, 20].

Thus the microbubble remains dormant under normal conditions, but when thrombin levels exceed the threshold for blood clotting, the microbubble produces a strong “on” signal. We hypothesize that activation will begin as the bubbles enter the local environment of an acute clot, and aptamer-thrombin interaction will increase as the bubbles pass through the vasculature of the clot, where thrombin concentration is expected to be highest, followed by continued activation in eddy currents on the downstream side of the clot. Enhanced signal should then be seen either within a clot, or immediately after the microbubbles clear the clot.

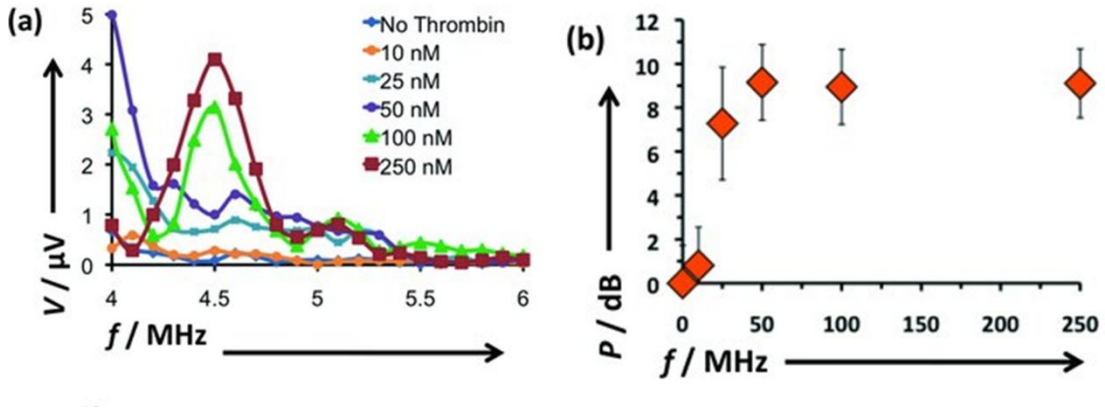

Figure 4.4: Analysis of thrombin-dependent ultrasound signal. Curves shown are the mean of 10 sequential trials, standard error shown. (a) Signal acquired from microbubbles after addition of thrombin in concentrations from 10 nM to 250 nM. (b) Change in side-scatter power from 4.0-5.5 MHz after addition of varying concentrations of thrombin.

4.4.5: Contrast enhanced ultrasound imaging in whole blood

Activation of the thrombin-detecting microbubbles was imaged in blood using a Siemens Acuson Sequoia 512 ultrasound scanner in contrast-

enhanced ultrasound mode. Microbubbles crosslinked with either TACS or SACS were diluted in EDTA-treated bovine blood to a concentration of 20 aM (10,000 bubbles per milliliter) and imaged at 2.0 MHz and 140 kPa inside an acoustically transparent phantom before and after addition of 100 nM thrombin. Prior to thrombin addition neither crosslinked bubble sample showed significant signal inside the phantom walls (**Figure 4.5**). The few bright spots in these images are most likely the result of a few large outlier bubbles, as very large bubbles will scatter signal easily even with a stiffened encapsulating shell, although in vivo large bubbles would be expected to be filtered by the lungs [21]. After the addition of thrombin, there was a substantial increase in harmonic signal for TACS microbubbles. There was no corresponding effect on microbubbles crosslinked by the scrambled SACS. This indicates that the activation is specific to the presence of thrombin. Brightness analysis using ImageJ showed a 10-fold increase in signal after thrombin addition (Figure 4e). This brightness value was similar to a sample containing the same concentration of PEG-DSPE stabilized bubbles, which is similar to an FDA-approved formulation and always retains shell flexibility (not shown). Unfortunately, earlier time points cannot be obtained using this method, as it is necessary to allow the microbubble suspension to settle and equilibrate in order to let the mixing currents subside. Our future investigations will work with a thrombosis flow model to further study the effects of microbubble activation immediately after exposure to thrombin.

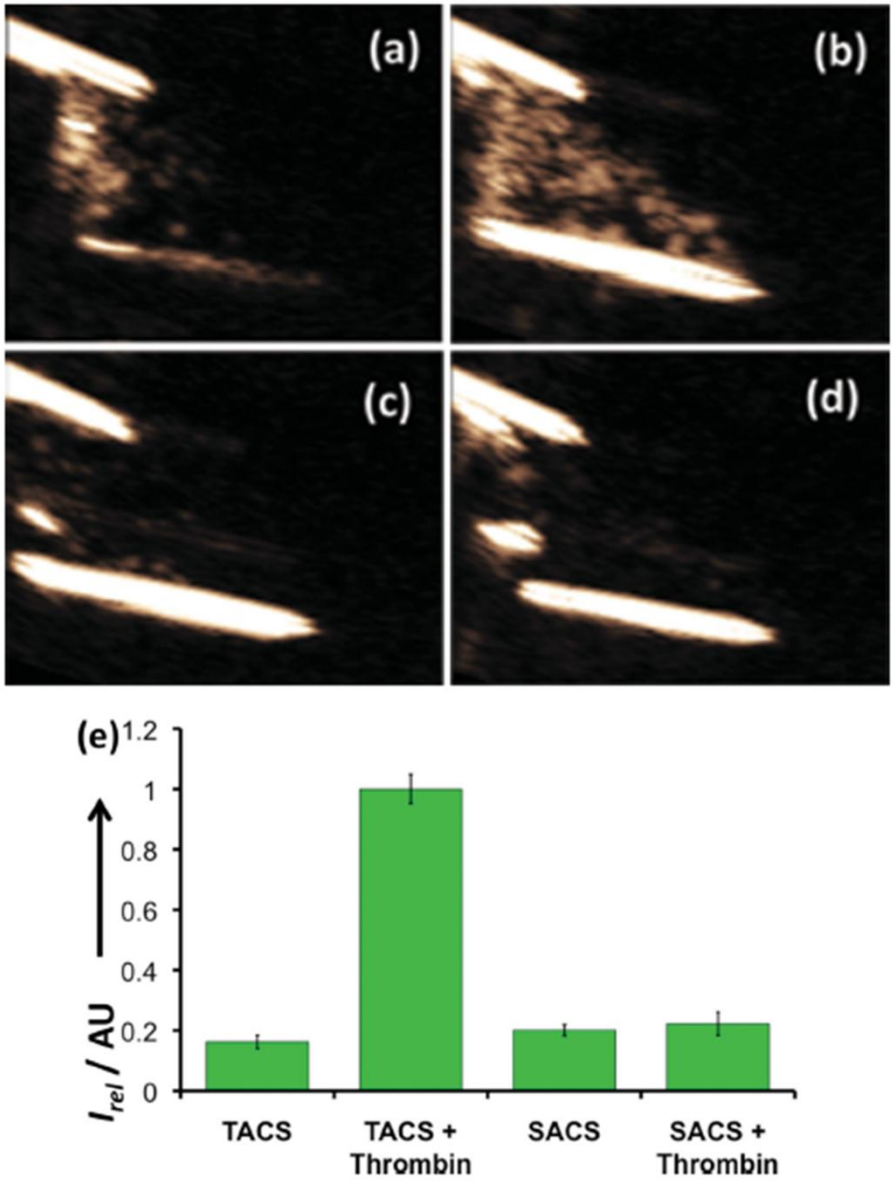

Figure 4.5: Contrast-enhanced ultrasound images of microbubble response to thrombin. Contrast-enhanced ultrasound images of TACS microbubbles EDTA-treated blood (a) prior to thrombin addition and (b) 3 min after thrombin addition. SACS microbubbles in EDTA-treated (c) prior to thrombin addition and (d) 3 min after thrombin addition. (e) Brightness analysis inside phantom of microbubble images.

4.4.6: Microbubble activation in actively-clotting whole blood

To demonstrate activation of the stimulus-responsive bubbles with naturally-generated thrombin, TACS and SACS microbubbles were added to blood freshly drawn from a one year old female New Zealand white rabbit. As soon as blood was removed from the animal, visible clotting in the tube was observed by eye (**Figure 4.6a**). At identical imaging conditions (2.0 MHz, 140 kPa), TACS microbubbles showed a fourfold increase in signal over SACS microbubbles (**Figure 4.6e**). The reduced increase in signal can be attributed to the active clotting occurring in the signal; as clotting decreases the acoustic transparency of the medium and the resulting signal generated by the activated microbubbles is substantially muted. Because of this decreased acoustic transparency, a 100-fold increase in microbubble concentration for all samples was necessary to observe any ultrasound signal. Again, the signal generated is comparable to a PEG-coated, freely oscillating microbubble with a formulation similar to those currently being used clinically. This sharp difference in the smart and scrambled bubbles was visible in as few as three minutes; this lag time is required to allow background signal generated by sample mixing to subside. This result also confirms that microbubble activation will occur faster than potential degradation by nucleases. Studies are currently underway to validate bubbles in a rabbit model with induced thrombosis.

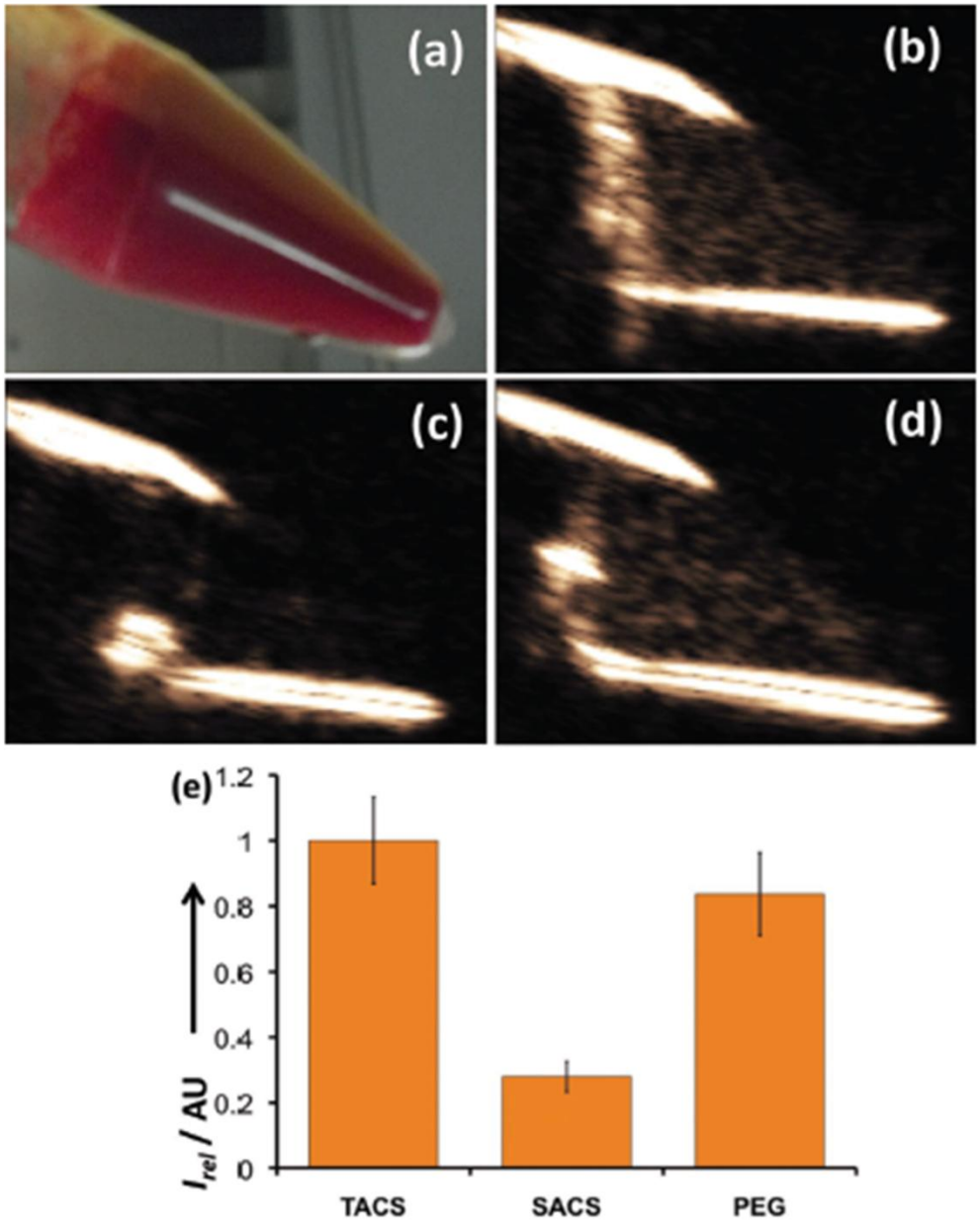

Figure 4.6: (a) Contrast-enhanced imaging of microbubbles in freshly drawn rabbit blood. (b-d) Contrast enhanced ultrasound sonographs of (b) TACS crosslinked microbubbles, (c) SACS crosslinked microbubbles, and (d) PEG-coated, freely oscillating microbubbles in freshly-drawn rabbit blood, 5 min after mixing. (e) Brightness analysis inside phantom of microbubble images.

4.5: Conclusions

In summary, we have demonstrated the first example of a stimulus-responsive contrast agent that generates ultrasound signal only in response to levels of thrombin found in active blood clots while remaining dormant in normal blood conditions. Contrast-enhanced ultrasound is ideal for imaging thrombosis, since it is both the primary modality for diagnosis and is safe, inexpensive, portable, and noninvasive. The development of a thrombin-sensitive contrast agent will help clinicians determine the activity of a clot and initiate proper therapy accordingly. In this work, microbubbles were found to activate in a fast, efficient manner at clinically relevant levels of thrombin in both fresh and preserved blood. These stimulus-responsive contrast agents have excellent potential for improving cardiovascular imaging techniques and the diagnostic power of an important imaging modality.

4.6: Acknowledgements

Biogen Idec graciously donated some of the laboratory consumables used in this experiment. We would also like to thank Prof. M. J. Heller at UCSD Nanoengineering for the use of his fluorometer, Prof. Z. Wu at UCSD Radiology for help in analyzing data, Mr. Christopher Barback with help in drawing rabbit blood, and the Ultrasound Group of Siemens Medical Solutions USA for providing their Sequoia 512 scanner through an equipment loan.

This material was reproduced in full from M. A. Nakatsuka, R. F. Mattrey, S. C. Esener, J .N. Cha, A. P. Goodwin, Advanced Materials, 2012, 24, 6010-6016. DOI: 10.1002/adma.201201484 – Reproduced by permission of John Wiley and Sons, Co.

4.7: References

[1] Heng Tan C, Bedi D, Vikram R. Sonography of thrombosis of the deep veins of the extremities: clinical perspectives and imaging review. J. Clin Ultrasound. 2012;40:31-43.

[2] Coley BD, Trambert MA, Mattrey RF. Perfluorocarbon-enhanced sonography: value in detecting acute venous thrombosis in rabbits. Am. J. Roentgenol. 1994;163:961-4.

[3] Jaffer FA, Tung CH, Gerszten RE, Weissleder R. In vivo imaging of thrombin activity in experimental thrombi with thrombin-sensitive near-infrared molecular probe. Arterioscl. Throm. Vas. 2002;22:1929-35.

[4] Tsien RY, Rink TJ, Poenie M. Measurement of cytosolic free Ca2+ in individual small cells using fluorescence microscopy with dual excitation wavelengths. Cell Calcium. 1985;6:145-57.

[5] Schutt EG, Klein DH, Mattrey RM, Riess JG. Injectable microbubbles as contrast agents for diagnostic ultrasound imaging: the key role of perfluorochemicals. Angew. Chem. Int. Edit. 2003;42:3218-35.

[6] Lanza GM, Wallace KD, Scott MJ, Cacheris WP, Abendschein DR, Christy DH, et al. A novel site-targeted ultrasonic contrast agent with broad biomedical application. Circulation. 1996;94:3334-40.

[7] Rychak JJ, Lindner JR, Ley K, Klibanov AL. Deformable gas-filled microbubbles targeted to P-selectin. J. Control. Release. 2006;114:288-99.

[8] Schumann PA, Christiansen JP, Quigley RM, McCreery TP, Sweitzer RH, Unger EC, et al. Targeted-microbubble binding selectively to GPIIb IIIa receptors of platelet thrombi. Invest. Radiol. 2002;37:587-93.

[9] Funovics M, Weissleder R, Tung CH. Protease sensors for bioimaging. Anal. Bioanal. Chem. 2003;377:956-63.

[10] Harris TJ, von Maltzahn G, Lord ME, Park JH, Agrawal A, Min DH, et al. Protease-triggered unveiling of bioactive nanoparticles. Small. 2008;4:1307-12.

[11] Unger EC, Porter T, Culp W, Labell R, Matsunaga T, Zutshi R. Therapeutic applications of lipid-coated microbubbles. Adv. Drug. Deliver. Rev. 2004;56:1291-314.

[12] Waters EA, Wickline SA. Contrast agents for MRI. Basic Res. Cardiol. 2008;103:114-21.

[13] Nakatsuka MA, Hsu MJ, Esener SC, Cha JN, Goodwin AP. DNA-coated microbubbles with biochemically tunable ultrasound contrast activity. Adv. Mater. 2011;23:4908-12.

[14] Church CC. The Effects of an Elastic Solid-Surface Layer on the Radial Pulsations of Gas-Bubbles. J. Acoust. Soc. Am. 1995;97:1510-21.

[15] Hoff L, Sontum PC, Hovem JM. Oscillations of polymeric microbubbles: Effect of the encapsulating shell. J. Acoust. Soc. Am. 2000;107:2272-80.

[16] Bock LC, Griffin LC, Latham JA, Vermaas EH, Toole JJ. Selection of Single-Stranded-DNA Molecules That Bind and Inhibit Human Thrombin. Nature. 1992;355:564-6.

[17] Nakatsuka MA, Lee JH, Nakayama E, Hung AM, Hsu MJ, Mattrey RF, et al. Facile one-pot synthesis of polymer-phospholipid composite microbubbles with enhanced drug loading capacity for ultrasound-triggered therapy. Soft Matter. 2011;7:1656-9.

[18] Nutiu R, Li Y. Structure-switching signaling aptamers. J. Am. Chem. Soc. 2003;125:4771-8.

[19] Kessels H, Beguin S, Andree H, Hemker HC. Measurement of thrombin generation in whole blood--the effect of heparin and aspirin. Thromb. Haemostasis. 1994;72:78-83.

[20] Nesheim M. Thrombin and fibrinolysis. Chest. 2003;124:33S-9S.

[21] Bouakaz A, de Jong N, Cachard C, Jouini K. On the effect of lung filtering and cardiac pressure on the standard properties of ultrasound contrast agent. Ultrasonics. 1998;36:703-8.

Chapter 5: In vivo ultrasound visualization of non-occlusive blood clots with thrombin-sensitive contrast agents.

5.1: Abstract

In this chapter, we report on the validation of a poly(ethylene glycol) PEG-stabilized, thrombin-activated microbubble (PSTA-MB) that shows increased acoustic activity in the presence of blood clots in vivo. Previously, we formulated microbubbles with tunable acoustic activity based on the presence or absence of DNA crosslinks within the encapsulating shell. By incorporating a thrombin-sensitive aptamer sequence within the crosslinking strand, the presence of thrombin was reflected by an increase in ultrasound signal. Incorporation of PEG into the shell increased stability such that the contrast agent could be used in vivo, with no change in biomarker sensitivity.

In the presence of actively clotting blood, PSTA-MBs showed a 5-fold increase in acoustic activity. Specificity for the presence of thrombin and stability under constant shear flow were demonstrated in a home-built in vitro model. PSTA-MBs were able to detect the presence of an active clot within the vena cava of a rabbit sufficiently small as to not be visible by current non-specific contrast agents.

5.2: Introduction

While ultrasound is widely used as an imaging tool, it is limited in distinguishing between normal and diseased soft tissues with similar acoustic impedances [1]. Introduction of contrast agents produces far greater ultrasound reflection, allowing imaging of smaller regions of interest with improved resolution and signal-to-noise ratios. For this, gas-filled microbubbles have been shown to be the most effective ultrasound contrast agents primarily because their nonlinear response to ultrasound creates echoes at frequencies that can be detected specifically using specialized pulse sequences [2-4]. However, microbubbles are inherently unstable in the circulation due to gas exchange in the lung, their sensitivity to significant changes in blood pressure as they circulate and when exposed to ultrasound, and shell disruption by adhesion of opsonization agents [5]. Significant progress has been made in prolonging the in vivo lifetime of microbubbles through optimization of bubble shell formulation. Bubbles can be stabilized by the introduction of thick, albumin protein shells such as with Optison® [6], polymer coatings such as poly(l-lactide-co-glycolide) (PLGA) [7], or the incorporation of poly(ethylene glycol) (PEG) lipid conjugates into phospholipid monolayers [8, 9]. Many such formulations are currently in trial or in clinical use.[2-4] However, due to their average diameters of 1-5 μm, microbubbles are limited to imaging and detecting abnormalities in the intravascular space.

As such, the main targets of microbubble detection are cardiovascular disease [10], tissue perfusion, and tumor angiogenesis [11, 12].

The microbubbles described in this work are designed to detect active clotting that can be used to distinguish acute deep vein thrombosis (DVT) from chronic DVT. Acute DVT affects patients particularly in the hospital setting following surgery, trauma, or childbirth, and it is potentially fatal if the clot embolizes to the lungs. Patients with acute DVT are treated aggressively with anticoagulants to prevent clot progression and promote lysis before the clot can organize and become adherent to the wall of the vein. Anticoagulation therapy, however, is of little benefit for chronic DVT and increases risk for internal bleeding. Since the clot is invisible to ultrasound, acute DVT is currently diagnosed by compression real-time ultrasound imaging, in which the inability to compress the vein along with the absence of Doppler flow signal provides indirect evidence of the physical presence of a clot. However, ultrasound is unable to consistently distinguish acute from chronic DVT, and in particular acute superimposed on chronic DVT, making treatment decisions difficult.

We propose here a new microbubble molecular imaging approach to not only recognize the presence of acute DVT but also distinguish active from chronic thrombosis. Ultrasound angiography with microbubbles has been proposed as a method to detect clot as filling defects [13, 14]. Because chronic thrombi will also appear as filling defects it is likely that this approach

will not aid in treatment management. Microbubbles have been proposed as molecular imaging agents to target receptors expressed on endothelial surfaces and blood elements [15-19]. However, immobilized bubbles can be dislodged or dissolved by shear stress caused by blood flow, and initial adhesion is limited by the total surface area and porosity of the clot [20]. If instead the microbubbles produced a signal only in response to elevated levels of soluble biomarkers, abnormalities could be diagnosed based on their local chemical environment even if they were otherwise too physically small to distinguish from background noise.

Here, we report the in vitro and in vivo validation of a PEG-stabilized, thrombin-activated microbubble (PSTA-MB) contrast agent capable of signaling the presence of active, non-occlusive blood clots. We previously designed microbubbles whose outer lipid monolayer shells contained a crosslinked network of hybridized DNA strands. These microbubbles became acoustically active at thrombin levels greater than 25 nM in static trials when diluted into sterile buffers, but they were insufficiently stable to survive circulation.[21, 22] We hypothesized that we could build a contrast agent with both stabilizing and stimulus-responsive agents in the same shell to allow bubble circulation without losing biomarker responsiveness. We found that incorporation of PEG-lipids improved the microbubble yield 4-fold over microbubbles without PEG in non-clotting blood, and were 25% more stable within the first 5 min of introduction into whole blood, with no effect on either

the initial silencing by crosslinking or thrombin-DNA crosslinker interaction. We were able to first validate the efficacy of these PSTA-MBs in a flow model as well as a rabbit DVT model. These PSTA-MBs were found to be especially useful for imaging actively-growing but non-occlusive blood clots, suggesting that these agents could be useful for early detection of malignant blood clot formation before the onset of vessel occlusion.

5.3: Materials and methods

5.3.1: Synthesis of DSPE-PAA-DNA

The synthesis of DSPE-PAA-DNA conjugate was described previously [21, 22]. Briefly, poly(acrylic acid) (PAA) was coupled to 1,2-distearoyl-*sn*-glycero-3-phosphoethanolamine (DSPE) via carbodiimide-mediated amidation, and two amine terminated DNA strands (5' H_2N–CCAACCACAAAA, 5' AAAACAACCCCA–NH_2) were attached to the carboxyl groups of the PAA similarly, with an average yield of 3.3 DNA strands per DSPE-PAA molecule.

5.3.2: Microbubble formulation and lifetime studies:

18 mg 1,2-palmitoyl-*sn*-glycero-3-phosphocholine (DPPC) and 2 mg 1,2-palmitoyl-*sn*-glycero-3-phosphatic acid (DPPA) were dissolved in 2 mL of chloroform and the solvent was subsequently removed by rotary evaporator (Büchi R215). The film was then rehydrated in 1X phosphate buffered saline (PBS, Gibco) to a final concentration of 4 mg/mL and stored at 4˚C. This

phospholipid mixture was subsequently mixed with varying amounts of DSPE-PEG-5000 (Avanti Polar Lipids) and the DSPE-PAA-DNA conjugate, heated and stirred at 75˚C for 30 min, and allowed to cool slowly to RT. The various phospholipid formulations are shown in **Table 5.1**. The phospholipid mixture was then probe sonicated (Branson) for 10 s under perfluorobutane gas (PFB), as described previously[23]. Bubbles were crosslinked via the addition of the complementary DNA strand GGTTGGTGTGGTTGGTGTTTTTTTTTGTGGTTGGTGTGGTTGG, referred to here forth as the thrombin aptamer crosslinking sequence (TACS). The symmetrical strand contains two 15-base aptamer sequences (GGTTGGTGTGGTTGG) on either end which possess a half-maximal inhibitory concentration (IC_{50}) of 25 nM for thrombin.[24] Nine of the fifteen bases of the aptamer are left unhybridized such that interaction with thrombin results in the displacement of the entire TACS strand. A control strand with the same crosslinking base pair sequences, but possessing scrambled unpaired ends with no affinity to thrombin, GTGTGTGTGGGTTGGTGTTTTTTTTTGTGGTTGGGTGTGTGTG, is referred to here as the scrambled aptamer crosslinking sequence (SACS). Either TACS or SACS was added to the prepared microbubble sample at a molar ratio of 1.5:1 relative to the available number of DNA sites, and allowed to hybridize at RT for 30 min. Microbubbles formed by this method had an

average diameter of 1.6±0.1 µm regardless of the amount of DSPE-PEG or DSPE-PAA-DNA.

A Multisizer 3 Coulter Counter (Beckman Coulter) with aperture size 1-30 µm was used to quantify the size and concentration of the microbubbles. 3 µL of microbubble solution was diluted into 15 mL of filtered isoton, and 100 µL was drawn per reading.

Table 5.1: Microbubble Formulations

	DPPC/DPPA	DSPE-PEG	DSPE-PAA-DNA
Pure PEG	1 mg/mL	0.3 mg/mL	0 mg/mL
0 mg/mL PEG	1 mg/mL	0 mg/mL	0.3 mg/mL
0.075 mg/mL PEG	1 mg/mL	0.075 mg/mL	0.3 mg/mL
0.225 mg/mL PEG	1 mg/mL	0.225 mg/mL	0.3 mg/mL

5.3.3: Static contrast enhanced ultrasound imaging

Freely oscillating PEG microbubbles containing 0.3 mg/mL DSPE-PEG and 0 mg/mL DSPE-PAA-DNA were diluted to various concentrations between 250 mL^{-1} and 250,000 mL^{-1} in either 2 mL of citrate-treated, non-clotting bovine blood (Lampire, Inc.), or 2 mL of blood which has been clotted through the addition of 500µL of 1 M aqueous calcium chloride in 1x PBS. The blood-bubble mixture was mixed and allowed to equilibrate for 3 min at RT, open to

the atmosphere, within the bulb of a plastic transfer pipet submerged underwater. Using a Siemens Acuson Sequoia C512, cadence mode images were taken at 7.0 MHz and an MI = 0.18. To quantify the signal generated by the microbubbles, the mean pixel brightness within the pipet bulb phantom was measured using ImageJ, and normalized to the mean brightness of the surrounding background. The area of the phantom was determined from first tracing the area of the image taken in B-Mode (not shown). Similar imaging and analysis was applied to PSTA-MB formulations which contained 0 mg/mL, 0.075 mg/mL or 0.225 mg/mL of DSPE-PEG, both in non-clotting and clotting conditions.

Additionally, the acoustic activity of bubbles with 0 mg/mL, 0.075 mg/mL and 0.225 mg/mL of DSPE-PEG were compared to that of freely oscillating microbubbles over a time period of 40 min in non-clotting citrate treated bovine blood as above. Bubble/blood mixtures were imaged every 5 min, and the normalized mean pixel brightness was measured and compared to the initial signal generated immediately after addition of bubble to the blood mixture.

5.3.4: In vitro flow model imaging

Two 1 mL syringes (BD) were cut down to 1”, keeping the sections with the Luer-slip. Between these two cut pieces, 4” of cellulose dialysis tubing (Fisher Scientific, MWCO = 3500, diameter = 1.1 cm) was affixed and sealed.

To form a clot within this cellulose section, it was filled with 2 mL of citrate-treated blood, to which 500 µL of a 1 M aqueous calcium chloride solution in 1x PBS was added and allowed to rest at RT undisturbed for 40 min.

Tygon tubing (internal diameter = 0.25”, Fisher Scientific) was used to form a closed loop between the syringe ends and a systolic pump (Fisher Scientific). The loop was filled with 25 mL of citrated blood, and blood was circulated at a speed of approximately 30 mL/min. The cellulose pouch containing the clot was imaged using a Sequoia Acuson C512 with and without the presence of a clot at a total system bubble concentration of 10,000 mL^{-1} in cadence mode. Activity of the PSTA-MBs crosslinked with the thrombin-aptamer crosslinking sequence (TACS) was compared to the activity of PSTA-MBs crosslinked with a scrambled-aptamer crosslinking sequence (SACS) to determine specificity towards thrombin. Again the mean pixel brightness within the cellulose walls was determined and normalized to the background signal over time as bubbles were allowed to circulate.

5.3.5: In vivo rabbit deep venous thrombosis model

This procedure was adapted from Coley et. al. [14] Female New Zealand white rabbits with an average weight of 3 kg were anesthetized with a cocktail of 35 mg/kg Ketamine and 5mg/kg Xylazine and the inferior vena cava (IVC) was exposed. The IVC was tied with a silk suture together with a blunted 18G needle just inferior to the renal veins. The distal IVC was clamped just

above the IVC bifurcation. 5000U of bovine thrombin was injected directly into the occluded IVC segment, and the clot allowed to form for five minutes. The distal clamp was removed allowing the blood to bathe the formed clot. The blunt needle was then removed leaving a tight infrarenal stenosis to prevent the formed clot to migrate to the lungs. The body cavity was filled with saline to eliminate trapped peritoneal air from interfering with imaging, and the incision closed. The rabbit was allowed to recover and the formed clot was imaged 6 h later.

For imaging, the rabbit was anesthetized with isofluorane and medical air, and 10 µL of Definity (Bristol-Meyers-Squibb) was injected intravenously into the ear vein in order to find and determine the shape of the clot. 10^7 microbubbles crosslinked with either TACS or SACS were then injected intravenously and microbubble response was charted at the clot site immediately after injection. Images were acquired of the clot using the CPS mode at 7.0 MHz and an MI = 0.18, and the increase in mean brightness contained within the vena cava was measured over time using ImageJ. The signal was not normalized to background as signal from background tissues is nearly totally suppressed by CPS imaging.

5.4: Results and discussion

5.4.1: Synthesis and characterization of PEGylated-DNA microbubbles

The stimulus-responsive mechanism of the microbubbles shown here derives from a DNA-aptamer switch that we have employed successfully in previous studies. [22, 25] Microbubbles formed from a mixture of DPPC and DPPA phospholipids were stabilized by a DSPE-PAA-oligonucleotide conjugate (**Figure 5.1**). Neighboring single-strand oligonucleotides were crosslinked by a complementary, aptamer-containing strand, which provided the encapsulating bubble shell with enhanced rigidity on the order of 25 pN per crosslink and greatly reduced the generation of nonlinear echoes. However, in the presence of clinically-relevant, elevated amounts of thrombin, the crosslinking aptamer strands preferentially bound to free thrombin, removing the crosslinks from the shell. This process caused the microbubble shells to become flexible, thus increasing their non-linear response when exposed to ultrasound, which can be distinguished from tissue signals using contrast specific imaging, such as CPS.

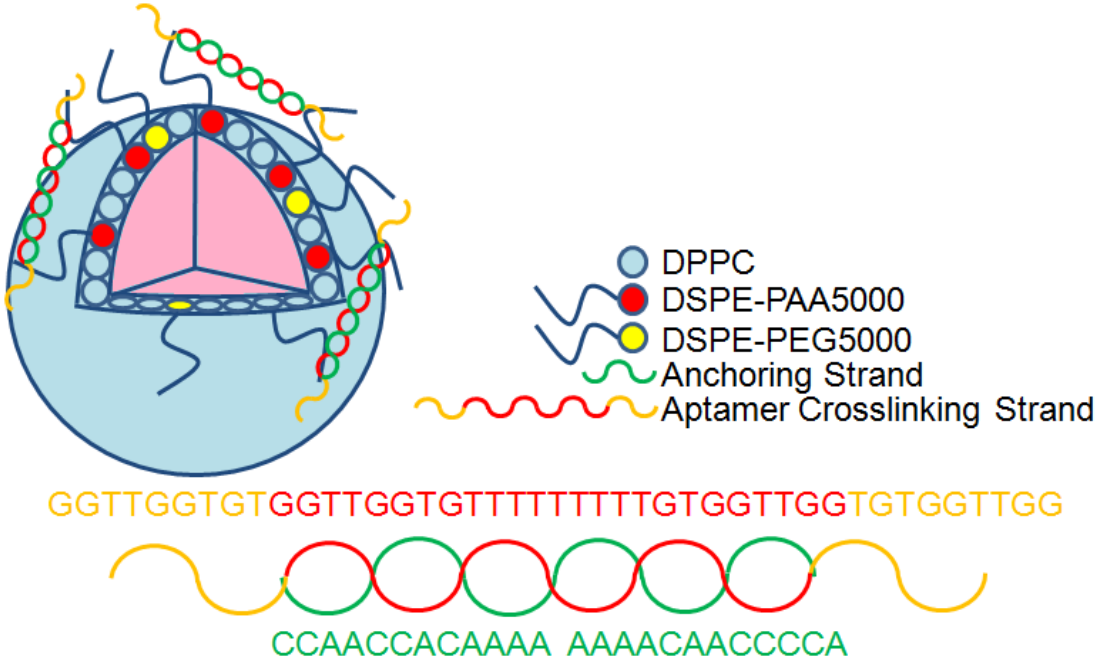

Figure 5.1: Diagram of Aptamer Crosslinked, PEGylated contrast agent. Poly(acrylic acid) (PAA) conjugated to the phospholipid DSPE is functionalized with the complementary DNA strand to a longer thrombin aptamer crosslinking sequence (TACS) The addition of the TACS causes crosslinks between neighboring phospholipid groups, and increasing the rigidity of the shell. In the presence of an acute blood clot, the unhybridized ends of the TACS will bind to the free thrombin and dislodge the strand from the bubble surface, reducing the number of crosslinks on the surface of the bubble and restoring acoustic ability.

In previous attempts to perform in vivo validation, these microbubbles as designed did not survive circulation at sufficient concentration to show a positive signal in a rabbit DVT model. We hypothesized that adding poly(ethylene glycol) (PEG) to our microbubble formulations would improve their stability without sacrificing their ability to interact with thrombin, as addition of DSPE-PEG as an emulsifying agent to gas-filled microbubbles has been applied previously for improving microbubble yield, homogeneity, and

stability compared to lipid-only formulations [9]. To add DSPE-PEG to the microbubbles, films of DPPC and DPPA phospholipids were melted in 1X PBS with varying amounts of the stabilizing agent DSPE-PEG5000 and crosslinking attachment site molecule DSPE-PAA5000-DNA, probe sonicated under perfluorobutane (PFB) to form bubbles, and mixed with the crosslinking strand. Four formulations were considered, all containing 1.0 mg/mL DPPC/DPPA: “Pure PEG”, “0 mg/mL PEG”, “0.075 mg/mL PEG” and “0.225 mg/mL PEG”. The exact formulations can be found in Table 1. After bubble preparation, bubble samples were measured by a Multisizer 3 Coulter Counter at varying time points to determine concentration (**Figure 5.2a**). As expected, microbubbles without DSPE-PEG showed the lowest initial concentration of about 1.2e8 mL^{-1}, while microbubbles with 0.3 mg/mL DSPE-PEG and no DSPE-PAA yielded about twice that. To our surprise, however, addition of 0.075 mg/mL DSPE-PAA to the mixture improved the yield by two-fold over bubbles with 0 mg/mL PEG, and 4-fold over DSPE-PAA only, indicating that this was an ideal formulation for future studies with PEG-stabilized, thrombin-activated microbubbles (PSTA-MBs).

Microbubble stability was also determined in citrate treated whole blood. The four formulations described previously were diluted to a concentration of 2500 mL^{-1} in 2 mL of citrate-treated non-clotting whole blood within the bulb of a transfer pipette and submerged underwater. The bubbles in the pipette were imaged by a Sequoia Acuson 512 in cadence mode, and

the mean pixel brightness, normalized to the background, was measured every five minutes to determine bubble viability (**Figure 5.2b**). When comparing the signal generated after 5 minutes of blood exposure to that signal generated immediately after bubble addition, we found that PSTA-MBs containing 0.075 mg/mL of DSPE-PEG were able to retain 95% of their acoustic activity while other formulations retained approximately 70% of their acoustic ability. While all microbubble formulations showed exponential decay in retained activity over time, PSTA-MB formulations with 0.075 mg/mL DSPE-PEG loadings were consistently 10% more active throughout the 40 min observation period, validating that the incorporation of small amounts of DSPE-PEG provide a boost in bubble lifetime, even in non-ideal environments such as in whole blood and open to air.

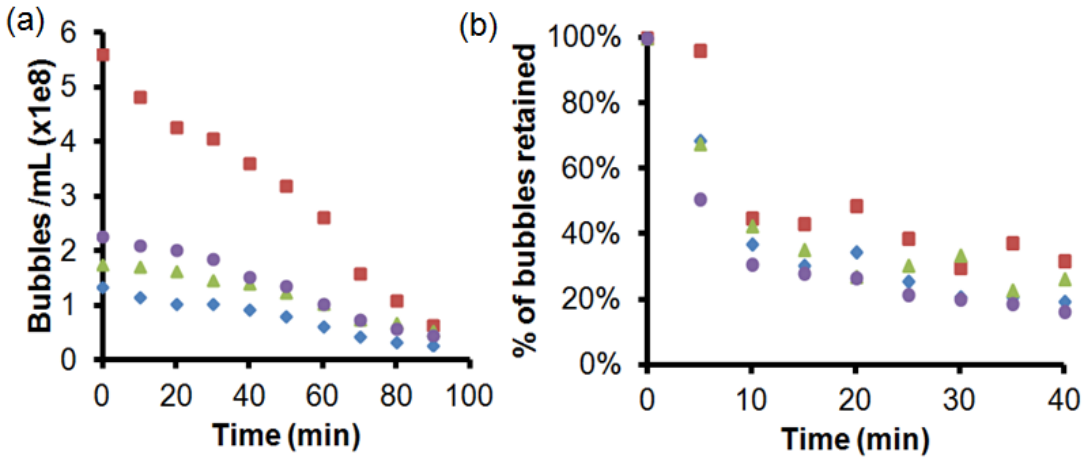

Figure 5.2: Comparison of bubble lifetime with various microbubble formulations in buffer (a), and amount of bubbles retained over time in citrate-treated non-clotting blood (b). Purple Circle = 0 mg/mL PAA-DNA, 0.3 mg/mL PEG, Blue Diamond = 0.3 mg/mL PAA-DNA 0 mg/mL PEG, Red Square = 0.3 mg/mL PAA-DNA, .075 mg/mL PEG, Green Triangle = 0.3 mg/mL PAA-DNA, .225 mg/mL PEG.

5.4.2: Activation of DNA-microbubbles in actively clotting blood:

Since PEG has been shown to retard the association of buried ligands with their protein targets, [26] addition of PEG to the microbubble shell may prevent thrombin from interacting with the crosslinking aptamer strands. It has also been shown that the addition of large amounts of PEGylated lipids to a microbubble shell can decrease the viscosity of the bubble, changing both its resonance frequency and corresponding acoustic behavior [27]. To ensure that the addition of DSPE-PEG to thrombin-activated microbubbles (PSTA-MBs) did not prevent silencing of signal, PSTA-MBs formulated with 0 mg/mL, 0.075 mg/mL and 0.225 mg/mL DSPE-PEG were evaluated in a static in vitro model in whole blood. First, we established an “acoustic concentration curve” by measuring the acoustic response of freely oscillating DSPE-PEG microbubbles without DSPE-PAA-DNA by diluting the bubbles to various concentrations in 2 mL in citrate-stabilized (non-clotting) whole blood within the bulb of a transfer pipette submerged underwater. Plotting mean pixel brightness after background subtraction against bubble concentration revealed a clear logarithmic relationship that enabled us to determine the number, or “effective concentration,” of freely-oscillating microbubbles associated with a given acoustic signal (**Figure 5.3**).

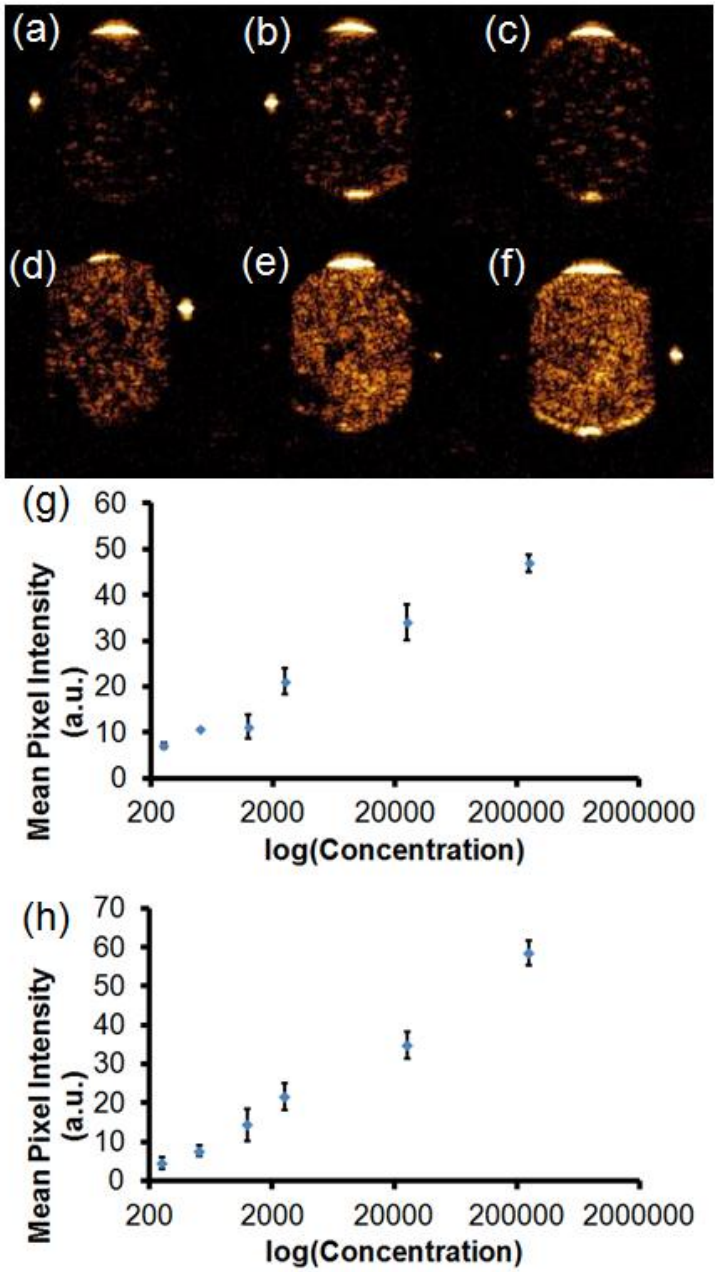

Figure 5.3: Contrast Enhanced Ultrasound Imaging of Freely Oscillating Microbubbles: Microbubbles with no DNA crosslinks in citrate treated blood are imaged at a concentration of 250 mL^{-1} (a), 500 mL^{-1} (b), 1250 mL^{-1}(c), 2500 mL^{-1} (d), 25,000 mL^{-1} (e), and 250,000 mL^{-1} (f). Acoustic activity vs. concentration is shown in (g). Each point is the average of three brightness analyses, error bars are the 95% confidence interval. An identical procedure was also carried out in clotting whole blood at the same concentrations, with a similar logarithmic relationship becoming apparent.

Next, PSTA-MBs were diluted to a concentration of 2500 mL^{-1} and measured as above. In non-clotting blood, the acoustic activity of DNA crosslinked microbubbles with no PEG incorporation at a concentration of 2500 mL^{-1} were found to be equivalent to an effective bubble concentration of approximately 215 mL^{-1}, indicating that crosslinking has prevented roughly 90% of these bubbles from generating acoustic signal (**Table 5.2**). The addition of DSPE-PEG appears to further reduce the signal generated from the crosslinked bubbles, although the small differences between the signals fall within 95% confidence intervals of each other. However, the clear difference between effective and actual concentration indicates that incorporation of DSPE-PEG within the microbubble shell did not prevent the formation of oligomer crosslinks, and the acoustic activity of the microbubbles was silenced accordingly.

To determine the response of bubbles to elevated thrombin levels, 1 M calcium chloride in 1X PBS was first added to the citrate-stabilized whole blood, causing the blood to initiate clotting. Bubbles were added immediately, the thrombin levels were allowed to increase for 3 min, and the acoustic signal was obtained as described above. To control for potential effects of clotting on acoustic signal, an effective concentration curve was obtained for freely-oscillating DSPE-PEG bubbles in clotting blood as well, with little change in the relationship between effective bubble concentration and mean pixel brightness (**Figure 5.4**) For DNA-crosslinked microbubbles without PEG

stabilization, acoustic signal increased roughly 5-fold, which equates to an effective concentration of 900 mL^{-1}. (**Table 5.2**) Effective microbubble concentrations for PSTA-MBs with 0.075 and 0.225 mg/mL DSPE-PEG in clotting blood were similar to this value, and again fell within their respective 95% confidence intervals. This increase in acoustic signal showed that the presence of DSPE-PEG did not prevent aptamer-thrombin interaction, although the presence of thrombin did not activate the microbubbles to their expected effective concentration. This “partial activation” effect was previously noted in our other DNA crosslinked microbubble systems, and we attributed this to the formation of an equilibrium between free thrombin, bound thrombin-aptamer, and hybridized aptamer that prevented complete dehybridization of the silencing strand.

Table 5.2: Effective bubble concentration calculated for various PEGylations of DNA-crosslinked microbubbles before and after the presence of thrombin as a function of mean pixel brightness.

	0 mg/mL PEG, No Clot	0 mg/mL PEG, Clot	0.075 mg/mL PEG, No Clot	0.075 mg/mL PEG, Clot	0.225 mg/mL PEG, No Clot	0.225 mg/mL PEG, Clot
Mean Pixel Intensity	5.08	12.96	3.95	13.37	3.42	14.04
Effective Concentration (mL^{-1})	215.75	911.23	178.40	961.78	163.35	1048.08
% Bubbles Active	8.63	36.45	7.14	38.47	6.53	41.92

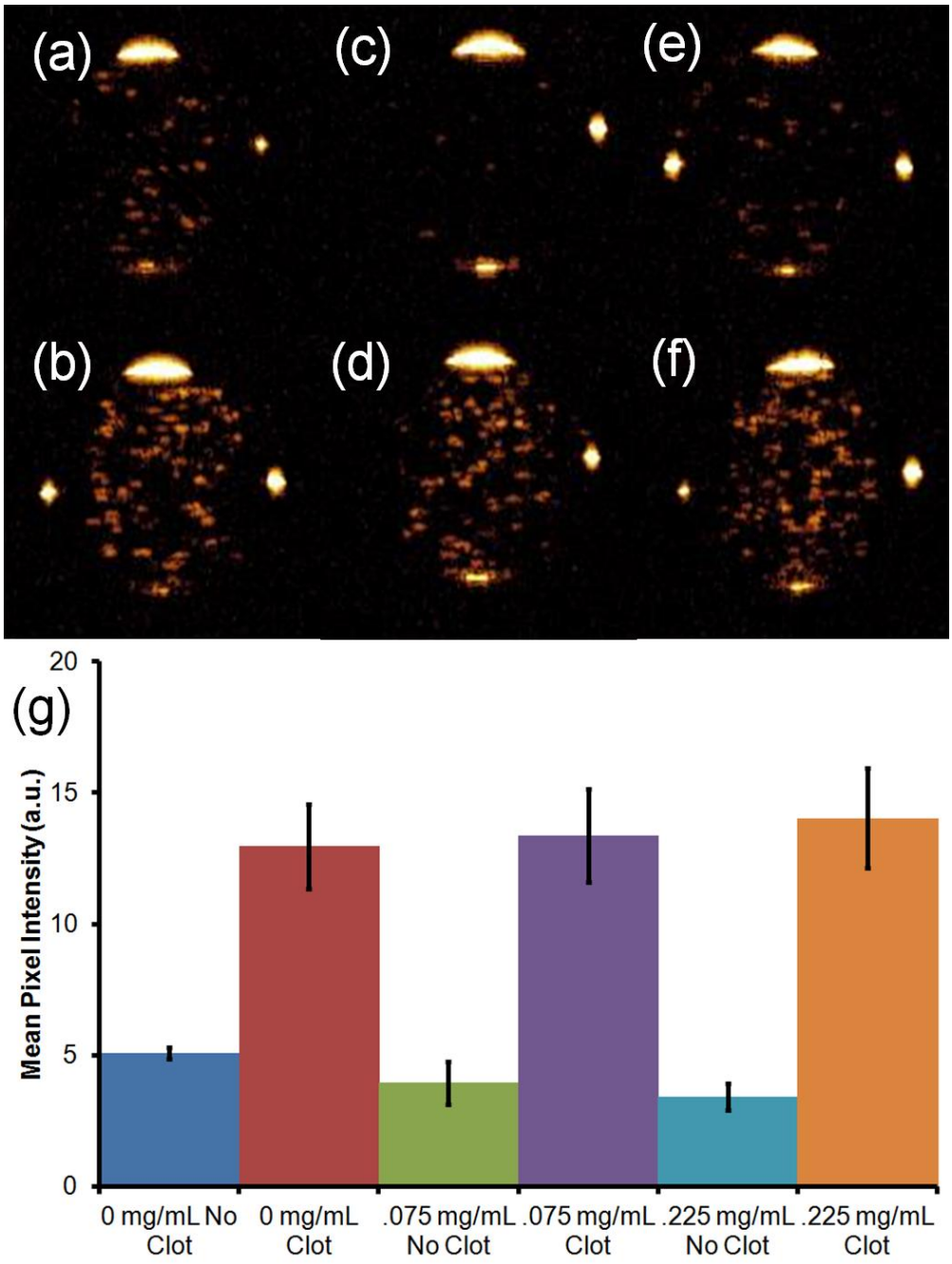

Figure 5.4: Static Contrast Enhanced Ultrasound Imaging: TACS crosslinked microbubbles with 0 mg/mL PEG loading in non-clotting (a) and actively-clotting blood (b), bubbles with .075 mg/mL PEG loading in non-clotting (c) and actively-clotting blood (d), and bubbles with .225 mg/mL PEG loading in non-clotting (e) and actively-clotting blood (f).(g) Average of three brightness analyses within the respective phantoms, error bars are the 95% confidence interval.

5.4.3: Contrast imaging in a flow model of an in vitro blood clot

While the previous experiment suggested that the acoustic signal of PSTA-MBs increased in a static area of high local thrombin concentration, this idealized case is not representative of the typical journey of a microbubble contrast agent through the bloodstream. To further assess the clinical viability of our microbubbles, we designed an in vitro model of clot formation based on the Wessler model [28] in order to better approximate in vivo conditions. In the Wessler model, an area within the jugular vein is physically isolated to restrict blood flow. Into this static “pouch”, thrombogenic material is injected, a clot is allowed to form, and then venous flow is restored. To form the pouch, cellulose dialysis tubing was partially filled with citrate-stabilized whole blood, air bubbles were removed from the tubing through manual compression, and a 1 M solution of calcium chloride in 1X PBS was added to induce thrombus formation. This resulted in a small, non-occlusive blood clot being formed on the walls of the cellulose dialysis tubing. The pouch was then connected within a closed Tygon loop, filled with citrate-stabilized blood, and connected to a peristaltic pump. This procedure preserved the local biochemical environment of the clot by retaining all of the thrombin produced during the formation of the clot.

Based on their performance in the static model and their resistance to degradation in whole blood, PSTA-MBs with 0.075 mg/mL were evaluated in the flow model. To measure the specificity of thrombin activation, PSTA-MBs

were prepared with one of two crosslinking strands: either a thrombin-aptamer crosslinking sequence TACS, or a scrambled-aptamer crosslinking sequence (SACS) that dampens acoustic signal but should not interact significantly with thrombin (see Methods for specific sequences). As a point of comparison, microbubbles were first introduced upstream of the pouch at a final dilution of 10,000 mL^{-1} in citrate-stabilized whole blood without the presence of a clot. Without the clot present, the PSTA-MBs generated little to no acoustic signal in the pouch region, regardless of crosslinking strand sequence (Figure 4). The few points of acoustic signal were most likely caused by either very large diameter bubbles, which will reflect signal very efficiently, or air bubbles generated by the shear flow in the model. Alternatively, the shear stress generated by the flow environment may caused weakening of some of the bubble shells; upon insonation, the bubble would then leave the rest of the shell, producing a freely-oscillating microbubble that would be generate nonlinear echoes quite efficiently, though it would be short-lived and non-specific in its activation [29, 30].

When the bubble samples were circulated with a clot present, signal generated from TACS bubbles, as determined by the mean pixel intensity within the clot site, increased approximately 5-fold as the microbubbles encountered the clot (**Figure 5.5**), while bubbles crosslinked with the SACS bubbles showed little overall change. As seen in Figure 4, PSTA-MBs circulate for approximately 15 seconds before dramatically changing their acoustic

activity. Because of the non-occlusive nature of the clot, blood flow within the pouch was not affected, and active microbubbles were allowed to clear the imaging site at the same rate that they were introduced. As such, after activation by exposure to thrombin, signal remained constant within the pouch until bubble loss began to take effect, at about 25 s after administration. Due to the constant circulation of calcium in addition to bubbles, clotting occurred rapidly throughout the system and led to substantial activation of bubbles even outside of the clot site within 30 s of introduction. Interestingly, signal for bubble samples crosslinked with the non-reactive SACS strand also showed a very small increase in signal in the presence of a clot. While the unhybridized ends of the SACS sequence (GTGTGTGTG) should not show any affinity towards thrombin, the hybridized hexamer sequence immediately preceding it (GGTTGG) has some affinity towards thrombin[31], allowing for some interaction and decrosslinking in these samples.

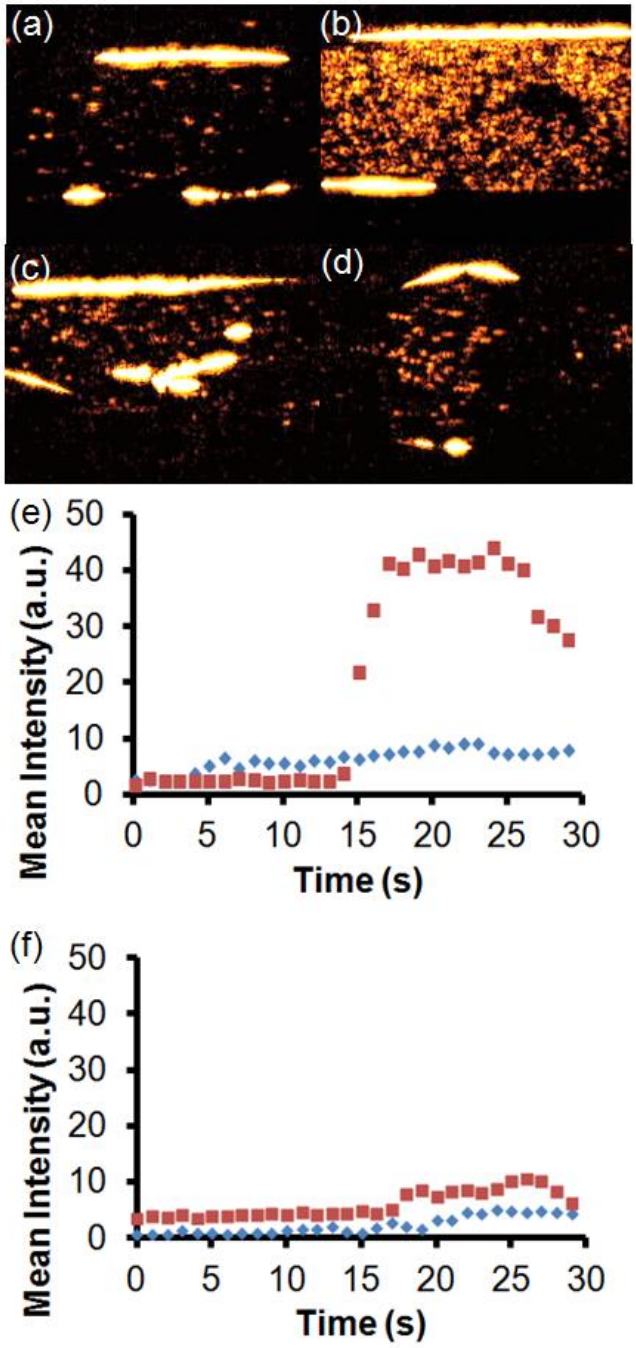

Figure 5.5: In Vitro Flow model: TACS crosslinked microbubbles when a clot is absent (a) or present (b), SACS crosslinked microbubbles in the absence (c) or presence (d) of an acutely formed clot Mean signal generated by TACS microbubbles (e) and SACS microbubbles (f) within the clot site in the presence (red) or absence (blue) of thrombin over time. T = 0 s corresponds to when blood first begins to circulate.

5.4.4: In vivo imaging of rabbit venous thrombosis

We further investigated the ability of the PSTA-MBs to act as site-specific contrast agents in a modified Wessler static thrombosis model in a rabbit. Briefly, a segment of the Inferior Vena Cava of the rabbit was temporarily occluded, and bovine thrombin added to generate a clot, followed by re-establishing flow and allowing the rabbit to recover for 6 h. Although this model does not produce a clot under natural conditions because blood flow at the clot site was stopped entirely for several minutes, in our hands, this procedure not only proved simpler and more reliable than other methods such as damaging the vessel wall or chemically inducing vascular damage, but it also ensured that the chemical environment around the clot remained relatively unaffected.

Under cadence mode imaging of the clot region, TACS and SACS bubbles were injected into the rabbits in separate trials. Unlike our in vitro model, blood flow was visibly reduced within the clot region and bubble clearance from the clot site was limited. For TACS bubbles, after the first few bubbles were detected at the clot site approximately 30 s after intravenous injection, signal increased constantly and dramatically over the next 10 s, peaking at a 5-fold increase in mean brightness within the blood vessel, as seen in **Figure 5.6**. The increase in signal differed from that observed in vitro because of an imbalance between microbubble activation and clearance allowing for gradual accumulation of active contrast agents within the clot site.

SACS bubbles showed no increase in acoustic signal over this same period. Only high concentrations of bubbles associated with full activation visibly changed the acoustic activity. Additionally, despite potential loss of bubbles during circulation, an injected concentration two orders of magnitude less than a typical diagnostic dose still remained viable roughly two minutes after injection, enough to detect and image the clot after several full cycles through the cardiovascular system.

It is noteworthy in these images that, despite the clear increase in acoustic activity and the saturation of the IVC with contrast agents, no specific clot can be distinguished. Current non-targeted contrast agents rely on the exclusion of signal, or filling defect, where the clot is present to detect and diagnose the presence of clots, and thus a clot must cause a significant displacement of blood within the vein to be visible by this method. Targeted contrast agents require bubbles to accumulate at the site of the clot, but because of the reduced flow velocity within the vein, even bubbles without targeting ligands cannot clear easily, reducing the clot-specific contrast. The immediate change in acoustic signal caused by local thrombin activation within an active clot, however, allow detection and diagnosis by the PSTA-MBs. Thus, these PEGylated, thrombin-activated microbubbles show excellent promise for improving early detection of active clot formation within the cardiovascular system and particular acute deep venous thrombosis.

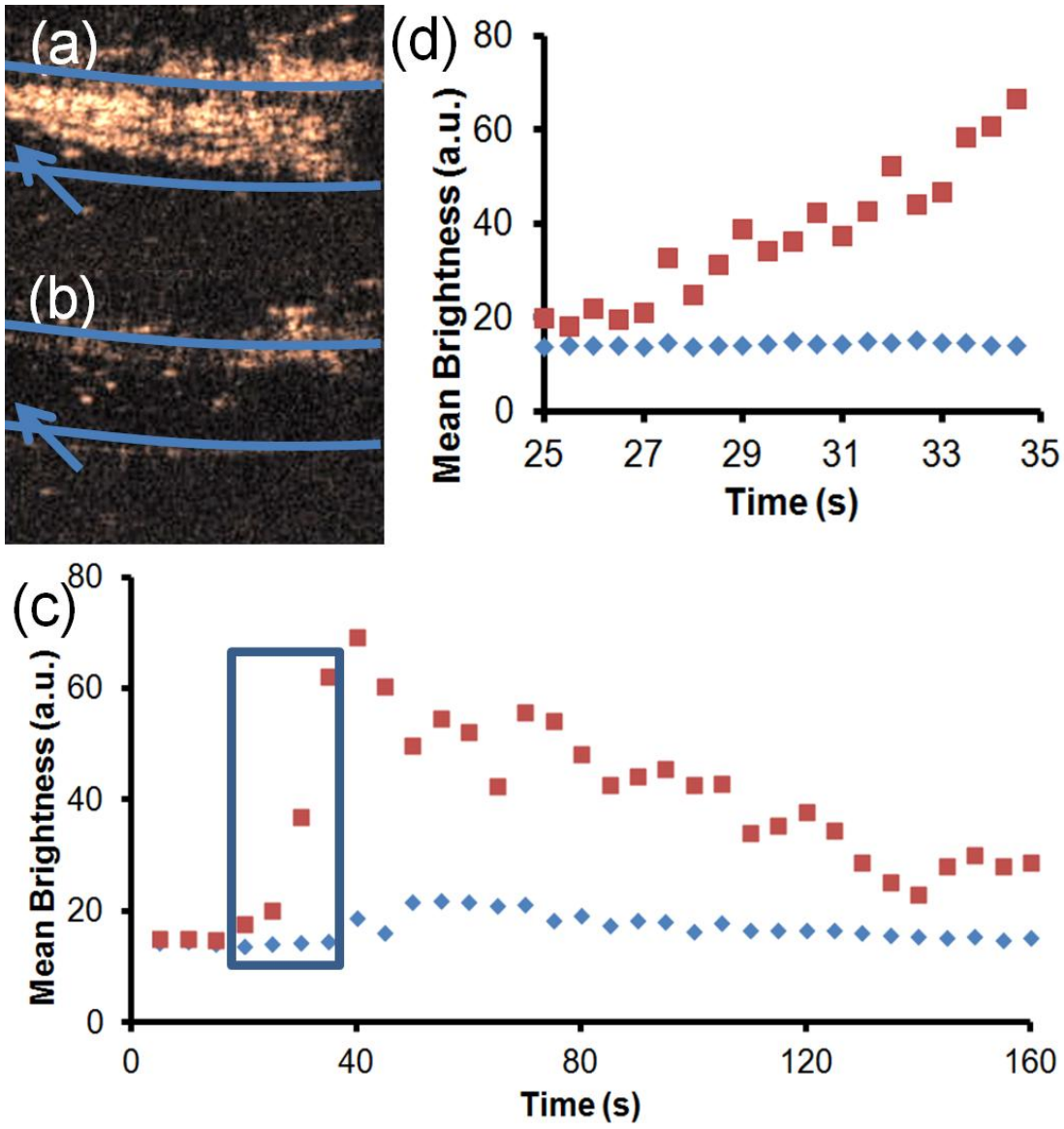

Figure 5.6: In Vivo Imaging of Deep Venous Thrombosis: Activation of TACS (a) crosslinked microbubbles and SACS (b) crosslinked microbubbles at clot site in cadence mode. Arrows point at probable clot site as determined by physical tie. Blue outlines indicate vena cava walls. (c) Acoustic signal generated within the clot site over time for TACS (red) or SACS (blue) within the inferior vena cava.(d) Acoustic signal generated as bubble encounter the clot and become active. This corresponds to area of interest highlighted in blue.

5.5: Conclusions

In this work we studied the effect of addition of DSPE-PEG to microbubbles capable of increasing their acoustic response in the presence of thrombin. The microbubbles responded to thrombin through interaction of this biomarker with DNA aptamer crosslinkers that rigidify the bubble shell, decreasing or eliminating its non-linear response to ultrasound. Adding DSPE-PEG to this formulation did not change the ability of the microbubbles to respond to elevated thrombin, while the addition of PEG resulted in a 2-fold increase in bubble yield, and a 25% increase in stability within the first 5 min of blood exposure, allowing them to be used under shear flow both in vitro and in vivo. The PSTA-MB contrast agent increased its acoustic signal five-fold in actively clotting blood. It also showed a sharp and immediate increase in signal when encountering a mature clot under shear flow when crosslinked with a DNA strand with an affinity towards thrombin, but very little change when crosslinked with a DNA strand with little affinity towards thrombin, demonstrating specificity of the activation mechanism. Finally, PSTA-MBs proved capable of imaging a non-occlusive clot in vivo, despite the clot being too small to see with traditional contrast enhanced imaging. These studies indicate that microbubbles functionalized with a combination of lipids, DSPE-PEG, and polymer-DNA conjugates represent a simple, non-invasive method for early, efficient diagnosis of deep venous thrombosis.

5.6: Acknowledgements

The authors would like to thank Professor Mark Borden at the University of Colorado Boulder for the use of his Sequoia Acuson C512 Ultrasound Imager for in vitro studies and his Beckman Coulter Multisizer 3, as well as the Ultrasound Group of Siemens Medical Solutions USA for providing their Sequoia 512 scanner to UCSD through an equipment loan for the in vivo studies. The authors would also like to thank Dr. Jameel Feshitan and Dr. Shashank Sirsi for instrument training, and Jacqueline Corbeil and Rosemarie Ramirez for aid during rabbit surgery.

This chapter is being prepared for submission for publication of this material. Matthew A. Nakatsuka, Christopher V. Barback, Kirsten R. Fitch, Alexander R. Farwell, Sadik C. Esener, Robert F. Mattrey, Jennifer N. Cha, and Andrew P. Goodwin contributed to this work.

5.7: References

[1] Schutt EG, Klein DH, Mattrey RM, Riess JG. Injectable microbubbles as contrast agents for diagnostic ultrasound imaging: the key role of perfluorochemicals. Angew. Chem. Int. Ed. 2003;42:3218-35.

[2] Ferrara KW, Borden MA, Zhang H. Lipid-shelled vehicles: engineering for ultrasound molecular imaging and drug delivery. Accounts Chem. Res. 2009;42:881-92.

[3] Sboros V. Response of contrast agents to ultrasound. Adv. Drug. Deliv. Rev. 2008;60:1117-36.

[4] Pancholi KP, Farook U, Moaleji R, Stride E, Edirisinghe MJ. Novel methods for preparing phospholipid coated microbubbles. Eur. Biophys. J. 2008;37:515-20.

[5] Lindner JR, Dayton PA, Coggins MP, Ley K, Song J, Ferrara K, et al. Noninvasive imaging of inflammation by ultrasound detection of phagocytosed microbubbles. Circulation. 2000;102:531-8.

[6] Kamaev PP, Hutcheson JD, Wilson ML, Prausnitz MR. Quantification of Optison bubble size and lifetime during sonication dominant role of secondary cavitation bubbles causing acoustic bioeffects. J. Acoust. Soc. Am. 2004;115:1818-25.

[7] Cui W, Bei J, Wang S, Zhi G, Zhao Y, Zhou X, et al. Preparation and evaluation of poly(L-lactide-co-glycolide) (PLGA) microbubbles as a contrast agent for myocardial contrast echocardiography. J. Biomed. Mater. Res. Part B. Appl. Biomater. 2005;73:171-8.

[8] Borden MA, Pu G, Runner GJ, Longo ML. Surface phase behavior and microstructure of lipid/PEG-emulsifier monolayer-coated microbubbles. Colloid Surface B. 2004;35:209-23.

[9] Borden MA, Longo ML. Dissolution behavior of lipid monolayer-coated, air-filled microbubbles: Effect of lipid hydrophobic chain length. Langmuir. 2002;18:9225-33.

[10] Lindner JR. Molecular imaging of cardiovascular disease with contrast-enhanced ultrasonography. Nat. Rev. Cardiol. 2009;6:475-81.

[11] Anderson CR, Hu X, Zhang H, Tlaxca J, Decleves AE, Houghtaling R, et al. Ultrasound molecular imaging of tumor angiogenesis with an integrin targeted microbubble contrast agent. Invest. Radiol. 2011;46:215-24.

[12] Willmann JK, Cheng Z, Davis C, Lutz AM, Schipper ML, Nielsen CH, et al. Targeted microbubbles for imaging tumor angiogenesis: Assessment of whole-body biodistribution with dynamic micro-PET in mice. Radiology. 2008;249:212-9.

[13] Heng Tan C, Bedi D, Vikram R. Sonography of thrombosis of the deep veins of the extremities: clinical perspectives and imaging review. J. Control. Release. 2012;40:31-43.

[14] Coley BD, Trambert MA, Mattrey RF. Perfluorocarbon-enhanced sonography: value in detecting acute venous thrombosis in rabbits. Am. J. Roentgenol. 1994;163:961-4.

[15] Maul TM, Dudgeon DD, Beste MT, Hammer DA, Lazo JS, Villanueva FS, et al. Optimization of ultrasound contrast agents with computational models to improve selection of ligands and binding strength. Biotechnol. Bioeng. 2010;107:854-64.

[16] Wang CH, Kang ST, Lee YH, Luo YL, Huang YF, Yeh CK. Aptamer-conjugated and drug-loaded acoustic droplets for ultrasound theranosis. Biomaterials. 2012;33:1939-47.

[17] Klibanov AL. Ligand-carrying gas-filled microbubbles: Ultrasound contrast agents for targeted molecular imaging. Bioconjugate Chem. 2005;16:9-17.

[18] Simberg D, Mattrey R. Targeting of perfluorocarbon microbubbles to selective populations of circulating blood cells. J. Drug Target. 2009;17:392-8.

[19] Shi G, Cui W, Benchimol M, Liu YT, Mattrey RF, Mukthavaram R, et al. Isolation of rare tumor cells from blood cells with buoyant immuno-microbubbles. PloS one. 2013;8:e58017.

[20] Takalkar AM, Klibanov AL, Rychak JJ, Lindner JR, Ley K. Binding and detachment dynamics of microbubbles targeted to P-selectin under controlled shear flow. J. Control. Release. 2004;96:473-82.

[21] Nakatsuka MA, Hsu MJ, Esener SC, Cha JN, Goodwin AP. DNA-coated microbubbles with biochemically tunable ultrasound contrast activity. Adv. Mater. 2011;23:4908-12.

[22] Nakatsuka MA, Mattrey RF, Esener SC, Cha JN, Goodwin AP. Aptamer-crosslinked microbubbles: smart contrast agents for thrombin-activated ultrasound imaging. Adv. Mater. 2012;24:6010-6.

[23] Nakatsuka MA, Lee JH, Nakayama E, Hung AM, Hsu MJ, Mattrey RF, et al. Facile One-Pot Synthesis of Polymer-Phospholipid Composite Microbubbles with Enhanced Drug Loading Capacity for Ultrasound-Triggered Therapy. Soft Matter. 2011;2011:1656-9.

[24] Nutiu R, Li Y. Structure-switching signaling aptamers. J. Am. Chem. Soc. 2003;125:4771-8.

[25] Caskey CF, Stieger SM, Qin S, Dayton PA, Ferrara KW. Direct observations of ultrasound microbubble contrast agent interaction with the microvessel wall. J. Acoust. Soc. Chem. 2007;122:1191-200.

[26] Borden MA, Zhang H, Gillies RJ, Dayton PA, Ferrara KW. A stimulus-responsive contrast agent for ultrasound molecular imaging. Biomaterials. 2008;29:597-606.

[27] Hosny NA, Mohamedi G, Rademeyer P, Owen J, Wu Y, Tang MX, et al. Mapping microbubble viscosity using fluorescence lifetime imaging of molecular rotors. Proc. Natl. Acad. Sci. USA. 2013.

[28] Wessler S. Studies in intravascular coagulation. I. Coagulation changes in isolated venous segments. J. Clin. Inves. 1952;31:1011-4.

[29] Miller DL. Frequency relationships for ultrasonic activation of free microbubbles, encapsulated microbubbles, and gas-filled micropores. J. Acoust. Soc. Am. 1998;104:2498-505.

[30] Postema M, Bouakaz A, Versluis M, de Jong N. Ultrasound-induced gas release from contrast agent microbubbles. IEEE T. Ultrason Ferr. 2005;52:1035-41.

[31] Bock LC, Griffin LC, Latham JA, Vermaas EH, Toole JJ. Selection of Single-Stranded-DNA Molecules That Bind and Inhibit Human Thrombin. Nature. 1992;355:564-6.